VILNIUS GEDIMINAS TECHNICAL UNIVERSITY

Mantas ATUTIS

ANALYSIS OF FLEXURAL BEHAVIOUR OF CONCRETE BEAMS PRESTRESSED WITH BASALT FIBER REINFORCED POLYMER BARS

DOCTORAL DISSERTATION

TECHNOLOGICAL SCIENCES,
CIVIL ENGINEERING (02T)

VGTU
LEIDYKLA
TECHNIKA
Vilnius 2018

Doctoral dissertation was prepared at Vilnius Gediminas Technical University in 2013–2018.

Supervisor

Prof. Dr Juozas VALIVONIS (Vilnius Gediminas Technical University, Civil Engineering – 02T).

The Dissertation Defence Council of Scientific Field of Civil Engineering of Vilnius Gediminas Technical University:

Chairman

Assoc. Prof. Dr Darius BAČINSKAS (Vilnius Gediminas Technical University, Civil Engineering – 02T).

Members:

Dr Nicholas FANTUZZI (University of Bologna, Italy, Civil Engineering – 02T),

Dr Shiho KAWASHIMA (Columbia University of the City of New York, United States, Materials Engineering – 08T),

Prof. Dr Romualdas KLIUKAS (Vilnius Gediminas Technical University, Civil Engineering – 02T),

Prof. Dr. Ričardas MAKUŠKA (Vilnius University, Chemical Engineering – 05T).

The dissertation will be defended at the public meeting of the Dissertation Defence Council of Civil Engineering in the Senate Hall of Vilnius Gediminas Technical University at **9 a. m. on 9 November 2018**.

Address: Saulėtekio al. 11, LT-10223 Vilnius, Lithuania.
Tel.: +370 5 274 4956; fax +370 5 270 0112; e-mail: doktor@vgtu.lt

A notification on the intend defending of the dissertation was send on 8 October 2018.
A copy of the doctoral dissertation is available for review at VGTU repository http://dspace.vgtu.lt/ and at the Library of Vilnius Gediminas Technical University (Saulėtekio al. 14, LT-10223 Vilnius, Lithuania).

VGTU Press TECHNIKA 2018-043-M research publication book

ISBN 978-609-476-132-4
© VGTU Press TECHNIKA, 2018
© Mantas Atutis, 2018
mantas.atutis@vgtu.lt

VILNIAUS GEDIMINO TECHNIKOS UNIVERSITETAS

Mantas ATUTIS

IŠ ANKSTO ĮTEMPTAIS BAZALTO PLUOŠTO STRYPAIS ARMUOTŲ LENKIAMŲJŲ BETONINIŲ ELEMENTŲ ELGSENOS ANALIZĖ

DAKTARO DISERTACIJA

TECHNOLOGIJOS MOKSLAI,
STATYBOS INŽINERIJA (02T)

VGTU
LEIDYKLA
Vilnius TECHNIKA 2018

Disertacija rengta 2013–2018 metais Vilniaus Gedimino technikos universitete.

Vadovas

prof. dr. Juozas VALIVONIS (Vilniaus Gedimino technikos universitetas, statybos inžinerija – 02T).

Vilniaus Gedimino technikos universiteto Statybos inžinerijos mokslo krypties disertacijos gynimo taryba:

Pirmininkas

doc. dr. Darius BAČINSKAS (Vilniaus Gedimino technikos universitetas, statybos inžinerija – 02T).

Nariai:

dr. Nicholas FANTUZZI (Bolonijos universitetas, Italija, statybos inžinerija – 02T),

dr. Shiho KAWASHIMA (Niujorko Kolumbijos universitetas, JAV, medžiagų inžinerija – 08T),

prof. dr. Romualdas KLIUKAS (Vilniaus Gedimino technikos universitetas, statybos inžinerija – 02T),

prof. dr. Ričardas MAKUŠKA (Vilniaus universitetas, chemijos inžinerija – 05T).

Disertacija bus ginama viešame Statybos inžinerijos mokslo krypties disertacijos gynimo tarybos posėdyje **2018 m. lapkričio 9 d. 9 val.** Vilniaus Gedimino technikos universiteto senato posėdžių salėje.

Adresas: Saulėtekio al. 11, LT-10223 Vilnius, Lietuva.
Tel.: (8 5) 274 4956; faksas (8 5) 270 0112; el. paštas doktor@vgtu.lt

Pranešimai apie numatomą ginti disertaciją išsiųsti 2018 m. spalio 8 d.

Disertaciją galima peržiūrėti VGTU talpykloje http://dspace.vgtu.lt/ ir Vilniaus Gedimino technikos universiteto bibliotekoje (Saulėtekio al. 14, LT-10223 Vilnius, Lietuva).

Abstract

In general, prestressed concrete (PC) is by far one of the most economical concrete construction techniques, but at the same time, it requires specific knowledge of the properties and behavior of this material. Precompression of the concrete by transferred prestressed force flexural stiffness can be increased and the main issue – cracking might be eliminated, correspondingly. Based on the development progress PC is widely being utilized in the construction of the structures for transport and energy sectors (bridges, viaducts, gasholders, reactors, oil&gas tanks, etc.). It has been used in order to store potentially dangerous materials during operation and to resist dynamic effects. However, even in PC case cracking appears, and it is common that it causes corrosion of conventional reinforcement. Finally, it influences the maintenance of existing infrastructure.

Within this research, the author develops the particular subject of concrete – application of new composite material – basalt fiber reinforced polymer (BFRP) to be used for prestressed concrete structures considering subsequent loading stages (stretching at the bulkheads, prestress transfer to concrete, application of service load, etc.). In order to design PC structures, it is significant to estimate effective prestress force with respect to the time-dependent process of concrete and reinforcement. In accordance with design codes requirements, typical formulas from regular concrete structures (RC) are to be used for the estimate of serviceability conditions of flexural PC members. However, a complete review of prestress losses and serviceability shall be employed in order to avoid errors in the structural prognosis of the PC structures with non-conventional composite reinforcement.

Unlike other composites, experimental test work and calculation methods have yet to be developed for BFRP reinforcement in order to determine stress relaxation behavior. Currently, this phenomena is not fully documented in the literature. Based on this, the author approached an innovative stress relaxation test method to describe the effect of stress relaxation and its impact on the final value of the effective prestress force. Full-scale testing beams were tested in order to evaluate the impact of prestress level (degree) to the flexural stiffness of concrete beams internally prestressed with BFRP bars.

The dissertation is structured within the introduction, three main chapters, verification of the results, the lists of references and author's publications on the subject of the dissertation.

The topic of the thesis has been discussed in 9 articles: 3 – in the journals with an Impact Factor, 5 – in scientific journals of other international databases and 1 in the conference proceedings referred by the Clarivate Analytics Web of Science.

Reziumė

Išankstinis įtempimas yra viena iš ekonomiškiausių statybinių konstrukcijų statybos būdų, tačiau iš inžinieriaus reikalauja gilesnių gelžbetonio mechanikos žinių. Iš anksto apgniuždant betoną galima padidinti statinių konstrukcijų standumą bei eliminuoti vieną iš esminių trūkumų – pleišėjimą. Vystantis pramonei įtemptasis gelžbetonis vis labiau naudojamas specialiųjų transporto, energetikos bei susisiekimo statiniuose (tiltai, viadukai, saugyklos, reaktoriai, naftos, suskystintųjų gamtinių dujų, trašų rezervuarai ir talpyklos) užtikrinant potencialiai pavojingų medžiagų sandėliavimą ar atsparumą dinaminių apkrovų poveikiui. Dėl aplinkos poveikio gelžbetoninėse konstrukcijose atsiranda nepageidaujami plyšiai, pradeda vystytis armatūros korozija, o tai gali įtakoti tolimesnės minėtų konstrukcijų eksploatacijos kaštų padidėjimą.

Šiame darbe plėtojama dar viena gelžbetonio mechanikos tyrimų kryptis – naujos kompozitinės medžiagos pritaikymas įtemptojo betono konstrukcijoms armuoti, kai ši armatūra įtempiama į atsparas. Norint tinkamai suprojektuoti įtemptąsias betonines konstrukcijas reikia tiksliai įvertinti efektyvios išankstinio įtempimo jėgos dydį atsižvelgiant į ilgalaikius procesus betone bei armatūroje t. y. armatūros įtempių nuostolius. Atsižvelgiant į normų reikalavimus, taikomi skaičiavimo metodai yra skirti įprastoms gelžbetoninėms konstrukcijoms, taip galimai apskaičiuojant galutinius įtempių nuostolius su paklaida, todėl yra reikalingas armatūros įtempių nuostolių skaičiavimo metodų ir eksperimentinių tyrimų tikslinimas, nes įtempiant armatūrą, keičiasi jos, kaip medžiagos mechaninės savybės, o tai turi įtakos efektyviosios išankstinio įtempimo jėgos nustatymui.

Skirtingai nuo kitų kompozitinių medžiagų mokslinių tyrimų rezultatų, šiuo metu pastebimas eksperimentinių tyrimų bei skaičiavimo metodų, tinkamų bazalto pluošto armatūros įtempių relaksacijos elgsenai įvertinti, trūkumas. Šiuo tikslu buvo parengta eksperimentinių tyrimų programa siekiant įvertinti armatūros įtempių relaksacijos įtaką išankstiniams armatūros įtempių nuostoliams bei išankstinio įtempimo jėgos dydžio įtaką betoninių elementų standumui. Todėl buvo atlikti natūralaus dydžio iš anksto įtemptais bazalto pluošto armatūros strypais armuotų lenkiamų betoninių sijų eksperimentiniai tyrimai.

Disertaciją sudaro įvadas, trys skyriai, bendrosios išvados, naudotos literatūros ir autoriaus publikacijų disertacijos tema sąrašai.

Disertacijos tema paskelbti 9 moksliniai strapsniai: 3 – žurnaluose turinčiuose citavimo rodiklį, 5 – kitų tarptautinių duomenų bazių leidiniuose ir 1 – konferencijų rinkinyje, referuojamame Clarivate Analytics Web of Science duomenų bazėje.

Notations

Symbols

A	– is the area of the beam cross-section;
A_c	– is the area of plain concrete net section;
A_{cc}	– is the area of the compressive concrete above the neutral axis around the top surface of the cross-section;
$\bar{A}_{eff}$	– is the area of the age-adjusted transformed cross-section;
A_g	– is the area of the gross cross-section;
A_p	– is the cross-sectional area of prestressing bar;
A_s	– is the cross-section area of steel rebar;
A_0	– is the area of the transformed cross-section at time;
C	– is the coefficient of pure creep;
C^*	– is the pure specific creep function;
$E_{c.eff}$	– is the effective modulus of elasticity of concrete;
$\bar{E}_{c.eff}$	– is the age-adjusted effective elasticity modulus for concrete;
E_{cm}	– is the secant modulus of elasticity of concrete;
$E_{cm.28}$	– is the elastic modulus of concrete at the age of 28 days;
E_p	– is the elastic modulus of the prestressing bar;

E_s – is the Young modulus of the steel;

E_0 – is the static elastic modulus of the polymer;

I – is the second moment of area of the beam cross-section;

I_{cr} – is the second moment of area of a cracked cross-section;

I_{cc}^{top} – is the second moment of area of the compressive concrete above the neutral axis around the top surface of the cross-section;

I_e – is the effective moment of inertia after cracking;

I_{eff}^{top} – is the second moment of area about the top surface of the transformed cross-section;

$\overline{I_{eff}^{top}}$ – is the second moment of the area about the top surface of the age-adjusted transformed cross-section;

I_g – is the second moment of area of the gross cross-section;

I_0^{top} – is the second moment of the transformed area about the top surface of the cross-section at time of prestress transfer;

M_a – is the moment due to the applied service load;

M_{cr} – is the cracking moment;

M_{dec} – is the decompression moment;

M_{ext} – is the externally applied moment;

N_{ext} – is the externally applied axial load;

P_0 – is the force at prestress transfer;

P_{max} – is the force imposed on the prestressing bar by the hydraulic jack;

$P_{m.t}$ – is the effective force in the prestressing bar at time after the time-dependent losses;

$P_{m.0}$ – is the initial force in the prestressing bar immediately after transfer after the instantaneous (short-term) losses;

S_c^{top} – is the first moment of area about the top surface of the concrete cross-section;

S_{cc}^{top} – is the first moment of area of the compressive concrete above the neutral axis around the top surface of the cross-section;

S_{eff}^{top} – is the first moment of area about the top surface of the transformed cross-section;

$\overline{S_{eff}^{top}}$ – is the first moment of area about the top surface of the age-adjusted transformed cross-section;

S_0^{top} – is the first moment of the transformed area about the top surface of the cross-section at prestress transfer;

a – is the coefficient;

b – is the coefficient; the width;

e	– is the eccentricity of the prestress; the base of the natural logarithm;
f_{cm}	– is the mean value of cylinder compressive strength of concrete;
f_{cm28}	– is the compressive strength of concrete at the age of 28 days;
f_u	– is the ultimate tensile strength of prestressing bar;
k	– is the spring elastic constant;
r_p	– is the relaxation function;
$1/r$	– is the curvature of the cross-section;
$s_{r.max}$	– is the maximum crack spacing;
t	– is the time being considered; the age of concrete (in days);
t_0	– is the time at the stretching (tensioning at bulkhead) of prestressing bars;
t_p	– is the time at prestress transfer to concrete cross-section;
t_q	– is the time at the service load applied;
w_k	– is the crack width;
y_p	– is the y-coordinate of the level of prestressing bar (tendon);
y_s	– is the y-coordinate of the level of steel reinforcement;
z_{cp}	– is the distance between the center of gravity of the concrete section and the tendons;
β_{cc}	– is the coefficient which depends on the age of the concrete;
ΔM	– is the restraining moment;
ΔN	– is the restraining axial force;
ΔP_c	– is the losses of prestress due to creep of concrete;
$\Delta P_{c.ext}$	– are the losses due to creep strain due to permanent service load;
ΔP_{c+s+r}	– are the time-dependent losses of prestress due to creep, shrinkage, and relaxation;
ΔP_{el}	– is the losses of prestress due to elastic shortening of the member;
ΔP_r	– are the losses due to intrinsic relaxation;
ΔP_s	– are the losses due to concrete shrinkage;
$\Delta P_\mu(x)$	– is the losses due to friction at any distance x from the jacking end;
ΔP_Θ	– is the losses due to to change in temperature;
$\Delta\sigma_{pr}$	– is the absolute value of the relaxation losses of the prestress;
$\Delta\overline{\sigma}_{pr}$	– is the reduced relaxation of prestressing bar;
ε_c	– is the compressive concrete strain;
ε_c^{tot}	– is the top fiber strain of the cross-section;
ε_{cs}, ε_{sh}	– is the shrinkage strain of concrete;

ε_p – is the strain in prestressing bar;

$\varepsilon_{p.dec}$ – is the strain in prestressing bar due to decompression;

$\dot{\varepsilon}$ – is the strain of composite element;

ε_1 – is the strain of spring;

ε_2 – is the strain of dash-pot;

ε_0 – is the instantaneous strain at the level of the reference axis at the time of prestress transfer;

η – is the viscous constant;

η_0 – is the Newtonian viscosity;

μ – is the coefficient of friction between the tendons and their ducts;

ρ_{1000} – is the value of relaxation loss (in %), at 1000 hours after tensioning and at a mean temperature of 20 °C;

σ – is the stress;

σ_c – is the compressive concrete stress;

$\sigma_{c.ext}$ – is the tensile stress in concrete at the centroid of the prestressing bar;

$\sigma_{c.QP}$ – is the stress in concrete at the centroid of the prestressing bar due to self-weight, initial prestress and other quasi-permanent live loads;

σ_p – is the stress in prestressing bar;

σ_{p0} – is the initial tendon stress for relaxation;

σ_{pi} – is the maximum tensile stress applied to the tendon minus the immediate losses occurred during the stressing process;

$\sigma_{pm.0}$ – is the initial stress in the prestressing bar immediately after transfer after the instantaneous (short-term) losses;

σ_ξ – is the average value of stress fulfilling Volterra‘s integral term;

σ_1 – is the stress of the spring;

σ_2 – is the stress of the dash-pot;

φ, φ_c – is the creep coefficient of concrete;

φ_p – is the relaxation coefficient of prestressing bar;

χ, χ_c – is the aging coefficient of concrete;

χ_p – is the aging coefficient of prestressing bar;

$\psi(t)$ – is the creep function.

Abbreviations

AAEMM	– age-adjusted effective moduli method;
ASSA	– average stress-strain approach;
AFRP	– aramid fiber reinforced polymer;
BFRP	– basalt fiber reinforced polymer;
CFRP	– carbon fiber reinforced polymer;
EMM	– effective moduli method;
FRP	– fiber reinforced polymer;
GFRP	– glass fiber reinforced polymer;
GM	– general method;
HSE	– health and safety environment;
LVDT	– linear variable displacement transducer;
RC	– reinforced concrete;
PC	– prestressed concrete;
ULS	– ultimate limit state;
SLS	– serviceability limit state;
QA	– quality assurance.

Contents

INTRODUCTION 1
Problem Formulation 1
Relevence of the Thesis 3
Object of the Research 4
Aim of the Thesis 4
Tasks of the Thesis 4
Research Methodology 5
Scientific Novelty of the Thesis 5
Pratical Value of the Research Findings 5
The Defended Statements 6
Approval of the Research Findings 6
Structure of the Dissertation 7
Acknowledgments 7

1. REVIEW OF THE PHYSICAL MODELS AND STRUCTURAL TYPES OF VISCOELASTIC MATERIALS 9
1.1. Prestressed Concrete for Structural Applications 10
1.2. Fiber Reinforced Polymer Composites for Structural Applications 14
1.2.1. Status Quo on the Development of Fiber Reinforced Polymers 16
1.2.2. Research on Fiber Reinforced Polymers Properties 18
1.2.3. Research on Prestressed Concrete Structures with Fiber Reinforced Polymer bars 19

1.2.4. Rheological Models of Viscoelastic Materials 20
1.3. Effects in Aging Linearly Viscoelastic Materials..... 23
1.4. Deflection Control..... 37
1.5. Cracking Control..... 39
1.6. Conclusions of Chapter 1 and Formulation of the Thesis Objectives 41

2. ASSESSMENT OF PRESTRESS LOSSES AND SERVICEABILITY OF FLEXURAL PRESTRESSED CONCRETE MEMBERS 43
2.1. Approximation of Relaxation Curve 44
2.2. Losses of Prestress Model by Means of Consewutive Phases..... 46
2.2.1. General Assumptions and Basic Principles..... 46
2.2.2. Calculation Algorithm..... 58
2.3. Analysis of Serviceability Behaviour..... 59
2.3.1. Proposal for Deflection Analysis 59
2.3.2. Proposal for Calculation of Crack Width..... 61
2.4. Conclusions of Chapter 2 63

3. COMPARISON BETWEEN ANALYTICAL AND EXPERIMENTAL RESULTS OF PRESTRESSED ELEMENTS..... 65
3.1. Experimental Test of Basalt Fiber Reinforced Polymers Anchorage..... 66
3.2. Experimental Test of Prestressed Concrete beams..... 67
3.2.1. Jacking Setup..... 68
3.2.2. Beam Specimens 69
3.2.3. Experimental Test Scheme..... 72
3.2.4. Discussion of the Test Results..... 73
3.3. Experimental Test of Stress Relaxation of Basalt Fiber Reinforced Polymer Bars..... 79
3.3.1. Experimental Program of Testing Bars 79
3.3.2. Test Specimens..... 81
3.3.3. Instrumentation..... 81
3.3.4. Results of the Experimental Work..... 83
3.4. Validation of Theoretical Predictions..... 86
3.4.1. Prestress Losses..... 86
3.4.2. Load-Deflection Response 90
3.4.3. Cracking Control 92
3.5. Conclusions of Chapter 3 95

GENERAL CONCLUSIONS 97

REFERENCES 99

LIST OF SCIENTIFIC PUBLICATIONS BY THE AUTHOR ON THE TOPIC OF THE DISSERTATION 109

SUMMARY IN LITHUANIAN 111

ANNEXES[1] 127
Annex A. Declaration of Academic Integrity..... 128
Annex B. The Co-Authors' Agreements to Present Publications Material in the Dissertation 129
Annex C. Copies of the Scientific Publications by the Author on the Topic of the Dissertation..... 133

[1]The annexes are supplied in the enclosed compact disc.

Introduction

Problem Formulation

European languages use the word *"carcass"* and pan-American refer to the *"skeleton"* of a building or structure upon which a living body is hung and integrated. Early development of structural materials started from materials resisting compression, starting with stones and bricks, then developing into concrete and more recently high-strength concrete. For materials resisting tension, people used bamboo and ropes, then iron bars and steel, then high-strength steel. Later, materials resisting both tension and compression, namely, bending were employed. Timber was utilized, then structural steel, reinforced concrete (RC) and finally prestressed concrete (PC) was developed.

In general, more concrete is produced than any other construction material in the world. There is no other material that could be used in lieu concrete to meet our demand for living infrastructure. PC, on the other hand, combines high-strength concrete and high-strength reinforcement in an "active" manner. This is achieved by prestressing reinforcement and keeping it against the concrete, thus putting the concrete into compression. This active combination results in a much better behavior of the two structural materials.

The historical development of prestressed concrete started in a different manner when prestressing was only intended to create permanent compression in

concrete to improve its tensile strength. Later it became clear that prestressing the reinforcement steel was also essential to the efficient utilization of high-tensile reinforcement.

It is a well-established fact that the initial prestressing force applied to the concrete element undergoes a progressive process of reduction over a period of the design life. Consequently, it is important to determine the level of the prestressing force at each loading stage, from the stage of transfer of the prestressing force to the concrete to the various stages of prestressing available at service load, up to the ultimate limit state (ULS). Essentially, the reduction in the prestressing force appears due to instantaneous (short-term) losses during the fabrication or construction process and time-dependent (long-term) losses such as creep, shrinkage and stress relaxation of reinforcement.

However, even concrete member is prestressed, corrosion of reinforcement is still most frequent and most serious form of degradation of the concrete structure and leads to excessive maintenance costs of the remaining design life of the structures. Concrete structures may also experience heating/cooling, freezing and wetting/drying cycles, which also promote concrete decay and subsequent steel corrosion. Non-metallic composite materials such as basalt fiber reinforced polymers (BFRP) posse attractive long-range potential because they are non-corrodible, non–magnetic and might be less sensitive to the environment of high temperatures. Mechanical properties of the basalt fiber polymers generally depend on the source of the basalt rock and the production process. Basalt fibers have high fire resistance and are much cheaper than the rest of the structural composites.

Unlike other construction materials, standard test methods have yet to be established for BFRP materials to determine constitutive properties regarding practical use. In case of prestress force, estimation of the prestress losses over the time requires that stress relaxation be known, but none of the codes provide significant information to determine it. The mechanical properties, in turn, must be clearly specified in the design codes. Until this task is complete, an interim work shall be keenly aware of the discrepancies that may exist between experimental test data and design code provisions. Engineering judgment is paramount in assessing and applying technical information regarding the performance and behavior of PC members with BFRP reinforcement.

The present research is focused on the complete analysis of PC flexural members reinforced with BFRP bars considering stress relaxation phenomena of BFRP and various initial prestress. An eye on details throughout the unique and innovative experimental work confirms expected serviceability behavior to be applicable in practice.

Relevance of the Thesis

Emerging breakthroughs in civil engineering suggest that concrete could be a part of the solution when it comes to planning for a sustainable development that encompasses economic growth and industrial progress while minimizing the ecological issues. Thus, RC and PC play a key role in meeting the demand for convenient infrastructure for the growing population, and thus its sustainability is of utmost importance. In the case of structural engineering, practicing engineers can choose either between traditional design code methods, analytical and numerical techniques or experimental work in order to analyze PC flexural members. Although design code methods ensure safe design, do not reveal the actual post cracking stress-strain behavior of the cross section and often lack physical interpretation in particular to FRP materials. Most of the research has focused on PC members with conventional steel reinforcement and research on PC flexural members reinforced with new type composites, such as BFRP, are scarce in the literature.

Stress relaxation of BFRP reinforcement, creep and shrinkage cause instantaneous (short-term) and time-dependent (long-term) deformations in PC structures. While it is generally accepted that the prestressing force and its losses do not affect the ultimate strength of PC member, a reasonably accurate prediction of the prestress losses is important to serviceability performance. If prestress losses are underestimated, and the limit of the tensile strength of concrete is reached it might cause much larger deflections than expected. On the other hand, if prestress losses are overestimated it could cause to greater camber (upward deflection) as well as unexpected cracking due to prestress.

Until today, the errors in predicting the exact prestress losses can be due to inaccuracy in the estimation of short-term and long-term material characteristics: stress relaxation of prestressing reinforcement, creep and shrinkage of concrete and inaccuracy of the method of analysis employed. The precise and adequate estimation of prestress losses leads to realistic effective prestressing as well as cracking and deformation analysis of PC flexural members. Within this study, analytical methods are proposed combining effects of creep and shrinkage of the concrete and stress relaxation of BFRP, deflections and cracking considered as an interrelated process. Experimental program and analytical calculations are performed in order to prove the reasonable accuracy of the results.

Speaking in general, PC members do require more care in design, construction, and erection than those of ordinary RC due to of the higher strength, smaller section, and sometimes delicate design features involved. The basic desirability of PC is almost self-evident, but its widespread application will be advanced by engineers' acquaintance with its principles and practice and further development

of new cost-effective composite materials such as BFRP, design, and construction.

Object of the Research

The object of present research is the influence of prestress level, and stress relaxation behavior of basalt fiber reinforced polymer (BFRP) bars to the flexural behavior of prestressed concrete members.

Aim of the Thesis

The aim of the thesis is to propose new analytical methods for the prediction of stress relaxation of BFRP and effective prestress that directly influence the deflections and cracking of PC flexural beams.

Tasks of the Thesis

To achieve the aim of the thesis, the following tasks have to be solved:

1. To review empirical and analytical methods for estimation of prestress losses as well as mathematical (mechanical) models with the emphasis on the viscoelastic (stress relaxation of BFRP reinforcement, creep and shrinkage of concrete) behavior.
2. To develop an analytical method for estimation of prestress losses by means of relaxation behavior and mechanical properties of BFRP.
3. To develop analytical methods for deflection and cracking analysis of flexural PC beams with BFRP reinforcement.
4. To perform a new experimental investigation on stress relaxation of BFRP reinforcement specimens in particular to a different level of prestress.
5. To perform an experimental investigation on a deflection and cracking of real scale flexural PC beams with different level of prestress under static four-point bending tests.
6. To evaluate analysis of the adequacy of developed analytical methods for deflections and cracking in comparison with the obtained experimental results.

Research Methodology

In order to achieve the aim of the thesis, qualitative research based on the theoretical continuum mechanics, analytical and experimental methods were performed. Evaluation of stress relaxation behavior of BFRP based on the differential equation of the process of deformation and approximation of stress relaxation function based on Maxwell's rheological model is proposed. The calculation method for prestress losses due to stress relaxation of BFRP is based on analysis of the issues related to stress-strain state methods among RC and PC. Regarding unique experimental program, stress relaxation rates for BFRP were observed based on stress relaxation functions. Also, an experimental program was expanded with the purpose to evaluate the influence of prestress level for flexural stiffness of the real scale concrete beams prestressed with BFRP bars.

Scientific Novelty of the Thesis

1. A new calculation method for estimation of prestress losses based on stress relaxation behavior of basalt fiber reinforced polymer (BFRP) bars, has been proposed.
2. As an alternative to the existing empirical methods in the design codes, new calculation methods for the determination of the deflections and cracking have been proposed.
3. Innovative experimental method for stress relaxation of BFRP has been proposed.
4. New experimental data on stress relaxation of BFRP bars are obtained.
5. New experimental results of concrete beams prestressed with BFRP bars under static short-term loading are obtained.

Practical Value of the Research Findings

In the present research a proposed analytical method for prestress losses estimation considering stress relaxation behavior of BFRP and certain consecutive phases of loading that cause degradation of initial prestress force. Also, calculation methods regarding deflection and cracking analysis of concrete beams prestressed with BFRP bars. Unique equipment capable of keeping constant strain

over relaxation time and stress relaxation test is proposed. The experimental program allows to investigate stress relaxation of BFRP reinforcement under several prestress levels. Based on experimental results, the stress relaxation coefficient for BFRP bars depending on prestress level is proposed. Experimental results shall be used by practicing engineers to use innovative composite materials as reinforcement for future PC structures.

The Defended Statements

1. The proposed calculation method of prestress losses based on stress relaxation of basalt fiber reinforced polymers (BFRP) adequately estimates the effective prestress force.
2. Stress relaxation rate (%) of BFRP bars is varying value and proportionally increases due to an immediate increase of initial prestress.
3. Calculation methods for deflection and cracking analysis based on decompression effect and stress relaxation of BFRP approach adequately assess serviceability limit state with respect to the concept of PC structures.

Approval of the Research Findings

The results of this dissertation have been published in 9 publications, 3 among them in the journals with an Impact Factor and 1 in the conference proceedings referred by the *Clarivate Analytics Web of Science*. The major results of the research presented in this dissertation have been reported by 5 presentations at the following 5 scientific conferences in Lithuania and abroad:

- 17th Conference of Lithuanian Young Scientists Science – *Future of Lithuania. A thematic conference „Civil Engineering*, Vilnius, Lithuania, 2014;
- 18th International Conference on *Composite Structures (ICCS 18)*, Lisbon, Portugal, 2015;
- 19th International Conference on *Composite Structures (ICCS 19)*, Porto, Portugal, 2016;
- 12th International Conference *Modern Building Materials, Structures and Techniques*, Vilnius, Lithuania, 2016;

– 3rd International Conference on *Mechanics of Composites (MECHCOMP3)*, Bologna, Italy, 2017.

Structure of the Dissertation

The dissertation consists of an introduction, three chapters, general conclusions, list of the references (135 publications), list of 9 scientific publications, published by the author on the research topic, summary in Lithuanian and three annexes. Dissertation consists of 126 pages, the text contains 61 pictures and 19 tables.

Acknowledgments

Peform Ph.D. research is a long and challenging endeavour, but the people I have met and contributed with along the way have made it great experience I will always cherish. I will remember the plentiful trips I took around the world to ex-ceptional research facilities and locations ranging from Lisbon, Cambridge to the City of New York. First and foremost, the author expresses his great appreciation to his supervisor Prof. Dr Juozas Valivonis, the Head of the Department of Reinforced Concrete Struc-tures and Geotechnics for providing the guidance, knowledge, and motivation over this research work. Numerous innovative experiments which were vital to disclose the nature of the phenomenas in the investigation would have not happe-ned without his leadership.

In particular, I would like to express my deepest gratitude to Prof. Dr Algirdas Jonas Notkus, Assoc Prof. Dr Bronius Jonaitis, Prof. Dr Charles Dolan, Prof. Dr Oral Büyüköztürk, Prof. Dr Vytautas Vaičaitis for significant support improving the quality of the dissertation. I am thankful to Dr Aidas Jokūbaitis for his willingness to help during the experimental works. Also, I would like to thank all of my collaborators at Vilnius Gediminas Technical University. This includes Assoc Prof. Dr Arnolas Šneideris, who always made a vast effort to ensure I had the necessary literature resources for completing my research work.

Lastly, I would like to thank my family for love and encouragement. And most of all for my loving, supportive, encouraging, and patient wife Eglė whose faithful support during all stages of this Ph.D. is utmost appreciated. Thank you.

The research presented was funded by Grant No. 09.3.3-LMT-K-712-04-0118 from the Lithuanian Science Council and covered by the European Union Structural Funds.

1

Review of the Physical models and Structural Types of Viscoelastic Materials

The first chapter presents a review of physical and mechanical properties of composite materials among those Basalt fiber reinforced polymers (BFRPs) posse attractive long-range potential as the reinforcement for PC structures. From this standpoint, BFRP is defined as viscoelastic material based on fundamentals of rheology. It is assumed that readers are already acquainted with PC principles that would help to understand the complexity of the issues related to flexural members from initial prestress application over the static loading process. Also, common and new methods for analysis of stress-strain, prestress losses, serviceability limit state (deflections and cracking) of flexural PC members are explained in detail. Throughout this chapter, photographs of significant structures designed and constructed in prestressed concrete using this fundamental concept are shown. Also, this chapter formulates the main objective and the tasks of the present research work. The review was partly presented in the articles published by Atutis (2010a), Atutis & Valivonis (2010b), Atutis *et al.* (2011), Atutis *et al.* (2013a), Atutis *et al.* (2013b), Atutis *et al.* (2015), Atutis *et al.* (2018a) and Atutis *et al.* (2018b).

1.1. Prestressed Concrete for Structural Applications

Prestressing has been revolutionary development, first as a material, but more importantly as a concept. As a concept, prestressing is valid and applicable practically to all structural materials.

Currently, a growing industry requires to use optimized and affordable engineering materials and methods for sustainable construction. Due to great compressive strength properties concrete is still very competitive among structural materials and have been successfully applied for construction engineering and other fields: energy (oil product storage units, gas pipelines and risers, gasholders, liquefied natural gas and terminals) and marine (cargo wharves, petroleum terminals, offshore platforms, piers, quays, jetties, dolphins, fender systems, bulkheads, floating barges and dry docks, etc.) infrastructure (FIP 1978, FIP 1982, Creazza *et al.* 1991, Gerwick 1992, Tsinker 1995, Tsinker 1997, Gaythwaite 2004, McConnell *et al.* 2004, DNV 2012, Meiswinkel *et. al*. 2013, Gaythwaite 2016, Ghali 2017) and transport sector (Meier 1987, Harding *et al.* 2010; Notkus 2010; Bhatt 2011; Kim 2014; Jokūbaitis *et. al.* 2016) (Fig. 1.1). The specifics of the environment of such an infrastructure requires of concrete to compete with high durability and quality requirements. The resistance of aggressive environmental conditions effects long-term maintenance of the infrastructure.

Regarding the energy industry by means of oil storage infrastructure, it often contains anaerobic bacterias which generate sulfides upon contact with seawater. In contact with oxygen, they convert to weak sulfuric acid, which can attack the surface of the concrete. Industry experts (FIP 1978, Gerwick 1992) indicate that if air is present over the crude oil, epoxy coating is warranted in the above-oil zones. The hydrogen sulfides (hereinafter – H_2S) and sulfuric acids (hereinafter – H_2SO_4) which may, however, cause corrosion of steel reinforcement and embedment details, refined products, such as gasoline, may be aggressive.

Marine structures rank among the foremost applications of concrete. It was early recognized as the optimal material for harbor and marine structures because it combines durability, strength, and economy. Considering that concrete is immersed in seawater, a chemical attack on the concrete is maximized, i. e. reactivity between alkali in cement, and reactive aggregates might be increased by accelerating corrosion of conventional steel. The most serious aggressive element is chlorides, carried to the concrete surface by the splash of seawater. In order to resist environmental conditions mentioned above durability of concrete undertakes a key performance role (Tsinker 1995; Tsinker 1997, Gaythwaite 2004, Gaythwaite 2016; Ghali 2017).

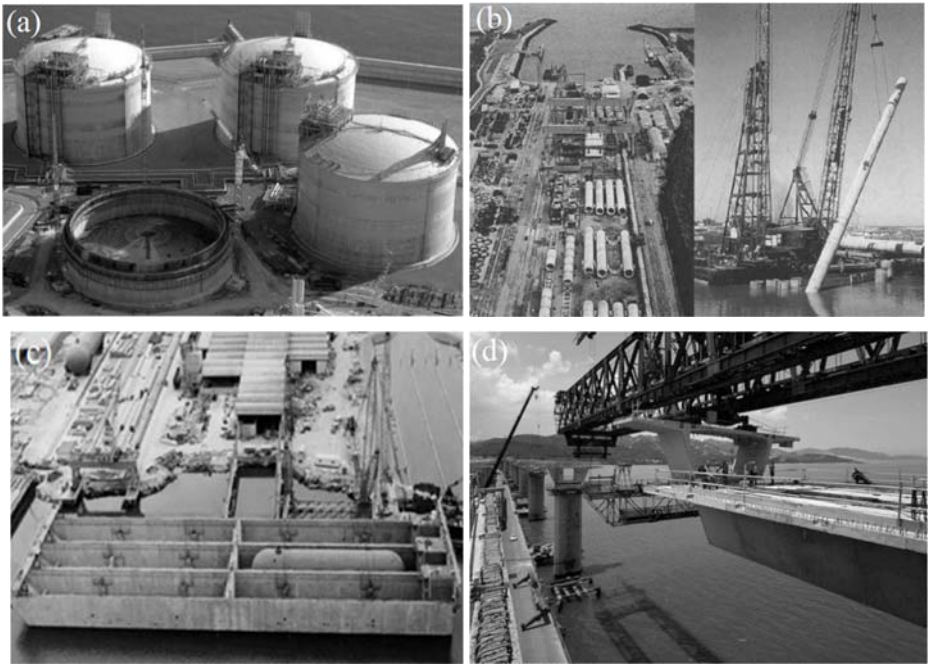

Fig. 1.1. Potential employment of prestressed concrete for: liquid storage tanks (Ghali 2017) (a); port deep piles (Tsinker 1997) (b); floating barge units (Gerwick 1992) (c); long-span bridges (Bhatt 2011) (d)

Lack of resistance of an aggressive environment can lead to unexpected cracking, corrosion of reinforcement, larger deformations, deflections, and failure of concrete structure (Leonhardt 1977). Thus, prestressed reinforcement can be used in order to prevent from cracking and to minimize the penetration of the air and water.

Also, PC has been shown excellent cryogenic properties at low temperatures, i. e. –160 ^{o}C (FIP 1982). However, even concrete member is prestressed, corrosion of reinforcement is still most frequent and most serious form of degradation of the concrete structure and can lead to necessary repair works and additional costs of the remaining operation time. In some cases, heating/cooling, freezing and wetting/drying cycles, can extremely impact concrete structures by causing corrosion of the reinforcement. Such mentioned consequences above provoked a considerable amount of research in order to find practible means of employing new composite materials such as fiber reinforced polymers (FRPs) (Abdelrahman *et al.* 1997, Sen *et al.* 1998, Lees *et al.* 1999, Torres *et al.* 2013, Atutis *et al.* 2015). Composite materials such as FRPs posse attractive potential due to good corrosion

resistance, mechanical properties and consequently are less sensitive to high temperatures, prestress losses than steel reinforcement (DNV2012). Thus, FRP could be a great alternative to conventional reinforcement. It was noticed that further research is required in order to evaluate the short-term and long-term properties. It is utmost important to ensure safe and optimum use of FRP materials in order to fulfill the requirements of the ultimate and serviceability limit states of prestressed concrete structures.

The main prestressing methods of FRP reinforcement were investigated by previous researchers (Fig. 1.2): 1) Stretching of the bars at bulkheads (prestressing bed) (Triantafillou et al. 1992; Meier 1995; Garden *et al.* 1998; Rosenboom *et al.* 2005; Abhijit *et al.* 2009; Diab *et al.* 2009; Atutis *et al.* 2015). In this case, FRP is being prestressed by hydraulic jacking system between external reaction frames (see Fig. 1.2a). Once the curing time of the epoxy adhesive is completed (ideal adhesive bond between FRP and concrete surface) prestressing force is transferred by releasing FRP reinforcement from external reaction frames (see Fig. 1.2b). In practice, such system can be used for in situ or precast concrete members where FRP plates or bars could be used as the reinforcement; 2) cambered-jacked beams (El-Hacha *et al.* 2001; Triantafillou *et al.* 1991). Regarding this method, beams are prestressed by FRP plate by means of cambering it to the upward direction, bonding the FRP reinforcement at the bottom (in tension zone). Jacking force is removed once the epoxy curing is completed (Fig. 1.2c). Practically, this system is applied to precast concrete structures for the strengthening purposes; 3) strengthening of existing beams by external prestress (Valivonis et al. 1995; Buyukozturk *et al.* 1998; Wight *et al.* 2001; El-Hacha *et al*. 2003; Kim *et al.* 2007; Woo *et al.* 2008; Yang *et al.* 2009; Pallegrino *et al.* 2009; Xue *et al*. 2010; Zhuo *et al.* 2009) (see Fig. 1.2d, e). This method is analogous to the conventional system by means of post-tensioning of unbonded FRP bars, and prestressing is transferred directly to the concrete member by pulling the anchor at one end, while the next one is fixed. In regard to installation matters, this system is complicated in order to strengthen existing structures with limited access to the supports (Fig. 1.2d).

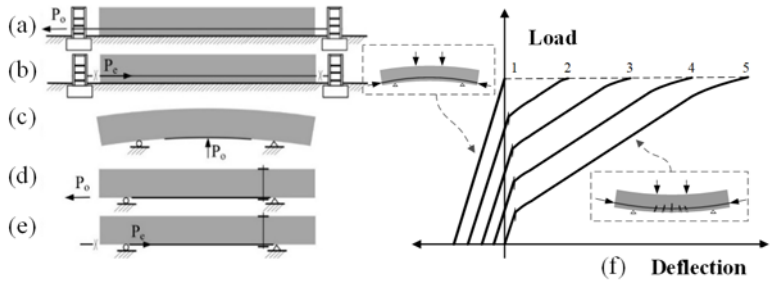

Fig. 1.2. Schematic principles of prestress: prestressing methods (a)–(e); Load-deflection relationship based on variation prestress level (f) (Marčiukaitis 2012)

Prestressing force effect has the influence of the stiffness of flexural member, but once the external load is applied to the member, it is very important to investigate the reduction of the prestressing force at any state of flexural behavior. Depending on prestress level, deformation and failure modes are different in comparison with non–prestressed member while the mechanical characteristics of the beams are uniform.

Consequently, diverse deflection represents diverse resultant of stress in reinforcement (Fig. 1.2e). Load-deflection diagram "1" shows that reinforcement observes the most of stress resultant and the beam is failed due to the elimination of the camber by the concrete stresses. In case of over reinforced cross-section, failure occurs due to the crushing of the concrete and non-effective use of the tensile strength of the reinforcement. By the increase of prestressing force value, the stresses of the concrete retake initial value by developing a certain deflection due to the appearance of the cracking. Further, the less stress of the reinforcement is contained (in case of less amount of reinforcement) the larger cracking and deflections are developed up to the failure. Once the concrete and reinforcement observe limit stress, the behavior of diagrams "3" and "4" show, that the failure of the beam can occur. According to the behavior of load – deflection diagram "5" where prestress level is equal to zero, the development of cracking and deflections reflects to the similar manner as in conventional RC.

From an economics point of view, Balafas *et al.* (2012) performed analysis method in order to predict optimal design and hence initial costs, of the RC and PC beams with FRP. A unique comparison of different alternative designs was drawn through a diagram of depth d plotted against flexural bar area A_p which allowed to identify ways in which FRP can be used at minimum cost, and to consider why FRPs are rarely used in practice. The diagrams (Figs. 1.3–1.4) were build up considering most of the governing constraints: ultimate strength conditions; deflection conditions; cost function and etc.

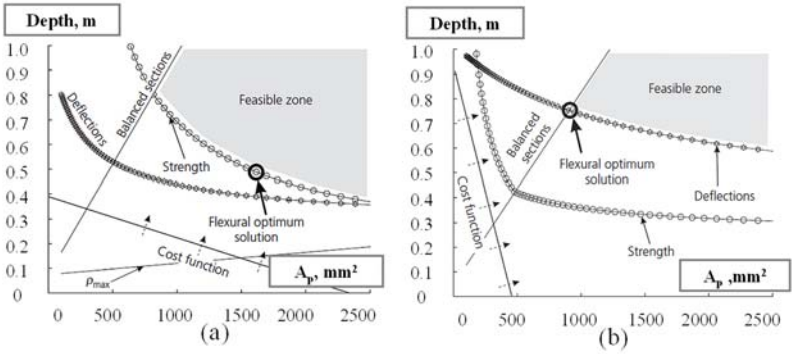

Fig. 1.3. Reinforced concrete beam with: steel rebar (a); fiber reinforced polymer rebar (b) (Balafas *et al.* 2012)

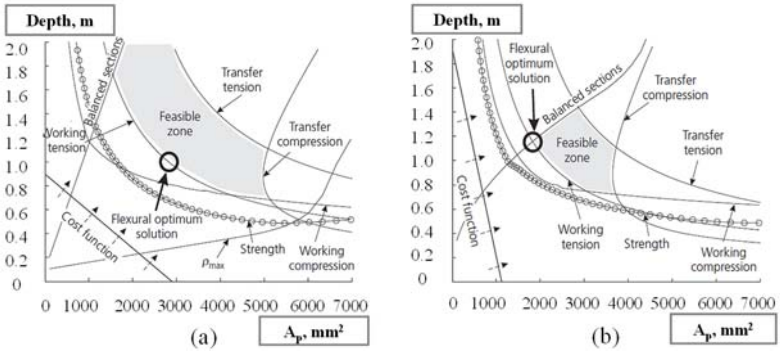

Fig. 1.4. Prestressed concrete beam with: steel tendon (a); fiber reinforced polymer tendon (b) (Balafas *et al.* 2012)

Considering RC beams, it is clear that steel is much cheaper (per unit volume) than FRP, so the constant cost line is much flatter (Fig. 1.3a, b). Beams with FRP need to be significantly deeper than with steel in order to comply with deflection conditions, but the amount of reinforcement required is less because of the tensile strength of the rebar. Comparison of the two plots for PC beams yields to conclusions that differ from those for RC sections (Fig 1.4). The optimum depth for both sections similar, which is logical given that prestressing allows the concrete to carry the load. Less material is needed for prestressing with FRP because those tendons are generally stronger, while the ultimate strength of the tendon enters by way of the balanced section criteria (Fig. 1.4b). In contrast to prestressed flexural elements, PC ought to be a logical application for FRP.

1.2. Fiber Reinforced Polymer Composites for Structural Applications

In general, considerable corrosion of RC and PC members accelerated the research on non-metallic materials like FRPs for structural applications as non-corrosive reinforcement (ACI 2004, ISIS 2008). FRP reinforcements are manufactured from thousands of small organic or inorganic fibers that are embedded in a polymer matrix (Fig. 1.5).

Because manufacturers vary the production process, there can be considerable variance in strength, even within the same brand of the composite. High strength fibers of FRPs can be made of glass, aramid, carbon and other polymers with a volumetric fiber ratio of 60–65%. Matrix resin is usually epoxy. FRP reinforcement is transversely anisotropic with the longitudinal axis being the strong axis.

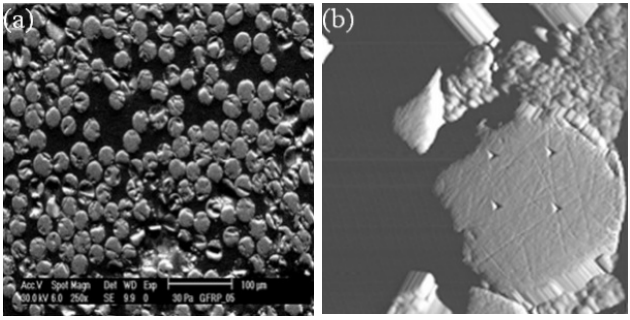

Fig. 1.5. Fiber and matrix distribution: over the domestic rebar cross-section (Sovják 2012) (a); incisions in fiber from the nanoindentation tip (Fornůsek *et al.* 2009) (b)

Moreover, the properties are affected by loading history and duration as well as environmental conditions. These factors are interdependent and, consequently, it is difficult to determine the effect of each one in isolation while the others are kept constant.

The surface texture of the FRP may range considerably between the different FRP products commercially available, for example, sand-coated surface, etc. Some examples of different surface textures are shown in Figure 1.6. The surface texture roughness is manufactured in such way that good bond between the concrete and FRP would be obtained. From this standpoint, FRP reinforcing bars can be configured in bars, rods, plates, and strands. Unlike traditional steel bars, there are no typical and standardized shape or surface configuration, the orientation of fiber and proportions among fiber and resin products. Moreover, there are no standard methods of FRP production (pultrusion, winding). Regarding FRP bars, there are various types of a cross-section such as round, solid, hollow, and square.

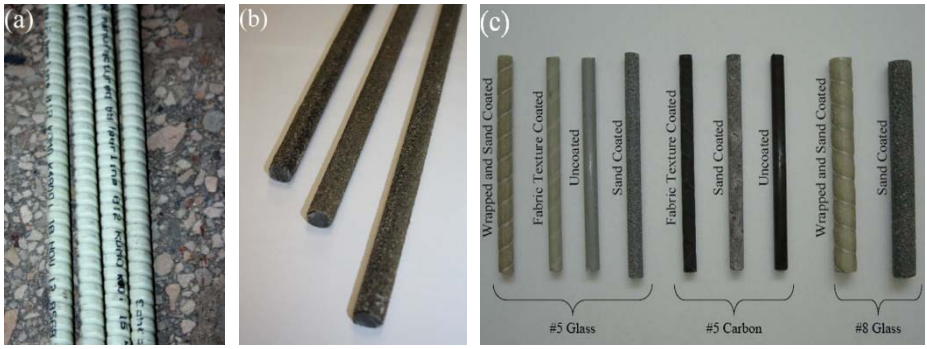

Fig. 1.6. Composite reinforcing bars: ribbed glass composite bars (Atutis *et al*. 2015) (a); sand coated basalt composite bars (Atutis *et al.* 2018) (b); various samples of glass and carbon composite bars (Fico 2004) (c)

1.2.1. Status Quo on the Development of Fiber Reinforced Polymers

In regard to the type of FRP, mainly three types of fibers were used for FRP reinforcement in concrete construction: glass (GFRP), carbon (CFRP) and aramid (AFRP). The physical and mechanical properties vary considerably between the different fiber types and may vary significantly for a given type of fiber as well. Some typical properties are given in Table 1.1.

The use of basalt FRP (BFRP) reinforcement is currently in the top research and development phase of composites (Wang *et al*. 2013, Wang *et al*. 2014a, Wang *et al*. 2014b, Wang *et al*. 2016a, Wang *et al*. 2016b, Atutis *et al*. 2018). The raw of basalt is a volcanic rock, and crushed stone melted at 1400-1500^{0}C and turned to the fibers. Mechanical properties of basalt fibers are very close or even better than remaining fibers (aramid, carbon, glass, etc.) (Kostikov 1995, Zoghi 2014). Properties of the basalt fiber generally depend on the source and the type of the basalt rock and the method of production. Basalt fibers have high-temperature resistance and are much cheaper than the rest of composite fibers (Bareišis *et al*. 2003, Kim 2014, Zoghi 2014). In particular, the price comparison of relevant composites is provided in Table 1.2.

BFRP is newly developed for application in civil infrastructure as a structural reinforcement material, displaying approximately 20% higher strength and modulus, similar cost, and more chemical stability compared to GFRP and a wider range of working temperatures and much lower cost than CFRP (Sim *et al.* 2005). Due to the lack of studies, the application of BFRP faces low utilization.

Table 1.1. Typical properties of fiber reinforced polymers and prestressing steel

Fiber type	Tensile strength, MPa	Moduli of elasticity, GPa	Ultimate strain	Density, kg/m^3	∅, mm	Author
Glass	1418	60.2	0.0236	2500	14.55	Atutis *et al.* (2015)
Carbon	2250	147	0.0157	1900	8.00	Abdelrahman *et al.* (1997)
Aramid	1330	80	0.0405	1250	15.00	Toutanji *et al.* (1999)
Basalt	1098	45	0.0246	2500	12.45	Atutis *et al.* (2017)
Steel (B500A)	525	200	0.0250	7850	n/a	CEN (2004)
Steel (Y1030)	830	205	0.0400	7850	n/a	CEN (2004)

Table 1.2. Material costs

Material	€/m³	€/kN/m (€ per m)	Reference
Concrete	$48 \cdot 145 e^{0.0178 f_{cm}}$		Balafas (2012)
Steel bar		0.015	Balafas (2012)
Steel tendon		0.012	Balafas (2012)
BFRP[a]		(0.75)	Galen
CFRP (CARBOPREE)[a]		(7.60)	Sireg SpA
CFRP (ARAPREE)[a]		(9.80)	Sireg SpA
GFRP		0.010	Balafas (2012)
FiBRA		0.055	Balafas (2012)

[a] personal communication

Thus, a comprehensive understanding of the creep and relaxation behavior of BFRP under prestress is critical for the application of BFRP as prestressing reinforcement and enhancing its utilization efficiency in construction.

In case of components, the polymer matrix of an FRP material consists of a resin binder and normally some fillers and additives. Primarily, the matrix has to bind the fibers together, provide lateral support to the fibers, protect the fibers from their surroundings and may beneficially influence some FRP material properties. Polymer matrix materials are highly viscoelastic. Upon loading, they exhibit elastic deformations, while under constant load, slow viscous deformations occur. At increased temperature, long-term loading, their response tends to be more ductile, while low temperature results in a rigid and brittle behavior.

Epoxy resins are more expensive than polyesters and vinyl esters but are largely used in high-performance composites as they have the best mechanical properties, adhesion properties and excellent resistance to chemicals. Some typical properties of polymer matrices are given in Table 1.3 below.

For structural fiber composites, among which FRP reinforcement for concrete, unsaturated polyester, vinyl ester, and epoxy are often used as the polymer binder. For these resins, polyesters are the most general purpose and frequently applied, given the good processability, fairly good properties, and low cost.

Table 1.3. Typical properties of resins (Triantafillou 1992)

Resin type	Tensile Strength, MPa	Modulus of elasticity, GPa	Density, kg/m³	Cure shrinkage
Polyester	35–104	2.1–3.5	1100–1400	0.05–0.12
Vinyl ester	73–81	3.0–3.5	1100–1300	0.05–0.10
Epoxy	55–130	2.8–4.1	1200–1300	0.01–0.05

Vinyl esters process essentially like polyesters but provide improved mechanical and chemical performance (Nanni *et al.* 1993).

1.2.2. Research on Fiber Reinforced Polymers Properties

In general, because the initial application of FRPs in civil infrastructure is the replacement of steel reinforcement in concrete structures under aggressive environment, the durability of FRP under high temperatures is of significant interest. Other composites like CFRP exhibits superior performance in resisting different corrosive effects, whereas the GFRP exhibits relatively weak resistance to alkali and acid (Wang *et al.* 2014). For the newly developed BFRP, fewer durability studies have been performed compared to other FRP composites.

Within the limited literature of the durability of BFRP, most of them emphasized alkali resistance and moisture absorption. Few studies investigated the degradation of BFRP sheets under seawater and analyzed the corrosion mechanism (Wei *et al.* 2011, Wu *et al.* 2014). Pearsosn *et al.* (2013) investigated that reduction of tensile strength of BFRP is equal or less in comparison with steel bars over long-term conditions. El Refai *et al.* (2013) observed good fatigue resistance of BFRP reinforcement. It was revealed in the previous studies (Wang *et al.* 2014) that BFRP sheets exhibited high resistance to salt corrosion. Among other corrosive environments, the degradation of BFRP bars shall still be further investigated.

Because the differences between FRP sheets and bars not only lies in the production technology but also in the matrix types (epoxy to vinyl ester), relevant forming temperatures and fiber volume fraction, those differences can impact the degradation behavior of BFRP under corrosive environments.

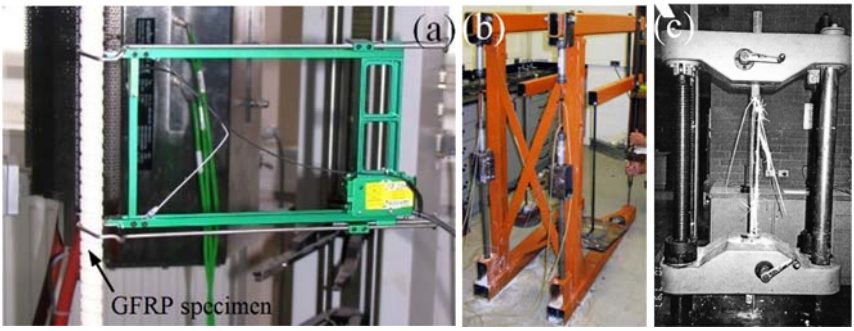

Fig. 1.7. Experimental testing equipment: tension – tension test of glass composite bar (Atutis *et al*. 2015) (a); creep test of basalt composite bar (Banibayat 2015) (b); tensile test setup for aramid fiber reinforced polymer bar (Zou 2003) (c)

Current studies emphasize the behavior of BFRP bars for prestressing applications in aggressive environment (Serbescu *et al.* 2014) and marine industry (Wang *et al.* 2014). Within the range of practical interest, Banibayat (2015) performed experimental creep test and defined relaxation function and coefficient based on logarithmic scale for time-dependent behavior of BFRP specimens (Fig. 1.7b):

$$r_{\mathrm{p}}(t) = 76 - 4.5\ln(t)\ ;\quad \varphi_{\mathrm{p}}(t) = 0.006\ln(t) + 0.045\ . \tag{1.1}$$

Shi *et al.* (2015) and Shi *et al.* (2016) performed creep and stress relaxation tests of BFRP tendons considering elimination of the impact of slippage at the anchor zone. The relaxation rates 4.2%, 5.3%, and 6.4% were estimated depending on initial prestress under 1000 hours tests.

1.2.3. Research on Prestressed Concrete Structures with Fiber Reinforced Polymer Bars

The most efficient way to use FRP is to apply it as a prestressed tension – only member rather than a normal reinforcement in concrete structures due to their relatively low modulus and high strength only in the longitudinal direction of fibers (Meier 1987, Wang *et al*. 2013, 2014). In prestressed structural members typically with prestressing levels of around 30–60 % of their tensile strength (f_{u}), creep, and relaxation behavior usually controls their applicability (ACI 2004). The high sustained load may cause large relaxation of prestressing force or even creep rupture of FRP materials. This phenomenon is different from the creep of steel reinforcement in reinforced concrete, which can only become dominant in the condition of extremely high temperatures (ACI 2004). Thus, the creep and relaxation behavior of FRP should be identified and creep rupture should be avoided when applying FRP for structural applications. However, for the typical types of FRP composites, namely glass, aramid and carbon, the creep rupture stress is limited to 0.2, 0.3 and 0.55 of their tensile strength, respectively (ACI 2006). This limitation leads to the fact that only CFRP can be used for prestressing, whereas GFRP and AFRP cannot be sufficiently used in prestressed application.

Previously, many researchers have investigated the short-term behaviour of concrete beams prestressed with either GFRP (Rubinsky 1958, Issa 1995, Gangarao and Vijay 1997, Noël and Soudki 2013, Noël and Soudki 2014, Atutis *et al.* 2015), CFRP (Arockiasamy *et al.* 1995, Abdelrahman *et al.* 1997, Fam *et al.* 1997, Abdelrahman *et al.* 1999, Park and Naaman 1999, Borosnyói 2002, Grace *et al.* 2003, Stanley and Soudki 2010, Xue *et al.* 2010, Heo *et al.* 2013, Grace *et al.* 2012, Grace *et al.* 2013) or AFRP (Nanni *et al.* 1992, Sen *et al*. 1998, Lees *et al.* 1999, Sen *et al*. 1999, Zou 2003a) (Fig. 1.8).

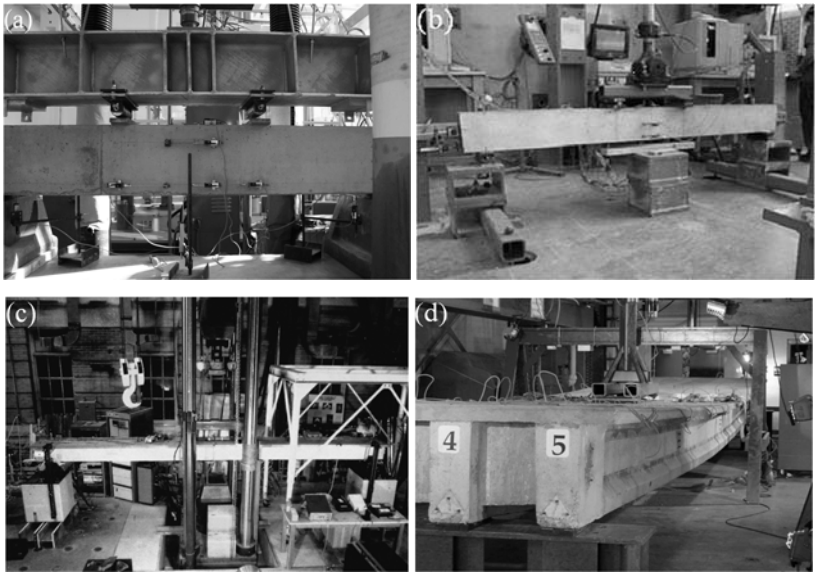

Fig. 1.8. Experimental works of prestressed concrete members with: glass composites (Atutis *et al*. 2015) (a); carbon composites (Mertol *et al.* 2007) (b); carbon composites (Abdelrahman *et al.* 1999) (c); bridge model with carbon composites (Grace *et al.* 2013) (d)

In case of long-term behavior, much less experimental research was carried out (Bryan *et al.* 1996, Zou 2003b, Karbhari *et al.* 2007) with regard to the analysis of serviceability and resistance of aggressive environmental conditions.

1.2.4. Rheological Models of Viscoelastic Materials

Based on rheology it is possible to consider the phenomenological approach of developing a constitutive model for linear *viscoelasticity*. Steel at elevated temperatures, concrete, and polymers are examples of viscoelastic behavior (Reddy 2013). The mathematical models of the viscoelastic constitutive behavior help enginers analytically or numerically determine the mechanical system response. Viscoelastic materials have a time-dependent stress response and even may have permanent deformation. The viscoelastic response characteristics of a material are determined often using creep or stress relaxation tests and dynamic response to loads varying sinusoidally with time. The creep test involves determining the strain response under constant stress, and it is done under uniaxial tensile stress owing to its simplicity. Application of a constant stress σ_0 produces a strain that, in general, contains three components: 1) an instantaneous; 2) plastic; and 3) delayed reversible components:

$$\varepsilon(t)=\left[J_{\infty}+\frac{t}{\eta_0}+\psi(t)\right]\sigma_0\,;\;\; \sigma(t)=\left[E_0+r_{\mathrm{p}}(t)\right]\varepsilon_0\,, \tag{1.2}$$

where $J_{\infty}\sigma_0$ is the instantaneous component of strain; η_0 is the Newtonian viscosity of the composite material; and $\psi(t)$ is the creep function. The relaxation test involves the determination of stress under constant strain. Application of a constant strain ε_0 produces stress that contains two components: E_0 is the static elastic modulus; and $r_{\mathrm{p}}(t)$ is the relaxation function.

A qualitative understanding of the actual viscoelastic behavior of materials can be gained through spring-and-dashpot models. For a linear response, combinations of linear elastic springs and linear viscous dashpots are used. Two simple spring-and-dashpot models are the *Maxwell model* and the *Kelvin-Voigt* model (Malkin 1994, Bareišis 2003, Reddy 2013). The Maxwell model characterizes a viscoelastic fluid while the Kelvin-Voigt model represents a viscoelastic solid. Other combinations of these models are also used. Based on rheological models it is possible to consider intermediate models of materials which are between *solid* and *Newtonian fluid mechanics*. The word viscoelastic is derived from the words "viscous"+ "elastic"; a viscoelastic material exhibits both viscous and elastic behavior. One can build up a model of linear viscoelasticity by considering combinations of the linear *elastic spring* and the linear *viscous dash-pot*; the dash-pot is a piston-cylinder (damper) arrangement, filled with a viscous fluid, a strain is achieved by dragging the piston through the fluid.

Considering the first model, which consists of an elastic spring element in series with a dash-pot element (Fig. 1.9a). One can divide the total strain into one for the spring ε_1 and one for the dash-pot ε_2. This model draws attention that nature consists of the bodies that connect elasticity and viscosity.

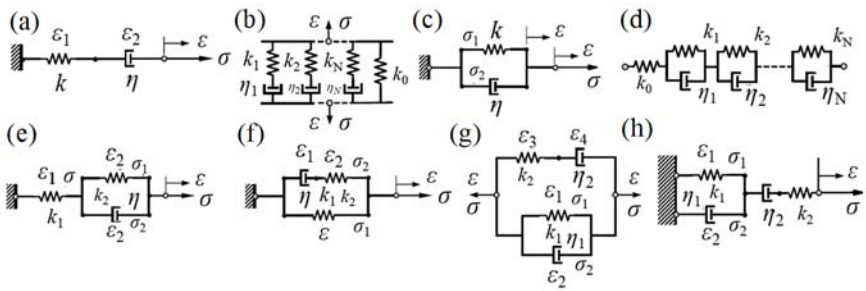

Fig. 1.9. Spring and dash-pot models: Maxwell element (a); the generalized Maxwell model (b); Kelvin-Voigt element (c); The generalized Kelvin-Voigt model (d); Three-element models (e, f); Four-element models (g, h)

Solids that suddenly deformed exhibit elastic behavior and deformation size is proportional to the load (*Hooke's law*). To the contrary, under slow deformation, the velocity of deformation of the solid is proportional to the value of the load (*Newton's law*).

The stress-strain relation for the model is developed using the following stress-strain relationships of individual elements:

$$\sigma = k \cdot \varepsilon \; ; \quad \sigma = \eta \cdot \dot{\varepsilon} \, , \tag{1.3}$$

where k is the spring elastic constant, η is the dash-pot viscous constant, and the superposed dot indicates time derivative.

It is understood that the spring element responds instantly to stress, while the dash-pot cannot respond instantly due to its response is rate dependent.
Note that when elements are connected in series, each element carries the same amount of stress while the strains are different in each element. Thus, it can be written as:

$$\dot{\varepsilon} = \varepsilon_1 + \varepsilon_2 = \frac{\dot{\sigma}}{k} + \frac{\sigma}{\eta} \, . \tag{1.4}$$

Once this system is loaded, at first spring element deforms and the rest of loading belongs to the flow of viscous fluid in the cylinder. Maxwell model considers only Hooke's elastic deformation and does not determine the elastic deformation of the polymer due to the straightening of macromolecules (Lemini 2014). Also, time is important in order to cause mentioned deformation. Such "delayed" deformation (strain) shall be described based on Kelvin's proposal below (Figs 1.9c– 1.9d).

The Kelvin-Voigt element (Fig. 1.9d) consists of a linear elastic spring and element in parallel with a dash-pot element. One can divide the total stress into one for the spring σ_1 and one for the dash-pot σ_2. The stress-strain relation for the model is derived as follows:

$$\sigma = \sigma_1 + \sigma_2 = k\varepsilon + \eta \frac{\mathrm{d}\varepsilon}{\mathrm{d}t} \, . \tag{1.5}$$

It is assumed that fluid is compressed in damper thus instantaneous load does not cause any of deformation in the viscous element. Elastic deformation appears after some time necessary for the displacement of the damper. Theories based on Maxwell and Kelvin-Voigt models compared with experimental work results shown that both models qualitatively reflect to the behavior of polymers. The first one better describes properties of linear polymers while the second one more belongs to the polymers with a mesh type structure.

There are *two three-element models* proposed in the literature (Figs. 1.9e and 1.9f). In the first one an extra spring element is added in series to the Kelvin-Voigt element, and in the second one, a spring element is added in parallel to the Maxwell element. The *four-element models* (Figs. 1.9g–1.9h) have constitutive relations that involve second-order derivatives of stress and strain (Thien 2013). Fornůsek *et al.* (2009) successfully performed experimental tests of GFRP prestressed slabs from the micro level point of view. In order to calculate the stress relaxation of the tendons two parallel Kelvin's chains viscoelastic model was assumed: one chain was used for glass fiber and the second was used for the matrix. Nanoindentation method was employed in order to determine the modulus of elasticity of both components. From the prestressed concrete point of view, more rigorous models, such as *Ross's* (Freudenthal *et al.* 1958) have been used to assist in approximately simulating the stress-strain-time behavior of concrete at the limit of proportionality with some limitations and predicting the creep strains (Nawy 2003).

1.3. Effects in Aging Linearly Viscoelastic Materials

There are quite many examples of viscoelastic materials with memory. As it was aforesaid concrete together with polymers (composites) are examples of viscoelastic behavior materials (Reddy 2013; Brinson&Brinson 2015). The mathematical models of the viscoelastic constitutive behavior are needed to analytically or numerically determine the structural system response in order to better understand and design of structures. According to linear theory of viscoelasticity the general formulation of the uniaxial strain-stress law of concrete drives to an integral form which is very complex from computational point of view, so that simplified models or approximate formulations of the integral form are great of interest, in order to obtain approximate results sufficiently refined for practical purposes without performing cumbersome structural calculations (Pisani 2000, Balevičius 2010, Balevičius *et al.* 2018).

In order to design PC elements, the value of effective prestressing force shall be known. There are several conditions such as materials used, fabrication practices and methods which cause the force in the prestressing reinforcement to decrease from initial force transferred by the jacking system. In general, prestress losses are defined as the reduction in the tensile stress in prestressing reinforcement. According to literature, they are categorized as either *instantaneous losses* or *time-dependent losses* (Lin *et al.* 1981, Collins *et al.* 1991, Kaklauskas *et al.* 2001b, Navrátil 2006, Marčiukaitis *et al.* 2007, Gilbert *et al.* 2011, Ghali *et al.* 2012, Marčiukaitis 2012, Marčiukaitis *et al.* 2013, Bažant *et al.* 2013, Gilbert *et al.* 2017). Instantaneous losses are affecting the prestress force as soon as it is

transferred to the concrete member at time t_0 and may vary along the length of reinforcement. With respect to Eurocode 2 (CEN 2004) and *fib* Model Code 2010 (*fib* 2013) these losses are the difference between the force imposed on the tendon by the hydraulic jack P_{max} and the force in the tendon immediately after transfer at a distance x from the active end of the reinforcement $P_{m0}(x)$ as shown in Fig. 1.10:

$$\Delta P_i(t) = P_{max} - P_{m0}(x) . \tag{1.6}$$

During the time $t = t_0$:

$$P_{m0}(x) = A_p \sigma_{pm.0}(x) . \tag{1.7}$$

The remaining losses occur gradually with a design life of PC element. These include losses caused by the gradual shortening of concrete at the prestressing reinforcement level due to creep and shrinkage and relaxation of the reinforcement. If we assume that $P_{m.t}(x)$ is a force in the prestressing tendon at x from the active end of the prestressing reinforcement after all losses, then:

$$\Delta P_{c+s+r}(t) = P_{m0}(x) - P_{m.t}(x) . \tag{1.8}$$

Mean value of prestress force at time period $t > t_0$ due to the type of method of prestressing shall be estimated:

$$P_{m.t}(x) = P_{m0}(x) - \Delta P_{c+s+r}(t) . \tag{1.9}$$

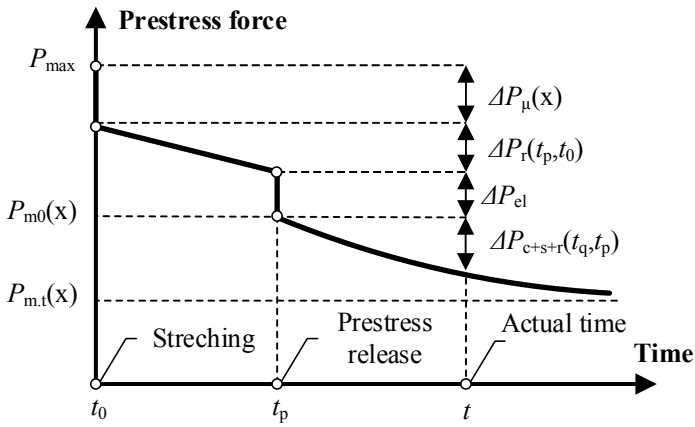

Fig. 1.10. Dependence of prestress force over the time by stretching reinforcement between the bulkheads according to CEN 2004 and *fib* 2013

Due to the fact that both immediate and time-dependent losses consist of several components Eq. (1.7) shall be expanded:

$$P_{m0}(x) = P_{max} - \Delta P_{el} - \Delta P_{r} - \Delta P_{\mu}(x) - \Delta P_{\Theta}, \tag{1.10}$$

where ΔP_{el} – elastic deformation losses; ΔP_{r} – intrinsic relaxation losses; $\Delta P_{\mu}(x)$ – losses due to friction at any distance x from the jacking end; ΔP_{Θ} – losses due to change in temperature.

Until about 25 years ago, a pilot knowledge and research contained little coverage of prestressing polymers and composites for concrete structures (Zavadskas 1974; Valivonis 1995; ACI 440.4R 2004; *fib* 2013). In case of the losses prediction methods for FRPs have been developed over the last years, but simple, practical solutions for accurate estimation of prestress losses have proved difficulties due to lack of successful experimental work results on a different kind of FRP.

The accurate estimation of losses requires more precise knowledge of material properties as well as the interaction between creep, shrinkage of concrete and the relaxation of the reinforcement. The current methods for the prediction of losses shall be classified according to their approach for the calculation of losses.

In terms of losses of stress in FRP tendons, the American Concrete Institute (ACI 440.4R 2004) and European regulations whether *Comité Euro-International du Béton* (CEB), *European Committee for Standardization* (CEN) and *Fédération Internationale du Béton* (*fib*) do not specify particular formulas for the prestress losses caused by major types of FRP relaxation, the Canadian Network of Centres of Excellence on Intelligent Sensing for Innovative Structures (ISIS) does, in particular to AFRP and CFRP. The values of stress relaxation proposed in these regulations are based on experimental test results (Odagiri *et al.* 1997; Dolan *et al.* 2000).

Looking to the Table 1.4 and Table 1.5 it is obvious that, current recommendations are not valid for calculation of prestress losses in flexural PC members due to stress relaxation of BFRP prestressing bars since they are based on steel tendon tests.

Table 1.4. Stress relaxation rates, %

Design Code	AFRP	BFRP	CFRP	GFRP
CEN 2004	–	–	–	–
ACI 440.4R 2004	6–18	–	2–8	–
ISIS 2008	6–18	–	1.04–3.59	–
fib 2013	11–25	–	2–10	4–14

Table 1.5. Formulas of stress relaxation in the bars

Reference	Formula	Conditions
CEN (2004)	$\frac{\Delta\sigma_{\mathrm{pr}}}{\sigma_{\mathrm{pi}}} = 5.39\,\rho_{1000}\,e^{6.7\mu}\left(\frac{t}{1000}\right)^{0.75(1-\mu)}10^{-5}$	Class 1 Relaxation loss (15.5–23.3%)
	$\frac{\Delta\sigma_{\mathrm{pr}}}{\sigma_{\mathrm{pi}}} = 0.66\,\rho_{1000}\,e^{9.1\mu}\left(\frac{t}{1000}\right)^{0.75(1-\mu)}10^{-5}$	Class 2 Relaxation loss (2.5–6.1%)
	$\frac{\Delta\sigma_{\mathrm{pr}}}{\sigma_{\mathrm{pi}}} = 1.98\,\rho_{1000}\,e^{8\mu}\left(\frac{t}{1000}\right)^{0.75(1-\mu)}10^{-5}$	Class 3 Relaxation loss (6.2–12.1%)
ISIS (2008)	$\frac{\Delta\sigma_{\mathrm{pr}}}{\sigma_{\mathrm{pi}}} = 3.38 + 2.88\log(t)$	AFRP
	$\frac{\Delta\sigma_{\mathrm{pr}}}{\sigma_{\mathrm{pi}}} = 0.231 + 0.345\log(t)$	CFRP
Sen *et al.* (1992)	$\Delta\sigma_{\mathrm{pr}} = \frac{\sigma_{\mathrm{pi}}}{100}\{0.75\log(t\cdot 24)+1.5\}$	GFRP
Saadatmanesh and Tannous (1999)	$\frac{\Delta\sigma_{\mathrm{pr}}}{\sigma_{\mathrm{p0}}} = \frac{\sigma_{\mathrm{p0}}/f_{\mathrm{u}} - [a - b\log(t)]}{\sigma_{\mathrm{p0}}/f_{\mathrm{u}}}$	CFRP

The loss of stress in a prestressing reinforcement occurs not only from reinforcement relaxation, but also from the losses due to concrete creep, shrinkage and elastic shortening, and these, in turn, reduce the relaxation of the tendon. Structural concrete member under stress continues to deform over a period of time due to the property of creep and steel under strain continues to lose stress over a period of time due to the property of relaxation. In addition, concrete shrinks due to loss of water as a result of drying and hydration. All these effects lead to losses of prestress over time, and this has to be taken into account within structural calculations.

Let the concrete beam be prestressed with the force at prestress transfer of P_0 applied at an eccentricity of e. The compressive stress in concrete at the centre of the tendon will be given by:

$$\sigma_{\mathrm{c}} = \frac{P_0}{A} + P_0 e\frac{e}{I}\ , \tag{1.11}$$

where A and I are the area and the second moment of area of the beams cross-section.

The compressive concrete strain will be given by:

$$\varepsilon_{\mathrm{c}} = \frac{\sigma_{\mathrm{c}}}{E_{\mathrm{cm}}(t)}, \tag{1.12}$$

where $E_{\mathrm{cm}}(t)$ is the secant modulus of elasticity of concrete at the time of prestress transfer and since stressing in prestressed concrete is done prior 28 days it shall be recalculated as below (CEN 2004):

$$E_{\mathrm{cm}}(t) = \left(\frac{f_{\mathrm{cm}}(t)}{f_{\mathrm{cm28}}}\right)^{0.3} E_{\mathrm{cm28}} . \tag{1.13}$$

Here E_{cm28} and f_{cm28} are elastic modulus and compressive strength at the age of 28 days.

If prestressing is applied prior 28 days after concrete hardening, the compressive strength of concrete at the age of t days shall be recalculated as below:

$$f_{\mathrm{cm}}(t) = \beta_{\mathrm{cc}}(t) f_{\mathrm{cm28}};\ \beta_{\mathrm{cc}}(t) = \exp\left\{0.25\left[1-\left(\frac{28}{t}\right)^{\frac{1}{2}}\right]\right\}, \tag{1.14}$$

here $\beta_{\mathrm{cc}}(t)$ is a coefficient which depends on the age of the concrete; t is the age of concrete in days.

Further, since prestressing reinforcement is fully bonded to concrete, the compressive strain in reinforcement is equal to the strain in concrete, and the compressive stress in prestressing reinforcement shall be given by:

$$\varepsilon_{\mathrm{p}} = \varepsilon_{\mathrm{c}};\ \sigma_{\mathrm{p}} = \varepsilon_{\mathrm{p}} E_{\mathrm{p}} = \sigma_{\mathrm{c}} \frac{E_{\mathrm{p}}}{E_{\mathrm{cm}}(t)} = \frac{P_0}{A}\left(1+\frac{Ae^2}{I}\right)\frac{E_{\mathrm{p}}}{E_{\mathrm{cm}}(t)} . \tag{1.15}$$

In case of elastic loss of force in the tendon shall be given as:

$$\Delta P_i = \sigma_{\mathrm{p}} A_{\mathrm{p}} = \left(\frac{P_0}{A}+\frac{P_0}{I}e^2\right)\frac{E_{\mathrm{p}}}{E_{\mathrm{cm}}(t)} A_{\mathrm{p}} = P_0\left(1+\frac{A_{\mathrm{p}}}{I}e^2\right)\frac{E_{\mathrm{p}}}{E_{\mathrm{cm}}(t)}\frac{A_{\mathrm{p}}}{A} . \tag{1.16}$$

With respect to time-dependent losses, is the secant modulus of elasticity of concrete at the time of prestress transfer $E_{\mathrm{cm}}(t)$ is going to be replaced by the long-term Young's modulus allowing creep deformation $E_{\mathrm{cm}}(t)/\varphi$, where φ is the creep coefficient.

Moreover, the loss of prestress due to creep could be expressed as:

$$\Delta P_{\mathrm{c}} = \left(\frac{P_0}{A}+\frac{P_0}{I}e^2\right)\frac{E_{\mathrm{p}}}{E_{\mathrm{cm}}(t)}\varphi A_{\mathrm{p}} = P_0\chi ; \tag{1.17}$$

$$\chi = \left(1 + \frac{A}{I}e^2\right)\frac{E_\mathrm{p}}{E_\mathrm{cm}(t)}\varphi\frac{A_\mathrm{p}}{A}.$$

The loss due to concrete shrinkage and relaxation of the tendon:

$$\Delta P_\mathrm{s} = \varepsilon_\mathrm{cs} E_p A_\mathrm{p}\,;\, \Delta P_\mathrm{r} = \Delta\sigma_\mathrm{pr} A_\mathrm{p}\,. \tag{1.18}$$

The loss due to creep strain due to permanent service loads which cause tensile stresses in concrete at the centroid of the tendon:

$$\Delta P_\mathrm{c.ext} = -\sigma_\mathrm{c.ext}\frac{E_\mathrm{p}}{E_\mathrm{cm}(t)}\varphi\,. \tag{1.19}$$

The final losses due to mentioned time-dependent effects above:

$$\Delta P_\mathrm{c+s+r} = \left(\varepsilon_\mathrm{cs} E_p + \Delta\sigma_\mathrm{pr} - \sigma_\mathrm{c.ext}\frac{E_\mathrm{p}}{E_\mathrm{cm}(t)}\varphi\right)A_\mathrm{p}\,. \tag{1.20}$$

Considering the force at the bulkheads (prestressing bed) at the time of transfer, the prestress force including final losses shall be defined as:

$$P_\mathrm{m.t} = P_\mathrm{max} - P_0\chi - \Delta P_\mathrm{c+s+r}\,. \tag{1.21}$$

Assuming $P_\mathrm{m.t} \approx P_0$, and solving for P_0 :

$$P_0 = \frac{P_\mathrm{max} - \Delta P_\mathrm{c+s+r}}{(1+\chi)}\,. \tag{1.22}$$

Thus Eq. (1.17) can be rewritten into absolute value:

$$\Delta P = P_0\chi + \Delta P_\mathrm{c+s+r} = \frac{P_\mathrm{max} - \Delta P_\mathrm{c+s+r}}{(1+\chi)}\chi + \Delta P_\mathrm{c+s+r} = \frac{(P_\mathrm{max}\chi + \Delta P_\mathrm{c+s+r})}{(1+\chi)}\,. \tag{1.23}$$

The numerator can be written as:

$$\left(\frac{P_\mathrm{max}}{A}\left(1 + \frac{Ae^2}{I}\right) - \sigma_\mathrm{c.ext}\right)\frac{E_\mathrm{p}}{E_\mathrm{cm}(t)}\varphi A_\mathrm{p} + (\varepsilon_\mathrm{cs} E_\mathrm{p} + \Delta\sigma_\mathrm{pr})A_\mathrm{p}\,. \tag{1.24}$$

Setting, that:

$$\sigma_\mathrm{c.QP} = \frac{P_\mathrm{max}}{A}\left(1 + \frac{Ae^2}{I}\right) - \sigma_\mathrm{c.ext}\,. \tag{1.25}$$

It is possible to obtain final losses of prestress in the tendon due to concrete creep and shrinkage as well as relaxation of the tendon:

$$\Delta P_{\mathrm{c+s+r}} = A_{\mathrm{p}} \frac{\left(\varepsilon_{\mathrm{cs}} E_{\mathrm{p}} + \Delta\sigma_{\mathrm{pr}} + \sigma_{\mathrm{c.QP}} \dfrac{E_{\mathrm{p}}}{E_{\mathrm{cm}}(t)} \varphi \right)}{[1+\chi]} . \tag{1.26}$$

Eurocode 2 (CEN 2004) express slightly simplified equation to Eq. (1.26) as shown in Table 1.6.

In order to perform time-dependent losses due to creep and shrinkage of concrete according to Eurocode 2 (CEN 2004), the total shrinkage strain $\varepsilon_{\mathrm{cs}}$ and creep coefficient $\varphi(t,t_0)$ shall be defined at certain time periods, i.e. at the time of prestress transfer (short-time) and the time between prestress transfer and applied service load (long-term).

Hence the value of total shrinkage strain $\varepsilon_{\mathrm{cs}}$ and related factors follow from:

$$\varepsilon_{\mathrm{cs}} = \varepsilon_{\mathrm{cd}} + \varepsilon_{\mathrm{ca}} ; \varepsilon_{\mathrm{cd}} = \beta_{\mathrm{ds}}(t,t_{\mathrm{s}}) k_{\mathrm{h}} \varepsilon_{\mathrm{cd.0}} ; \beta_{\mathrm{ds}}(t,t_{\mathrm{s}}) = \frac{(t-t_{\mathrm{s}})}{(t-t_{\mathrm{s}}) - 0.04\sqrt{h_0^3}} ; \tag{1.27}$$

$$\varepsilon_{\mathrm{cd.0}} = 0.85\left[(220 + 110\alpha_{\mathrm{ds1}}) \exp\left(-\alpha_{\mathrm{ds2}} \frac{f_{\mathrm{cm}}}{f_{\mathrm{cm.0}}} \right) \right] \cdot 10^{-6} \cdot \beta_{\mathrm{RH}} ; \tag{1.28}$$

$$\beta_{\mathrm{RH}} = 1.55\left[1 - \left(\frac{RH}{RH_0} \right)^3 \right] ; \varepsilon_{\mathrm{ca}} = \beta_{\mathrm{as}} \varepsilon_{\mathrm{ca}}(\infty) ; \tag{1.29}$$

$$\varepsilon_{\mathrm{ca}}(\infty) = 2.5(f_{\mathrm{ck}} - 10) \cdot 10^{-6} ; \ \beta_{\mathrm{as}} = 1 - \exp(-0.2 t^{\frac{1}{2}}) , \tag{1.30}$$

where $\varepsilon_{\mathrm{cd}}$, $\varepsilon_{\mathrm{ca}}$, $\varepsilon_{\mathrm{cd.0}}$ are the drying shrinkage strain, the autogenous shrinkage strain, and the basic drying shrinkage strain; k_{h} is a coefficient depending on the notional size h_0 which shall be defined as $h_0 = 2A_{\mathrm{c}}/u$; A_{c} is the concrete cross-section area, and u is the perimeter of that part of the cross-section which is exposed to drying, and t, t_{s} are the age of the concrete at the moment considered, and the age of concrete at the beginning od drying shrinkage (or swelling), in days. Coefficients $\varepsilon_{\mathrm{ds1}}$, $\varepsilon_{\mathrm{ds2}}$ depends on the type of cement; RH is the ambient relative humidity and RH = 100%; f_{cm}, f_{ck} are the mean compressive strength of concrete (MPa) and characteristic compressive cylinder compressive strength (MPa), f_{cm} = 10 MPa.

The creep coefficient $\varphi(t,t_0)$ shall be calculated accordingly:

$$\varphi(t,t_0) = \varphi_0 \beta_{\mathrm{c}}(t,t_0) ; \tag{1.31}$$

$$\varphi_0 = \varphi_{\mathrm{RH}} \beta(f_{\mathrm{cm}}) \beta(t_0) ; \ \varphi_{\mathrm{RH}} = \left[1 + \frac{1 - RH/100}{0.1\sqrt[3]{h_0}} \alpha_1 \right] \alpha_2 ; \tag{1.32}$$

Table 1.6. Formulas of time-dependent prestress losses

Reference	Formulae
CEN (2004)	$\Delta\sigma_{\mathrm{c+s+r}} = \dfrac{\varepsilon_{\mathrm{cs}} E_{\mathrm{p}} + 0.8\Delta\sigma_{\mathrm{pr}} + \dfrac{E_{\mathrm{p}}}{E_{\mathrm{cm}}}\varphi(t,t_0)\sigma_{\mathrm{c,QP}}}{1 + \dfrac{E_{\mathrm{p}}}{E_{\mathrm{cm}}}\dfrac{A_{\mathrm{p}}}{A_{\mathrm{c}}}\left(1 + \dfrac{A_{\mathrm{p}}}{I_{\mathrm{c}}} z_{\mathrm{cp}}^2\right)\left[1 + 0.8\varphi(t,t_0)\right]}$.
Zamblauskaitė (2005)	$\Delta\sigma_{\mathrm{s}} = E_{\mathrm{p}}\varepsilon_{\mathrm{sh}}(t,t_{\mathrm{s}})$. $\Delta\sigma_{\mathrm{s}} = E_{\mathrm{p}}\left(\varepsilon_{\mathrm{cr}}(t,t_0) - \varepsilon_{\mathrm{c}}(t_0)\right)$.
Karbhari (2007)	$\Delta\sigma_{\mathrm{c+s+r}} = E_{\mathrm{p}}\left\{k_{\mathrm{A}}\left(\Delta\varepsilon_{\mathrm{c+s}}\right) + y_{\mathrm{p}}\left[\dfrac{k_{\mathrm{I}}\Delta\dfrac{1}{r} + k_{\mathrm{c}}\left(\Delta\varepsilon_{\mathrm{c+s}}\right)}{h}\right]\right\} + k_{\mathrm{p}}\Delta\overline{\sigma}_{\mathrm{pr}}$
Balevičius (2018)	$\Delta\sigma_{\mathrm{c}} = E_{\mathrm{p}}\sigma_{\xi}(t,t_0)C(t,t_0)$. $\Delta\sigma_{\mathrm{s}} = E_{\mathrm{p}}\left[\varepsilon_{\mathrm{c}}^{top}(t,t_0) + y_{\mathrm{p}}(\varepsilon_{\mathrm{sh}}(t,t_0)k_{\mathrm{sh}}\right]$.
Pisani (2000)	$\Delta\sigma_{\mathrm{c+s+r}} = \sigma_{\mathrm{p0}} D_{\mathrm{p}} \times \left\{\dfrac{r_{\mathrm{p}}(t,t_{\mathrm{p}})}{E_{\mathrm{p}}}\dfrac{D_{\mathrm{p}}[\chi_{\mathrm{p}}(t,t_0)-1]\varphi_{\mathrm{p}}(t,t_0) + (1-D_{\mathrm{p}})[\chi_{\mathrm{c}}(t,t_0)-1]\varphi_{\mathrm{c}}(t,t_0)+1}{1+\chi_{\mathrm{c}}(t,t_0)\varphi_{\mathrm{c}}(t,t_0) - D_{\mathrm{p}}[\chi_{\mathrm{c}}(t,t_0)\varphi_{\mathrm{c}}(t,t_0) - \chi_{\mathrm{p}}(t,t_0)\varphi_{\mathrm{p}}(t,t_0)]} + \dfrac{\left[r_{\mathrm{p}}(t,t_{\mathrm{p}}) - \dfrac{r_{\mathrm{p}}(t,t_{\mathrm{p}})}{E_{\mathrm{p}}} r_{\mathrm{p}}(t,t_{\mathrm{p}})\right]\dfrac{1+\chi_{\mathrm{p}}(t,t_0)\varphi_{\mathrm{p}}(t,t_0)}{E_{\mathrm{p}}}}{1+\chi_{\mathrm{c}}(t,t_0)\varphi_{\mathrm{c}}(t,t_0) - D_{\mathrm{p}}[\chi_{\mathrm{c}}(t,t_0)\varphi_{\mathrm{c}}(t,t_0) - \chi_{\mathrm{p}}(t,t_0)\varphi_{\mathrm{p}}(t,t_0)]}\right\}$. $D_{\mathrm{p}} = \dfrac{1/E_{\mathrm{p}}A_{\mathrm{p}}}{\dfrac{1}{E_{\mathrm{p}}A_{\mathrm{p}}} + \dfrac{1}{E_{\mathrm{cm28}}A_{\mathrm{c}}} + \dfrac{e^2}{E_{\mathrm{cm28}}I_{\mathrm{eff}}}}$

$$\beta(f_{\mathrm{cm}}) = \frac{16}{\sqrt{f_{\mathrm{cm}}}}\ ;\ \beta(t_0) = \frac{1}{\left(0.1 + t_0^{0.20}\right)}\ ;\ \beta_{\mathrm{c}}(t,t_0) = \left[\frac{(t-t_0)}{\left(\beta_H + t - t_0\right)}\right]; \tag{1.33}$$

$$\beta_{\mathrm{H}} = 1.5\left[1 + (0.012RH)^{18}\right]h_0 + 250\alpha_3 \le 1500\alpha_3\,; \tag{1.34}$$

$$\alpha_1 = \left[\frac{35}{f_{\mathrm{cm}}}\right]^{0.7}\ ;\ \alpha_2 = \left[\frac{35}{f_{\mathrm{cm}}}\right]^{0.2}\ ;\alpha_3 = \left[\frac{35}{f_{\mathrm{cm}}}\right]^{0.5}, \tag{1.35}$$

where φ_0, φ_{RH} are the notional creep coefficient and a factor to allow for the effect humidity on the notional creep coefficient; $\beta_c(t,t_0)$, $\beta_c(f_{cm})$, $\beta(t_0)$ are coefficient to describe the development of creep with time after loading, and a factor to allow for effect of concrete strength on the notional creep coefficient, and a factor to allow the effect of concrete age at loading on the notional creep coefficient, respectively; β_H is a coefficient depending on the relative humidity (*RH* in %) and the notional member size (h_0); α_1, α_2, α_3 are coefficients to consider the influence of the concrete strength.

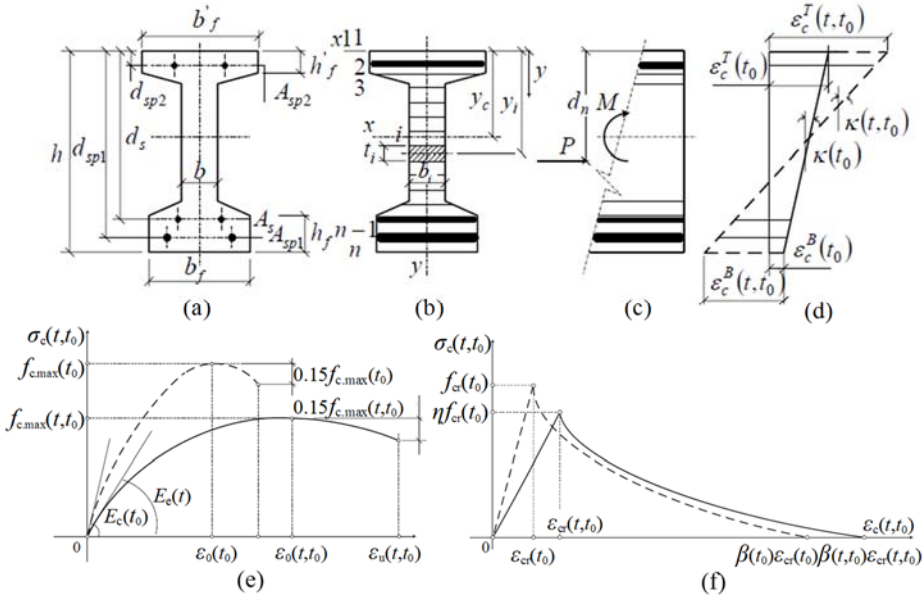

Fig. 1.11. Integral constitutive model: general shape (a); layered cross-section (b); elevation and forces induced on reinforcement (c); strain distribution (d); stress-strain curves for concrete in compression (e); for concrete in tension (f) (Zamblauskaitė 2005)

Zamblauskaitė (2005) extended the *Integral flexural constitutive model* (Kaklauskas *et al.* 2001a, 2004) for short-term and long-term deformation analysis of flexural PC members in particular to shrinkage and creep analysis, and tension stiffening effect (Fig. 1.11). In this case, prestress losses estimation is based on *Effective modulus method* proposed by McMillan (1916) and Faber (1927) (Bažant *et al.* 1988). Having used this modulus of elasticity in the calculation of the effects of the external load (prestressing), long-term deformations will occur directly. Thus the creep function is to be expressed through the creep coefficient:

$$\varepsilon_c(t,t_0) = \sigma_c(t_0)\frac{1+\varphi(t,t_0)}{E_c(t_0)}\left[1+\varphi(t,t_0)\right] + \varepsilon_{cs}(t,t_s) =$$

$$\frac{\sigma_{\mathrm{c}}(t_0)}{E_{\mathrm{c.eff}}(t,t_0)} + \varepsilon_{\mathrm{cs}}(t,t_s)\,; \tag{1.36}$$

$$E_{\mathrm{c.eff}}(t,t_0) = \frac{E_{\mathrm{c}}(t_0)}{1+\varphi(t,t_0)}\,. \tag{1.37}$$

Eqs. (1.36) and (1.37) state, that the effective modulus of elasticity is related to sustained actions that maintain a constant value of stresses with time. Based on this proposal the cross-section of PC element is divided into a number of horizontal layers and longitudinal strain $\varepsilon_{\mathrm{ci}}(t,t_0)$ is to be estimated as:

$$\varepsilon_{\mathrm{ci}}(t,t_0) = \varepsilon_{\mathrm{c}}^{top}(t,t_0) + y_i\frac{1}{r}(t,t_0)\,, \tag{1.38}$$

where y_{i} is the distance of the i-th layer from the top fiber of the cross-section. $\varepsilon_{\mathrm{c}}^{top}(t,t_0)$, $1/r(t,t_0)$ are the top fiber strain and curvature, respectively, and are obtained from the expressions in Table 1.7. Considering these values, the losses due to creep and shrinkage can be estimated based on expressions in Table 1.6.

Later, Karbhari *et al.* (2007) presented a method to calculate the long-term prestress losses in PC flexural members with either CFRP or AFRP reinforcement. This method states that in PC member, the two ends of the prestressing tendon constantly move forward each other because of creep and shrinkage of concrete, thereby reducing the tensile stress in the tendon. In this case, a reduced relaxation value $\Delta\overline{\sigma}_{\mathrm{pr}}$ (Ghali 2012) and dimensionless coefficient χ_{r} as proposed by Saadatmanesh *et al.* (1999) for AFRP tendon is equal to much less initial stress and is given by:

$$\Delta\overline{\sigma}_{\mathrm{pr}} = \chi_{\mathrm{r}}\Delta\sigma_{\mathrm{pr}}\,;\ \chi_{\mathrm{r}} = \int_0^1 \frac{\lambda(1-\Omega\zeta)-(a'-5b')}{(1-\Omega\zeta)(\lambda-(a-5b))}\mathrm{d}\zeta\,; \tag{1.39}$$

$$a' = \lambda(1-\Omega\zeta)-0.03\,;\ b' = \frac{\lambda(1-\Omega\zeta)-0.027}{23}\,; \tag{1.40}$$

$$a = \lambda - 0.03\,;\ b = \frac{\lambda-0.27}{23}\,;\ \Omega = -\frac{\Delta\sigma_{\mathrm{p.c+s+r}}-\Delta\sigma_{\mathrm{pr}}(t)}{\sigma_{\mathrm{p0}}}\,, \tag{1.41}$$

where $\lambda = \sigma_{\mathrm{p1}}/f_{\mathrm{pu}}$; σ_{p1} is the stress in the tendon 1 hour after the release of stress. Ratios $\sigma_{\mathrm{p1}}/\sigma_{\mathrm{p0}}$ in the tests varied between 0.91 and 0.96 with the average 0.93; a, a', b, b' are tabulated variables given for $\lambda = 0.4$ and $\lambda = 0.6$; ζ is a dimensionless time function defining the shape of the tendon stress-strain curve; Ω is the ratio of the difference between the total stress losses $\Delta\sigma_{\mathrm{c+s+r}}$ and intrinsic relaxation $\Delta\sigma_{\mathrm{pr}}(t)$ to the initial stress σ_{p0}. This method differs from the one proposed by

Zamblauskaitė (2005) due to the principle of the effective modulus of elasticity and consideration of prestressing reinforcement relaxation.

Based on this method, in order to define the artificial restraining force, ΔN and related moment ΔM, the elastic modulus of the concrete is transferred to as *age-adjusted modulus* of concrete and given by:

$$\overline{E}_{\text{c.eff}}(t,t_0) = \frac{E_{\text{c}}(t_0)}{1+\chi\varphi(t,t_0)}. \tag{1.42}$$

Eq. (1.42) is defined from well known Age-adjusted effective modulus method proposed by Trost (1967) (Bažant *et al.* 1988). Considering the aging coefficient $\chi(t,t_0)$, the Eq. (1.36) shall be rewritten as:

$$\varepsilon_{\text{c}}(t,t_0) = \sigma_{\text{c}}(t_0)\frac{1+\varphi(t,t_0)}{E_{\text{c}}(t_0)} + \frac{\sigma_{\text{c}}(t)-\sigma_{\text{c}}(t_0)}{E_{\text{c}}(t_0)}\left[1+\varphi(t,t_0)\right] =$$

$$\frac{\sigma_{\text{c}}(t_0)}{E_{\text{c.eff}}(t,t_0)} + \frac{\sigma_{\text{c}}(t)-\sigma_{\text{c}}(t_0)}{\overline{E}_{\text{c.eff}}(t_0)}. \tag{1.43}$$

This method is related to the case of variable stresses between $\sigma_{\text{c}}(t_0)$ and $\sigma(t_0)$. Finally, the strain and curvature are obtained from the expressions based on Ghali's (2012) equations (Table 1.7). Considering Fig. 1.12 it is obvious, that in comparison with steel bars, FRP bars (due to lower modulus of elasticity) produced less time-depending prestress losses. Also, based on the tests of AFRP bars, it shows that AFRP bars produced stress relaxation at the beginning of the prestress. Contrary, steel bars produce the same amount of stress relaxation at the level of prestress greater than 50%.

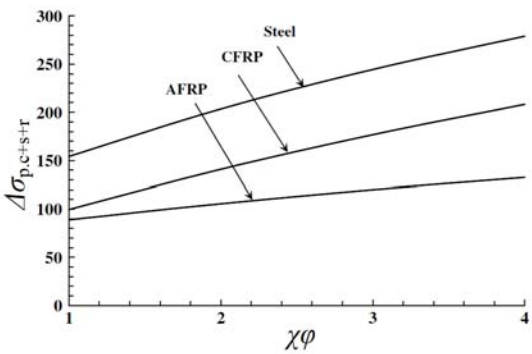

Fig. 1.12. Effect of creep and relaxation on time-dependent losses in prestressed concrete member with aramid, carbon composites and steel tendons (Karbhari 2007)

From creep analysis point of view, Balevičius (2010) proposed an average stress-strain method (ASSA) in a sense to fulfill Volterra's integral term in time interval elapsed after loading and predicting of an actual state at the time considered. In this case, Eq. (1.36) becomes (Jirásek *et al.* 2001; Balevičius *et al.* 2018):

$$\varepsilon_{\mathrm{c}}(t,t_0)=\frac{\sigma_{\mathrm{c}}(t)}{E_{\mathrm{c}}(t)}-\int_{t_0}^{t}\sigma_{\mathrm{c}}(\tau)\frac{\partial J(t,\tau)}{\partial\tau}\mathrm{d}\tau+\varepsilon_{\mathrm{cs}}(t,t_{\mathrm{s}})\,, \tag{1.44}$$

where $J(t,\tau)=1/E_{\mathrm{c}}(\tau)+C(t,\tau)$ is the creep compliance due to unit stress of concrete, $E_{\mathrm{c}}(\tau)$ is the modulus of elasticity of concrete at age τ, $C(t,\tau)$ is the specific creep of concrete; $t_{\mathrm{s}}=t_0$ is age of the concrete (in days) at the beginning of the development of drying shrinkage.

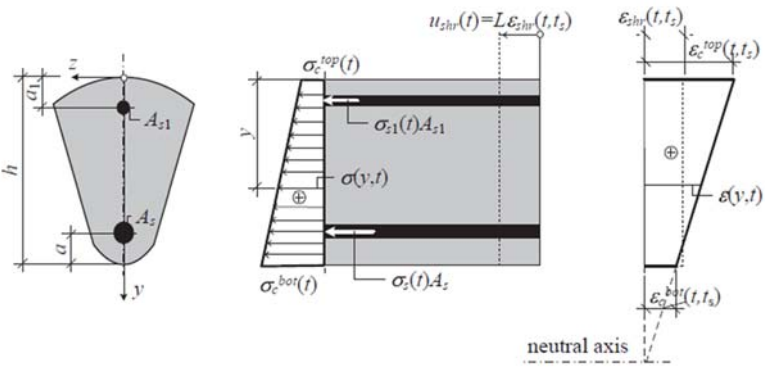

Fig. 1.13. Shrinkage displacement-induced stress-strain state of reinforced concrete element (Balevičius 2018)

The application of the first mean value theorem to the integration of Eq. (1.44) gives (Balevičius 2010):

$$\varepsilon_{\mathrm{c}}(t,t_0)=\frac{\sigma_{\mathrm{c}}(t)}{E_{\mathrm{c}}(t)}+\sigma_{\xi}(t,t_0)C^{*}(t,t_0)+\varepsilon_{\mathrm{cs}}(t,t_{\mathrm{s}})\,, \tag{1.45}$$

here $C^{*}(t,t_0)=1/E_{\mathrm{c}}(t_0)-1/E_{\mathrm{c}}(t)+C(t,t_0)$ is the specific creep, involving a partly recovered instantaneous strain.

$$\sigma_{\xi}(t,t_0)=\sigma_{\mathrm{c}}(\xi)=-C^{*}(t,t_0)^{-1}\int_{t_0}^{t}\sigma_{\mathrm{c}}(\tau)\frac{\partial J(t,\tau)}{\partial\tau}\mathrm{d}\tau\,, \tag{1.46}$$

Table 1.7. Algorithms for strain and curvature estimation by various authors

Reference	Formulae
Ghali (2012) Gilbert& Mickleborough (1988)	$\varepsilon_{\mathrm{c}}^{top}(t,t_0)=\dfrac{-\overline{S_{\mathrm{eff}}^{top}}\Delta M_{\mathrm{c+s+r}}(t,t_0)+\overline{I_{\mathrm{eff}}^{top}}\Delta N_{\mathrm{c+s+r}}(t,t_0)}{\overline{E}_{\mathrm{c.eff}}(t,t_0)\left(A_{\mathrm{eff}}\overline{I_{\mathrm{eff}}^{top}}-\left(\overline{S_{\mathrm{eff}}^{top}}\right)^2\right)}$
	$\dfrac{1}{r}(t,t_0)=\dfrac{-A_{\mathrm{eff}}\Delta M_{\mathrm{c+s+r}}(t,t_0)-\overline{S_{\mathrm{eff}}^{top}}\Delta N_{\mathrm{c+s+r}}(t,t_0)}{\overline{E}_{\mathrm{c.eff}}(t,t_0)\left(A_{\mathrm{eff}}\overline{I_{\mathrm{eff}}^{top}}-\left(\overline{S_{\mathrm{eff}}^{top}}\right)^2\right)}$
Zamblauskaitė (2005)	$\varepsilon_{\mathrm{c}}^{top}(t,t_0)=\dfrac{S_{\mathrm{eff}}^{top}\Delta M_{\mathrm{c+s}}(t,t_0)+I_{\mathrm{eff}}^{top}\Delta N_{\mathrm{c+s}}(t,t_0)}{E_{\mathrm{c.eff}}(t,t_0)\left(A_{\mathrm{eff}}I_{\mathrm{eff}}^{top}-\left(S_{\mathrm{eff}}^{top}\right)^2\right)}$
	$\dfrac{1}{r}(t,t_0)=\dfrac{A_{\mathrm{eff}}\Delta M_{\mathrm{c+s}}(t,t_0)+S_{\mathrm{eff}}^{top}\Delta N_{\mathrm{c+s}}(t,t_0)}{E_{\mathrm{c.eff}}(t,t_0)\left(A_{\mathrm{eff}}I_{\mathrm{eff}}^{top}-\left(S_{\mathrm{eff}}^{top}\right)^2\right)}$
Balevičius (2018)	$\varepsilon_{\mathrm{c}}^{top}(t,t_0)=\varepsilon_{\mathrm{sh}}(t,t_{\mathrm{s}})\dfrac{\overline{I_{\mathrm{eff}}^{top}}A_{\mathrm{c}}-\overline{S_{\mathrm{eff}}^{top}}S_{\mathrm{c}}^{top}}{\overline{I_{\mathrm{eff}}^{top}}A_{\mathrm{eff}}-\left(\overline{S_{\mathrm{eff}}^{top}}\right)^2}$

here $\sigma_{\xi}(t,t_0)$ is average stress of concrete in a sense to fulfill the Volterra's integral term in $[t,t_0]$; $\sigma_{\mathrm{c}}(\xi)$ is the value of the function $\sigma_{\mathrm{c}}(\tau)$, for $\xi\in[t,t_0]$. In general, the latter unknown strains $\varepsilon_{\mathrm{c}}^{top}(t,t_0)$ or $\varepsilon_{\mathrm{c}}^{bot}(t,t_0)$ cannot be expressed explicitly after the inversion of the Volterra's integral due to mathematical complexity of the age-varying creep and the instantaneous-elastic strain functions. The solution can be given by numerical approach when the recurrence algebraic equations are substituted for the integral equations within the apparently small-time intervals (Balevičius 2018). The numerical prediction can be transformed into the explicit formuale if the shrinkage-induced coefficient is known in advance. Having assessed $E_{\mathrm{c}}(t)=E_{\mathrm{c}}(t_0)$, $C^*(t,t_0)=C(t,t_0)$:

$$\chi(t,t_0)=\frac{\sigma_{\xi}(t,t_0)-\sigma_{\mathrm{c}}(t_0)}{\sigma_{\mathrm{c}}(t)-\sigma_{\mathrm{c}}(t_0)}\,; \tag{1.47}$$

$$\sigma_{\xi}(t,t_0)=\sigma_{\mathrm{c}}(t_0)+\chi(t,t_0)\left[\sigma_{\mathrm{c}}(t)-\sigma_{\mathrm{c}}(t_0)\right]=\chi(t,t_0)\sigma_{\mathrm{c}}(t)\,; \tag{1.48}$$

$$\varepsilon_{\mathrm{c}}(t,t_0) = \frac{\sigma_{\mathrm{c}}(t)}{E_{\mathrm{c}}(t_0)}[1 + \chi(t,t_0)C(t,t_0)E_{\mathrm{c}}(t_0)] +$$

$$\varepsilon_{\mathrm{cs}}(t,t_{\mathrm{s}}) = \frac{\Delta\sigma_{\mathrm{c}}(t)}{\overline{E}_{\mathrm{c.eff}}(t,t_0)} + \varepsilon_{\mathrm{cs}}(t,t_{\mathrm{s}})\,. \tag{1.49}$$

In order to perform the estimation of losses in stress of the tendon (Table 1.6) within definition of unknown strains $\varepsilon_{\mathrm{c}}^{top}(t,t_0)$ or $\varepsilon_{\mathrm{c}}^{bot}(t,t_0)$ (Table 1.7) Balevičius (2018) have been used age-adjusted modulus based on AAEM approach proposed by Trost (1967) and later proved the results based on basic equilibrium by Gilbert *et al.* (1988) (Balevičius 2010).

Pisani (2000) proposed a general method (GM) for both the cross-section analysis and losses in the stress of PC flexural members with AFRP tendons. This is based on a *visco-elastic constitutive law* from continuum mechanics. It was assumed that both, concrete and AFRP are made as the visco-elastic hereditary material. Thus, the viscoelastic constitutive law of mentioned materials are written in the forms:

$$\varepsilon_{\mathrm{c}}(t,x,y) = \sigma_{\mathrm{c}}(t_0,x,y)J_{\mathrm{c}}(t,t_0) + \int_{t_0}^{t} \mathrm{d}\sigma_{\mathrm{c}}(\tau,x,y)J_{\mathrm{c}}(t,\tau) + \varepsilon_{\mathrm{sh}}(t,t_0)\,; \tag{1.50}$$

$$\varepsilon_{\mathrm{pj}}(t) = \sigma_{\mathrm{pj}}(t_0)J_{\mathrm{p}}(t,t_0) + \int_{t_0}^{t} \mathrm{d}\sigma_{\mathrm{pj}}(\tau)J_{\mathrm{p}}(t,\tau)\,. \tag{1.51}$$

Due to McHenry superposition principle:

$$\varepsilon_{\mathrm{pj}} = \sigma_{\mathrm{pj}}(t_{\mathrm{p0}})J_{\mathrm{p}}(t,t_{\mathrm{p0}}) + \int_{t_0}^{t} \mathrm{d}\sigma_{\mathrm{pj}}(\tau)J_{\mathrm{p}}(t,\tau) - \sigma_{\mathrm{pj}}(t_{\mathrm{p}})J_{\mathrm{p}}(t,t_0) + \sigma_{\mathrm{pj}}(t_0)J_{\mathrm{p}}(t,t_0) +$$

$$\int_{t_0}^{t} \mathrm{d}\sigma_{\mathrm{pj}}(\tau)J_{\mathrm{p}}(t,\tau)\,, \tag{1.52}$$

here $\varepsilon_{\mathrm{pj}}(t)$ is the total strain, that is the sum of the compatible strain; $J_{\mathrm{p}}(t,t_0)$ is the creep function of AFRP; t_{p} is the age of the concrete (in days) immediately prior cut loose of the bars from the bulkheads; t_{p0} is the age of concrete (in days) due to streching of the bars.

Whereas to determine the stress distribution in the PC cross-section a Volterra integral equation by means of numerical integration over each time interval shall be solved. At the same time the algebraic method transforming the Volterra integrals into algebraic formulas by means of the assumption that the stress-dependent axial strain $\varepsilon_{\mathrm{p}}(t) - \varepsilon_{\mathrm{n}}(t)$ at time t can be approximated by a linear function of the relaxation coefficient of the AFRP material:

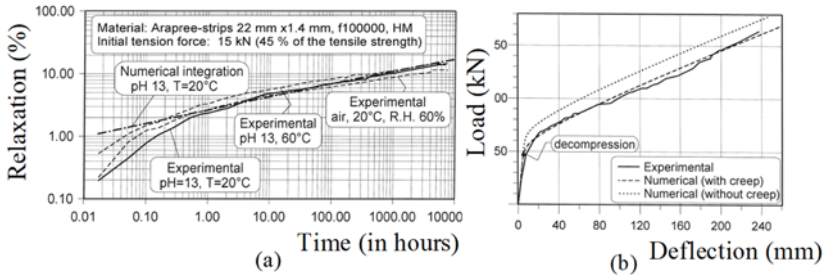

Fig. 1.14. Comparison of numerical output (Pisani 2000) and experiments: numerical relaxation rate versus experimental (a); Load-deflection curve: numerical versus experimental by Arockiasamy et al. (1995) (b)

$$\varepsilon_{\mathrm{p}}(t) - \varepsilon_{\mathrm{n}}(t) = \frac{\sigma_{\mathrm{p}}(t_0)}{E_{\mathrm{p}}(t_0)} + \varepsilon_1 \varphi_{\mathrm{p}}(t, t_0)\ , \tag{1.53}$$

here $\varepsilon_{\mathrm{p}}(t)$ is a generic strain of AFRP tendon; $\varepsilon_{\mathrm{n}}(t)$ is a stress-independent inelastic strain; ε_1 is an unknown term; $\varphi_{\mathrm{p}}(t) = b[24(t - t_0)]^a$ is the relaxation coefficient, where $a = 0.21$, $b = 4.38\times10^{-2}$.

In spite of crude approximation, the solution for losses in the stress of PC member with AFRP tendons was proposed in particular to the algebraic equation which allows to overcome the problem of computing the Volterra integrals that affect common structural analysis, once the aging or relaxation coefficients of both concrete and tendons are available (Table 1.6).

1.4. Deflection Control

European regulation CEN (2004), *fib* (2013) present empirical method of calculation of the member stiffness (*EI*) taking into account gross and cracked sections of the reinforced concrete element. At the gross section linear elastic behavior is typical for both concrete and reinforcement, while after cracking tension force in the section belongs to reinforcement:

$$(1/r) = (1-\zeta)(1/r)_{\mathrm{I}} + \zeta(1/r)_{\mathrm{II}}, \tag{1.54}$$

here $(1/r)_{\mathrm{I}}$ and $(1/r)_{\mathrm{II}}$ are the curvatures at gross (uncracked) and cracked sections, respectively.

With respect to prestressed concrete, gradual value of deflection can be calculated in regard to the equation below:

$$\delta = -\delta_{\mathrm{p}} + \delta_{\mathrm{q}} + \delta_{\mathrm{cs}}\ , \tag{1.55}$$

here – δ_p is a camber due to prestressing force; δ_q is a deflection due to applied external load; δ_{cs} is a deflection due to shrinkage of concrete. A coefficient ζ is the interpolation factor which refers to the tension stiffening effect and can be defined:

$$\zeta = 1 - \beta\left(\frac{M_{cr}}{M_a}\right)^2 . \tag{1.56}$$

The cracking moment M_{cr} is determined from elastic flexure formula and M_a represents the applied service load moment at which deflection is being calculated. The factor β refers to the type of the applied load (in case of short-term loading, long-term and cyclic loading β belongs to 1 and 0.5, correspondingly).

In accordance with ACI 440.4R (2004) a modified Branson‘s equation is proposed in order to predict the short-term deflection of FRP prestressed beams as follow:

$$I_e = \left(\frac{M_{cr}}{M_a}\right)^m \beta_d I_g + \left[1 - \left(\frac{M_{cr}}{M_a}\right)^m\right] I_{cr} \le I_g , \tag{1.57}$$

where I_g is the gross moment of inertia; β_d is a factor to soften the effective moment of inertia in order to get more suitable correspondence to experimental results.ACI Commity 440 recommends to use such formula $\beta_d = 0.5[E_p/E_s+1]$. E_p is the modulus of elasticity of FRP tendons; E_s is the modulus of elasticity of steel, and I_{cr} is the cracked moment of inertia.

Table 1.8. Proposals for effective moment of inertia estimation by various authors

Reference	Formulae
Bischoff (2005)	$I_e = \dfrac{I_{cr}}{1 - \beta_c \cdot \eta \cdot (M_{cr}/M_a)} = \dfrac{I_{cr}}{1 - (1 - \frac{I_{cr}}{I_g})(M_{cr}/M_a)^2}$
Ghali (1993) ISIS (2008)	$I_e = \dfrac{I_g I_{cr}}{I_{cr} + [1 - 0.5(M_{cr}/M_a)^2](I_g - I_{cr})}$
Toutanji *et al.* (2000)	$I_e = \left(\dfrac{M_{cr}}{M_a}\right)^m \beta_d I_g + \left[1 - \left(\dfrac{M_{cr}}{M_a}\right)^m\right] I_{cr} \le I_g$ $m = 6 - 10\rho E_p / E_s ,\ \rho E_p / E_s < 0.3$

In common, a value of 3 for the power m shall be used for conventional reinforcement matters. For the same type of FRP Toutanji *et al.* (2000) suggested to take into account $m = 6 - 10\rho E_p/E_s$ when $\rho E_p/E_s<0.3$. With respect to full-scale studies by Bischoff (2005) and Bischoff *et al.* (2011) it was found that the ratio I_g/I_{cr} has an impact to accuracy of the original Branson's equation (Table 1.8) for effective moment of inertia and tension stiffening effect depends on the power m and ratio I_g/I_{cr}, and is overestimated for values $I_g/I_{cr}>3$ when m is equal 3. Yost *et al.* 2003 indicated that power m should be used higher than 3 for FRP reinforcement. The factor β_c represents tension stiffening and is assumed to equal M_{cr}/M_a. Also, based on Ghali's (1993) proposal ISIS (2008) adopted another type of formulae for I_e estimation (Table 1.8).

In regard to prestressed concrete, it has been observed that in order to avoid a significant overestimation of the deflection, decompression moment M_{dec} has to be defined as the moment that produces zero stress at the extreme fiber of the concrete section (Atutis *et al*. 2015):

$$M_{\text{dec}} = P_{\text{e}}e + \frac{P_{\text{e}}I_{\text{g}}}{A_{\text{g}}y_{\text{g}}}. \tag{1.58}$$

The mathematical formulae for the mentioned parameters and the methods for structural analysis of serviceability limit state (SLS) are given in the current codes such as ACI 440.4R (2004), CEN (2004) and *fib* (2013). These formulations, which rely on traditional concepts, have the advantage of simplicity but involve a large degree of uncertainty. Mota *et al.* 2006 performed database of 197 beams analysis in order to find an accurate and conservative equation to estimate deflections of FRP reinforced concrete members. It was pointed out that there is a critical need for reliability analysis of FRP code equations (Mousavi *et al.* 2012). It was noted that with an increasing number of samples in the database, results change dramatically. Extensive research efforts are being done by national and international concrete community for this topic (Gilbert *et al*. 1988, Valivonis *et al.* 1995, Jokūbaitis and Kamaitis 2000, Pisani 2000, Kaklauskas *et al.* 2001, Zou 2003c, Balaguru *et al.* 2009, Ghali 2012, Mias *et al.* 2013, Jakubovskis *et al.* 2014, Mias *et al.* 2015), most of it motivated by prestressed concrete techniques or flexural behavior of concrete due to effect of concrete creep and shrinkage.

1.5. Cracking Control

Design code (ACI 2004) recommendations of structural concrete with various type of FRP bars indicates that calculation of the maximum probable crack width

could be based on equation independently from the type of reinforcement (steel or FRP):

$$w_{\mathrm{k}} = \left({}^{2\sigma_{\mathrm{p}}}\!/_{E_{\mathrm{p}}} \right) \cdot \beta \cdot k_{\mathrm{b}} \cdot \sqrt[3]{d_{\mathrm{c}}^2 + \left({}^{s}\!/_{2} \right)^2} \ , \tag{1.59}$$

where σ_{p}, E_{p} are reinforcement stress and modulus of elasticity; β is ratio of distance between neutral axis and tension face to distance between the neutral axis and centroid of reinforcement; d_{c} is the thickness of cover from tension face to center of closest reinforcement; s is spacing of the bar; k_{b} is a coefficient that accounts for the degree of bond between FRP bar and surrounding concrete. It is indicated that k_{b} can vary from those of steel bars or tendons (ACI 2004).

Crack width calculation according to CEN (2004) for steel reinforced concrete members are as follows:

$$w_{\mathrm{k}} = s_{\mathrm{r.max}} \cdot (\varepsilon_{\mathrm{sm}} - \varepsilon_{\mathrm{sm}}) \ , \tag{1.60}$$

where $\varepsilon_{\mathrm{sm}}$ is the mean strain in the reinforcement at design loads; $\varepsilon_{\mathrm{cm}}$ is the mean strain in the concrete between the cracks; $s_{\mathrm{r.max}}$ is the maximum crack spacing.

Maximum spacing between adjacent cracks can be calculated by the equation below:

$$s_{\mathrm{r.max}} = 3.4 \cdot c + 0.425 \cdot k_{\mathrm{b}} \cdot k_2 \cdot \Phi / \rho_{\mathrm{p.eff}} \ , \tag{1.61}$$

where Φ is the bar diameter; c is the clear cover to the longitudinal reinforcement; k_2 is the coefficient that accounts strain distribution, with $k_2 = 0.5$ for bending and $k_2 = 1$ for pure tension. The difference between the mean strain in the reinforcement and the mean strain in the concrete may be taken as:

$$(\varepsilon_{\mathrm{sm}} - \varepsilon_{\mathrm{cm}}) = {}^{\sigma_{\mathrm{p}}}\!/_{E_{\mathrm{p}}} - k_{\mathrm{t}} \cdot \left({}^{f_{\mathrm{ct.eff}}}\!/_{E_{\mathrm{p}} \rho_{\mathrm{p.eff}}} \right) \cdot \left(1 + \alpha_{\mathrm{e}} \cdot \rho_{\mathrm{p.eff}} \right) \geq 0.6 \frac{\sigma_{\mathrm{p}}}{E_{\mathrm{p}}} \ , \tag{1.62}$$

where $f_{\mathrm{ct.eff}}$ is the mean value of the axial tensile strength of concrete at the time cracking is expected; k_{t} is the factor that depends on the duration of loading and belongs to 0.4 and 0.6 due to long-term and short-term loading, respectively.

Experimental results by Borosnyói (2002) indicated that in the case of PC members with steel tendons stabilized of crack pattern occurs under much lower average strain of reinforcement ($\varepsilon_{\mathrm{sm.rn}}$) than in PC with CFRP tendons, independently of applied reinforcement ratio due to high bond capacity of sand coated surface of CFRP tendons: $\varepsilon_{\mathrm{sm.rn}} = \varepsilon_{\mathrm{sm}} - \mathrm{K} \cdot \rho_{\mathrm{eff}}$; K is the bond parameter.

Based on fracture mechanics and experimental works Jokūbaitis *et al.* (2000) proposed a relation between effective prestressing force and crack width at fracture state:

$$P_e = \frac{2 \cdot f_{ct}}{\lambda \cdot \Delta_c} \cdot w_k \cdot \left[\frac{S_{c.eff}}{h_{cr}} - A_{c.eff} \cdot \left(1 - \frac{\lambda \cdot \Delta_c}{w_k} \right) \right], \tag{1.63}$$

here Δ_c is concrete constant; h_{cr} is a depth of the flexural crack; λ is the longitudinal reinforcement coefficient. In this case, prestressing force depends on mentioned measured cracking pattern parameters and vice versa.

1.6. Conclusions of Chapter 1 and Formulation of the Objectives of the Thesis

Based on the literature review, the following conclusions can be drawn:

1. BFRP shows advantageous chemical and mechanical properties and is cost-competitive among the remaining FRPs. Therefore, the use of BFRP as a prestressing reinforcement in concrete structures is currently in the research and development phase. Like relevant FRPs, BFRP can be regarded as a viscoelastic material, consisting of high-strength fibers integrated into a resin matrix, thus exhibit stress relaxation. While design codes provide particular values of stress relaxation for commonly used FRPs (aramid, carbon, and glass), stress relaxation behavior of BFRP remains unclear. Limited experimental relaxation tests of BFRP bars are available.
2. The comparison of existing empirical design code formulas for stress relaxation of conventional steel and FRP reinforcements show different results. With an increase of initial stress level stress relaxation increase proportionally from the very beginning of prestressing of FRP. In case of steel reinforcement, the same proportional increase of stress relaxation appears at the higher choice of the initial stress level. It might be concluded that contrary to prestressed steel bars increase of initial stress level produces more constant relaxation rate for FRPs for the same time interval.
3. In order to assess the effective prestress of PC members with prestressed BFRP, prestress losses should be determined appropriately. While creep and shrinkage of concrete are well documented in design codes and validated with numerous experimental data, inaccurate estimation of stress relaxation of BFRP would lead to underestimation or overestimation of prestress losses.
4. Accurate estimation of prestressing is frequently associated with the serviceability of PC members. Prestressing, by itself, improves durability by preventing cracking, which in turn minimizes the penetration of water

and air. However, cracking is an inevitable and natural phenomenon even for such structures. Most of design codes and recommendations handle crack width calculation for PC members in a manner similar to that for RC members. Since the bond interface among reinforcement and concrete plays a key role in determining crack width, methods used for steel bars shall not be used for BFRP bars without the improvements from experimental tests.

5. The design of FRP prestressed concrete members is typically governed by serviceability limit state requirements. The lower modulus of FRP bars can lead to greater deflections. Thus calculation method to predict expected deflection with a reasonably high degree of accuracy is needed. With respect to the principles of PC, the camber due to decompression force shall be estimated for the final deflection calculation. It requires revision of approximate methods proposed by the design codes. Stress relaxation of BFRP, as well as creep and shrinkage of concrete, have the impact to the variation of deflection over the time. The analytical analysis shall be proved by the experimental tests. No experimental tests of prestress level effect to flexural stiffness of PC members reinforced with BFRP bars are available.

In regard to the conclusions of the literature review, the following tasks are addressed to this doctoral thesis:

1. To develop an analytical method for estimation of prestress losses by means of relaxation behavior and mechanical properties of BFRP.
2. To develop analytical methods for deflection and cracking analysis of flexural PC beams with BFRP reinforcement.
3. To perform a new experimental investigation on stress relaxation of BFRP reinforcement specimens in particular to a different level of prestress.
4. To perform an experimental investigation on a deflection and cracking of real scale flexural PC beams with different level of prestress under four-point bending tests.
5. To evaluate the adequacy of the developed analytical methods in comparison with the obtained experimental results.

2

Assessment of Prestress Losses and Serviceability of Flexural Prestressed Concrete Members

This chapter describes the complex analysis of effective prestress and serviceability limit state of PC beams with BFRP reinforcement based on stress relaxation behavior of BFRP considering consecutive stages of the loading of the flexural PC members. Proposed methods for prestress losses, deflection and cracking estimation are based on the concept of PC mechanics within particular assumptions. Moreover, a viscoelasticity theory was used to evaluate the stress relaxation of BFRP bars through the concept of Maxwell's rheological model. It would allow to disclose the nature of the phenomena of the stress relaxation behavior of BFRP bars as viscoelastic material prior to experimental work.

Herewith, alternative methods to analyze the deflections and crack widths of concrete beams prestressed with BFRP bars are proposed. Mentioned serviceability methods are based on strain and curvature analysis, effective moment of inertia including decompression effect and early (free) shrinkage of the concrete. Finally, the relevant recommendations for the approximation of the stress relaxation, deflection and cracking control of flexural PC members are presented in the conclusions section of this chapter. This chapter includes the material presented in journal publications by Atutis *et al*. (2015), Atutis *et al.* (2018a), Atutis *et al.* (2018b).

2.1. Approximation of Relaxation Curve

Firstly, it is assumed that relaxation is the reduction of stress over time subjected to sustained strain. With respect to the topic of this thesis, relaxation is a property of the composite prestressing reinforcement (FRP) and is independent of concrete properties, and also is defined as the loss of stress in a material held at constant length (Fig. 2.1).

Let us consider the model which consist of the elastic spring element in series with a dash-pot element (Fig 1.9a). In this case, the total strain can be divided into one for the spring ε_1 and one for the dash-pot ε_2. Therefore, the releation between elasticity and viscosity will be reflected by resin and fibers of linear composite (FRP). In this case, solids that suddenly deformed exhibit elastic behavior and deformation size is proportional to the load (Hooke's law). To the contrary, under slow deformation, the velocity of deformation of the solid is proportional to the value of the load (Newton's law). It is obvious that the spring element responds instantly to stress, while the dash-pot cannot respond in the same way due to its response is rate dependent. Note that once elements are connected in series each element carries the same amount of stress while the strains are different in each element. Deformation of the composite element at any of time will be expressed below:

$$\dot{\varepsilon} = \varepsilon_1 + \varepsilon_2 \,. \tag{2.1}$$

Once the system is loaded, at first spring element deforms and the rest of loading belongs to the flow of viscous fluid in the cylinder. Only Hooke's elastic strain will be considered, and elastic strain of the polymer due to the straightening of the macromolecules will not be determined.

Based on classical mechanics approach the elastic deformation of the spring and stresses is bounded by the Hooke's law:

$$\varepsilon = \frac{\sigma}{E}, \tag{2.2}$$

where E is the elastic modulus of the spring.

For a certain stress value, the elastic deformation suddenly appears as an instantaneous one as the velocity of deformation variation depends on the velocity of the stress variation:

$$\frac{\mathrm{d}\varepsilon_1}{\mathrm{d}t} = \frac{1}{E} \cdot \frac{\mathrm{d}\sigma}{\mathrm{d}t} \,. \tag{2.3}$$

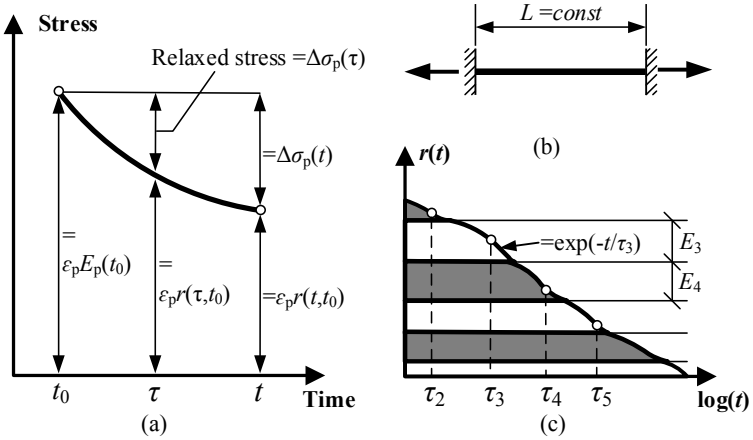

Fig. 2.1. Stress relaxation phenomenon: variation of stress with time and maintained strain constant thereafter (a); maintained length constant over time (b); approximation of relaxation curve at loading (c)

As mentioned earlier (Section 1.2.4), both elements of Maxwell's model are connected sequentially, so that the viscous element is exposed by the same stress as the elastic element. Further, according to Newton's law, increasing strain-inducting the viscous solid, the velocity of the flow of high-velocity viscous solid increases proportionately:

$$\sigma = \eta \cdot v, \tag{2.4}$$

where η is the viscosity of solid.

It can be assessed, that $v = \mathrm{d}\varepsilon_2/\mathrm{d}t$, thus it gives:

$$\frac{\mathrm{d}\varepsilon_2}{\mathrm{d}t} = \frac{\sigma}{\eta}. \tag{2.5}$$

Further, writing the received deformation values into the equation (2.3), we deduce the differential equation for the deformation process:

$$\frac{\mathrm{d}\varepsilon}{\mathrm{d}t} = \frac{1}{E} \cdot \frac{\mathrm{d}\sigma}{\mathrm{d}t} + \frac{\sigma}{\eta}. \tag{2.6}$$

The differential equation above allows us to describe cases of relaxation of stress in a composite polymer, when ε = const, and assuming that the stresses in FRP decrease to zero, i.e. $\mathrm{d}\varepsilon_2/\mathrm{d}t = 0$, then we obtain from equation (2.6):

$$\frac{\mathrm{d}\sigma}{\sigma} = -\frac{E}{\eta}\mathrm{d}t. \tag{2.7}$$

Integrating from 0 to t and from σ_0 to σ and assuming $E/\eta = \tau$, we obtain:

$$\int_{\sigma_0}^{\sigma} \frac{\mathrm{d}\sigma}{\sigma} = -\frac{E}{\eta}\int_{0}^{t} \mathrm{d}t \,. \tag{2.8}$$

$$\ln \sigma - \ln \sigma_0 = -\frac{E}{\eta} \,. \tag{2.9}$$

$$\sigma(t) = \sigma_0 \exp(-t/\tau) \,, \tag{2.10}$$

where τ time of stress relaxation.

Assuming $\tau = t$, we obtain:

$$\sigma(t) = \sigma_0 / \mathrm{expl} \,. \tag{2.11}$$

According to Eq. (2.11) we get that τ shows how long the initial stresses have decreased e times. Also, equation (2.11) shows that for a very long experimental time (i.e. $t >> \tau$):

$$\sigma(t) = \sigma_0 / \mathrm{exp}\infty \,. \tag{2.12}$$

In this case, the stress is approaching to zero, but this phenomenon shall be confirmed by the experiments what is not common and yet not comfortable practice due to specifics of required experimental equipment. Mathematically relaxation curve at loading shall be approximated by a sum of exponentials (Fig. 2.1 c). Analyzing the relationship between the deformation and stress relaxation time of structural material, it can be seen that the time duration increases if the viscosity of the solid, in which the piston moves, increases, and the spring elasticity decreases.

2.2. Losses of Prestress Model by Means of Consecutive Phases

2.2.1. General Assumptions and Basic Principles

The proposed model is based in the following assumptions: 1) instantaneous losses due to relaxation of BFRP occur at the beginning of prestress force appli-

cation (release from bullheads); 2) the cross-section of PC member remains homogenous at uncracked and post-cracking behavior; 3) linear-elastic properties are assumed for non-prestressed steel and prestressing BFRP reinforcements as well as concrete; 4) plane sections remain plane and, as a consequence, the strain distribution is linear over the depth of the section; 5) perfect bond exists between the bonded reinforcement and concrete; 6) tensile stress in the concrete does not contribute to the cross-sectional properties; 7) in case of time-dependent prestress losses, stress-strain state is to be calculated based on age-adjusted effective modulus method (Trost *et al.* 1967).

There are three critical phases of the design of PC members for serviceability. The first phase is instantaneous after the prestress is transferred to the concrete, i.e., when the member is subjected to the maximum prestress force and the external load is usually at a minimum. Instantaneous losses have taken place, but no final losses have yet occurred (Fig. 2.2).

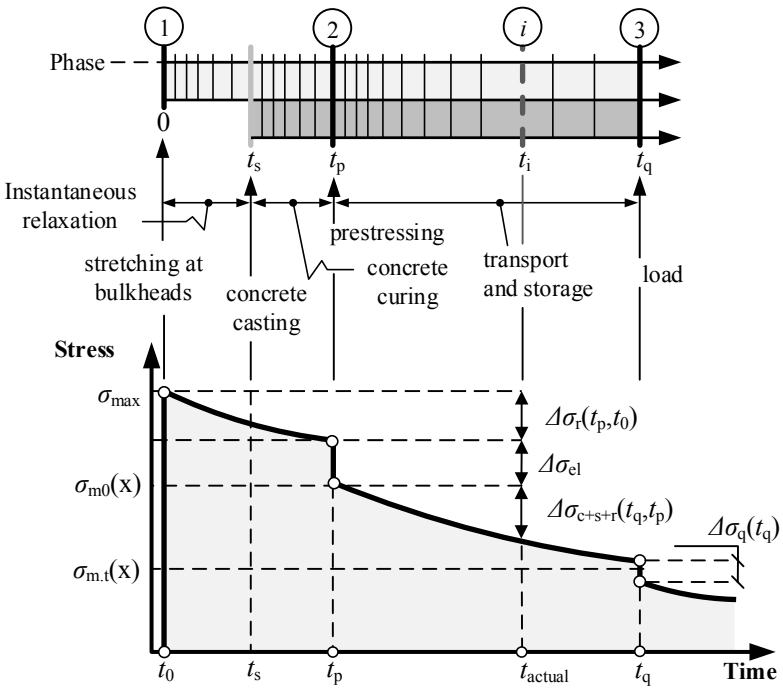

Fig. 2.2. Proposed prestress losses model based on consecutive phases: correlation between absolute time scale and losses due to the execution stage

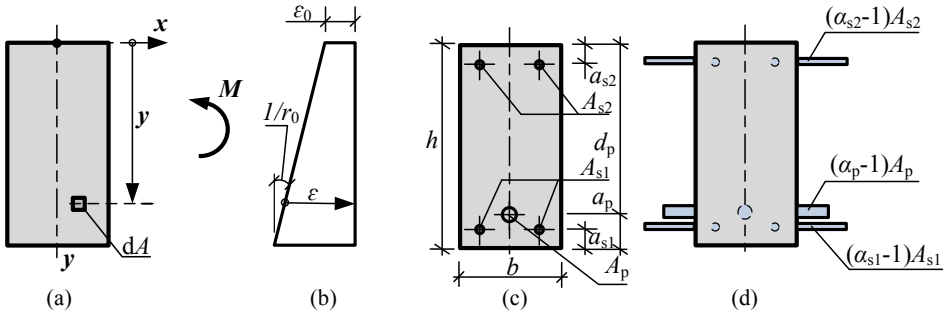

Fig. 2.3. Analysis of strain in a cross-section: generic cross-section and positive M, and y (a); strain diagram (b); an example of the cross-section (c); transformed uncracked cross-section (d)

In this case, prestress force at or immediately after the transfer is given as:

$$P_{\mathrm{m0}} = P_{\max} - A_{\mathrm{p}} \Delta\sigma_{\mathrm{p}}(t_{\mathrm{p}}), \tag{2.13}$$

where P_0 is the initial jacking force.

The instantaneous prestress change (the loss) in prestressing BFRP bar at the time of transfer is (Fig. 2.4):

$$\Delta\sigma_{\mathrm{p}}(t_{\mathrm{p}}) = \left(E_{\mathrm{p}} \varepsilon_0(t_{\mathrm{p}}) + y_{\mathrm{p}} \frac{1}{r_0}(t_{\mathrm{p}}) \right). \tag{2.14}$$

In this respect, the cross-sectional analysis is going to be employed in order to determine two unknowns that define the strain diagram: strain ε_0 at the level of the reference axis and the curvature of the cross-section $1/r_0$ (Fig. 2.3). The strain and stresses at any depth y below the reference axis are given by basic equations:

$$\varepsilon = \varepsilon_0 + y \frac{1}{r_0}; \tag{2.15}$$

$$\sigma = E \left(\varepsilon_0 + y \frac{1}{r_0} \right). \tag{2.16}$$

The stresses and its moments about the reference axis when integrating over the area give the stresses resultants:

$$N_{\mathrm{i}} = \int_A \sigma \mathrm{d}A = E \varepsilon_0 \int_A \mathrm{d}A + E \frac{1}{r_0} \int_A y \mathrm{d}A; \tag{2.17}$$

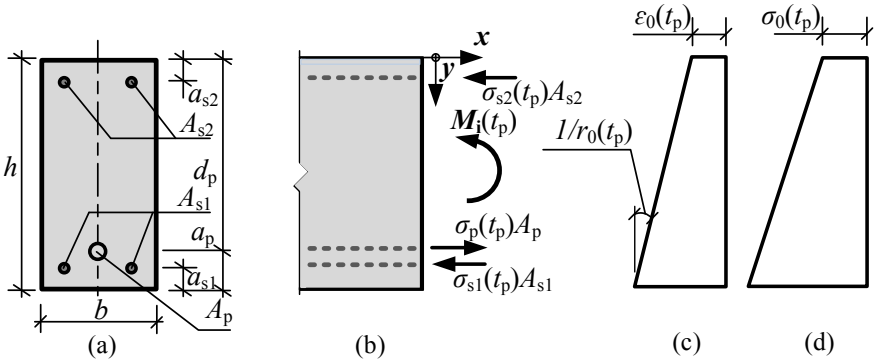

Fig. 2.4. Strain and stresses distribution at prestress transfer: section (a); elevation and forces induced on reinforcement (b); strain (c); stresses in concrete (d)

$$M_{\mathrm{i}} = \int_A \sigma y \mathrm{d}A = E\varepsilon_0 \int_A y \mathrm{d}A + E\frac{1}{r_0}\int_A y^2 \mathrm{d}A \,. \tag{2.18}$$

When the two unknowns ε_0 and $1/r_0$ are calculated from the Eqs. (2.15, 2.16) the internal actions are determined from the stresses using Eqs. (2.17, 2.18). This procedure forms the basis of both the instantaneous and time-dependent losses of prestress within this chapter.

For the instantaneous analysis the linear elastic stress-strain relationship of the concrete and reinforcement shall be applied:

$$\sigma_{\mathrm{c}} = E_{\mathrm{c}}\varepsilon_0; \tag{2.19}$$

$$\sigma_{\mathrm{si}} = E_{\mathrm{si}}\varepsilon_0, \tag{2.20}$$

where σ_{c}, σ_{si} represent the stresses in the concrete, in the i-*th* non-prestressed reinforcing bar (with $i = 1, ..., m_{\mathrm{s}}$).

At this stage, a BFRP bar is stretched between the bulkheads (before casting) at the prestressing bed in the form in which the concrete beam is cast. In this case, prestressing BFRP bar will be subjected to a constant strain, and the stresses in the bar will decrease with time t_{p} to maintain the state of constant strain. This reduction in stresses is known as instantaneous relaxation $\Delta\sigma_{\mathrm{pr}}$ and will be derived from a relationship of the form:

$$\Delta\sigma_{\mathrm{pr}} = E_{\mathrm{pj}}\left(\varepsilon_{\mathrm{pj}} - \varphi_{\mathrm{p}}(t,t_0)\cdot\varepsilon_{\mathrm{pj}}\right), \tag{2.21}$$

where $\varphi_{\mathrm{p}}(t,t_0)$ is relaxation coefficient. Due to the lack of theoretical and experimental data it will be defined based on extensive work by Pouya Banibayat (2015):

$$\varphi_{\mathrm{p}}(t,t_0) = 0.006\ln(t,t_0) + 0.0465 \ . \tag{2.22}$$

Finally, stresses σ_{pi} in the j-th prestressing BFRP bar (with $j = 1,...,m_{\mathrm{p}}$) immediately after prestress transfer:

$$\sigma_{\mathrm{pj}} = E_{\mathrm{pj}}\varepsilon_0 + \Delta\sigma_{\mathrm{pr}} \ . \tag{2.23}$$

After the concrete is hardened, the bond between reinforcement and surrounding concrete is established. The internal axial force and moment resisted by the component materials forming the cross-section and shall be given by equilibrium:

$$\begin{cases} \sum H = 0, \ \int\limits_{A_{\mathrm{c}}} \sigma_{\mathrm{c}} \mathrm{d}A_{\mathrm{c}} + \sum\limits_{i=1}^{m_{\mathrm{s}}} \sigma_{\mathrm{si}} A_{\mathrm{si}} + \sum\limits_{j=1}^{m_{\mathrm{p}}} \sigma_{\mathrm{pj}} A_{\mathrm{pj}} - N_{\mathrm{i}} \\ \sum M^{top} = 0, \ \int\limits_{A_{\mathrm{c}}} y\sigma_{\mathrm{c}} \mathrm{d}A_{\mathrm{c}} + \sum\limits_{i=1}^{m_{\mathrm{s}}} y_{\mathrm{si}} \sigma_{\mathrm{si}} A_{\mathrm{si}} + \sum\limits_{j=1}^{m_{\mathrm{p}}} y_{\mathrm{pj}} \sigma_{\mathrm{pj}} A_{\mathrm{pj}} - M_{\mathrm{i}} \end{cases} . \tag{2.24}$$

The internal axial force N_{i} and moment M_{i} shall be expressed in terms of the actual geometry and elastic modulus of the materials forming the cross-section:

$$N_{\mathrm{i}} = \left(A_{\mathrm{c}} E_{\mathrm{cm}} + \sum_{i=1}^{m_{\mathrm{s}}} A_{\mathrm{si}} E_{\mathrm{si}} + \sum_{j=1}^{m_{\mathrm{p}}} A_{\mathrm{pj}} E_{\mathrm{pj}} \right) \varepsilon_0 +$$

$$\left(S_{\mathrm{c}} E_{\mathrm{cm}} + \sum_{i=1}^{m_{\mathrm{s}}} y_{\mathrm{si}} A_{\mathrm{si}} E_{\mathrm{si}} + \sum_{j=1}^{m_{\mathrm{p}}} y_{\mathrm{pj}} A_{\mathrm{pj}} E_{\mathrm{pj}} \right) \frac{1}{r_0} + \sum_{j=1}^{m_{\mathrm{p}}} A_{\mathrm{pj}} \Delta\sigma_{\mathrm{pr}} \ ; \tag{2.25}$$

$$M_{\mathrm{i}} = \left(S_{\mathrm{c}} E_{\mathrm{cm}} + \sum_{i=1}^{m_{\mathrm{s}}} y_{\mathrm{si}} A_{\mathrm{si}} E_{\mathrm{si}} + \sum_{j=1}^{m_{\mathrm{p}}} y_{\mathrm{pi}} A_{\mathrm{pj}} E_{\mathrm{pj}} \right) \varepsilon_0 +$$

$$\left(I_{\mathrm{c}} E_{\mathrm{cm}} + \sum_{i=1}^{m_{\mathrm{s}}} y_{\mathrm{si}}^2 A_{\mathrm{si}} E_{\mathrm{si}} + \sum_{j=1}^{m_{\mathrm{p}}} y_{\mathrm{pj}}^2 A_{\mathrm{pj}} E_{\mathrm{pj}} \right) \frac{1}{r_0} + \sum_{j=1}^{m_{\mathrm{p}}} y_{\mathrm{pj}} A_{\mathrm{pj}} \Delta\sigma_{\mathrm{pr}} \ . \tag{2.26}$$

In addition, due to aforesaid general assumptions, the cross-sectional properties will be calculated by transforming the section into equivalent areas of the constituent materials. In this case, both reinforcements A_{si} and A_{pj} will be transformed into equivalent areas of concrete:

$$A_{\mathrm{s.eff}} = \alpha_{\mathrm{si}} A_{\mathrm{si}}; \ A_{\mathrm{p.eff}} = \alpha_{\mathrm{pj}} A_{\mathrm{pj}}, \tag{2.27}$$

where $\alpha_{si} = E_{si}/E_{cm}$ is the modular ratio of the i-th steel bar; and $\alpha_{pj} = E_{pj}/E_{cm}$ is the modular ratio of the j-th prestressing BFRP bar (Fig. 2.3).

The computation of axial and flexural stresses in a PC section due to prestressing, and external loads and moments, requires a determination of the area, and the moment of inertia (second moment of area) of the section. The other properties frequently used to facilitate the computation of stresses are determined from these basic properties.

It is assmed that the top fiber of the cross-section is the reference axis. The area, the first moment and the second moment of the transformed area about mention reference axis at prestress transfer t_p will be calculated from:

$$A_0 = A_g + \sum_{i=1}^{m_s}(\alpha_{si} - 1)A_{si} + \sum_{i=1}^{m_p}(\alpha_{pi} - 1)A_{pi}\,; \tag{2.28}$$

$$S_0^{top} = A_g y_c + \sum_{i=1}^{m_s}(\alpha_{si} - 1)A_{si} y_{si} + \sum_{i=1}^{m_p}(\alpha_{pi} - 1)A_{pi} y_{pi}\,; \tag{2.29}$$

$$I_0^{top} = I_g + A_g y_c^{\,2} + \sum_{i=1}^{m_s}(\alpha_{si} - 1)A_{si} y_{si}^{\,2} + \sum_{i=1}^{m_p}(\alpha_{pi} - 1)A_{pi} y_{pi}^{\,2}\,. \tag{2.30}$$

From structural mechanics point of view, Eqs. 2.17, 2.18 could be written in the matrix form:

$$\{R\} = E[H]\{\varepsilon\}\,, \tag{2.31}$$

where $\{R\}$ is a vector of stresses resultants; $[H]$ is area property matrix of the cross-section; $\{\varepsilon\}$ is strain distribution vector. The general form shall be written as:

$$\begin{Bmatrix} N_i \\ M_i \end{Bmatrix} = E\begin{bmatrix} \int \mathrm{d}A & \int y\mathrm{d}A \\ \int y\mathrm{d}A & \int y^2\mathrm{d}A \end{bmatrix}\begin{Bmatrix} \varepsilon_0 \\ 1/r_0 \end{Bmatrix}, \tag{2.32}$$

where dA is the elemental area.

Eq. (2.32) can, therefore, be refined in the more general form:

$$\begin{Bmatrix} N_i \\ M_i \end{Bmatrix}_{t_p} = E_{cm}\begin{bmatrix} A_0 & S_0^{top} \\ S_0^{top} & I_0^{top} \end{bmatrix}\begin{Bmatrix} \varepsilon_0^{top} \\ 1/r_0 \end{Bmatrix}_{t_p}. \tag{2.33}$$

From Eqs. (2.32, 2.33) strain, curvature and the stresses at the top fiber immediately after prestress transfer t_p:

$$\varepsilon_0^{top}(t_\mathrm{p}) = \frac{1}{E_\mathrm{cm}(t_\mathrm{p})}\left(\frac{N_\mathrm{i}(t_\mathrm{p}) - \frac{S_0^{top}}{I_0^{top}} M_\mathrm{i}(t_\mathrm{p})}{A_0 - \frac{\left(S_0^{top}\right)^2}{I_0^{top}}}\right) = \frac{I_0^{top} N_\mathrm{i}(t_\mathrm{p}) - S_0^{top} M_\mathrm{i}(t_\mathrm{p})}{E_\mathrm{cm}(t_\mathrm{p})\left(A_0 I_0^{top} - \left(S_0^{top}\right)^2\right)}\ ; \tag{2.34}$$

$$\frac{1}{r_0}(t_\mathrm{p}) = \frac{1}{E_\mathrm{cm}(t_\mathrm{p})}\left(\frac{M_\mathrm{i}(t_\mathrm{p}) - \frac{S_0^{top}}{A_0} N_\mathrm{i}(t_\mathrm{p})}{I_0^{top} - \frac{\left(S_0^{top}\right)^2}{A_0}}\right) = \frac{A_0 M_\mathrm{i}(t_\mathrm{p}) - S_0^{top} N_\mathrm{i}(t_\mathrm{p})}{E_\mathrm{cm}(t_\mathrm{p})\left(A_0 I_0^{top} - \left(S_0^{top}\right)^2\right)}. \tag{2.35}$$

Stresses in the concrete are to be defined by replacing Eq. (2.35) into Eq. (2.19):

$$\sigma_0^{top}(t_\mathrm{p}) = \frac{I_0^{top} N_i(t_\mathrm{p}) - S_0^{top} M_\mathrm{i}(t_\mathrm{p})}{\left(A_0 I_0^{top} - \left(S_0^{top}\right)^2\right)}. \tag{2.36}$$

Prior application of Eq. (2.34–2.36), we shall combine stresses resultants with prestressing forces into equivalent normal force and a moment:

$$\begin{Bmatrix} N_\mathrm{equivalent} \\ M_\mathrm{equivalent} \end{Bmatrix}_{t_\mathrm{p}} = \begin{Bmatrix} N_\mathrm{i}(t_\mathrm{p}) - \sum P_\mathrm{j}(t_\mathrm{p}) - A_\mathrm{pj}\Delta\sigma_\mathrm{pr}(t_\mathrm{p}) \\ M_\mathrm{i}(t_\mathrm{p}) - \sum P_\mathrm{j}(t_\mathrm{p}) y_\mathrm{pj} - A_\mathrm{pj} y_\mathrm{pj}\Delta\sigma_\mathrm{pr}(t_\mathrm{p}) \end{Bmatrix}, \tag{2.37}$$

where the subscript j refers to the j-th prestressing BFRP bar and y_pj is its distance below the reference axis. In case of stresses, resultants are known, the instantaneous axial strain and curvature at prestress transfer are given by:

$$\begin{Bmatrix} \varepsilon_0^{top} \\ \frac{1}{r_0} \end{Bmatrix}_{t_\mathrm{p}} = \frac{1}{E_\mathrm{cm}(t_\mathrm{p})}\begin{bmatrix} A_0 & S_0^{top} \\ S_0^{top} & I_0^{top} \end{bmatrix}^{-1} \begin{Bmatrix} N \\ M \end{Bmatrix}_\mathrm{equivalent}. \tag{2.38}$$

Having inverted 2x2 matrix Eq. (2.38) is to be refined:

$$\begin{Bmatrix} \varepsilon_0^{top} \\ \frac{1}{r_0} \end{Bmatrix}_{t_\mathrm{p}} = \frac{1}{E_\mathrm{cm}(t_\mathrm{p})\left(A_0 I_0^{top} - \left(S_0^{top}\right)^2\right)}\begin{bmatrix} I_0^{top} & -S_0^{top} \\ -S_0^{top} & A_0 \end{bmatrix} \begin{Bmatrix} N \\ M \end{Bmatrix}_\mathrm{equivalent}. \tag{2.39}$$

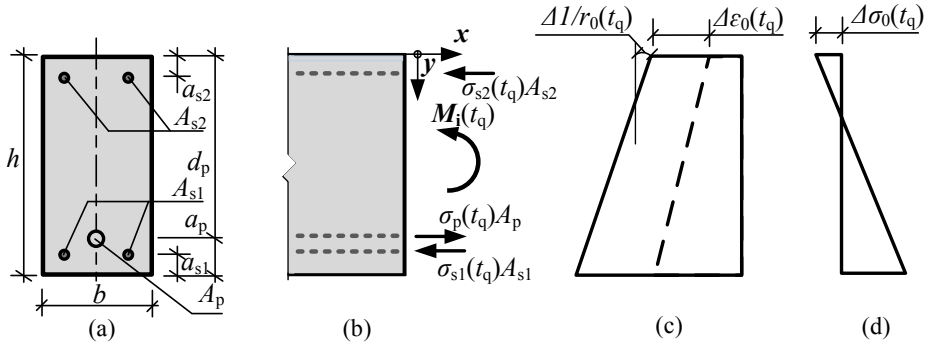

Fig. 2.5. Changes caused by creep, shrinkage, and relaxation after a lifetime of prestress: section (a); elevation and forces induced on reinforcement (b); strain (c); stresses in concrete (d)

The second phase is reflected to the final losses that took place when the full-service load is applied to the flexural PC member (Fig. 2.5). In example, at time t_p when the prestressing force is at a minimum, and the external service load is at a maximum.

The prestressing force at this phase is referred as the effective prestress. Mentioned prestress force after the design life of prestressing ($t_q - t_p$) shall be defined as:

$$P_{mt} = P_{m0} - A_p \Delta\sigma_p(t_q), \tag{2.40}$$

where $\Delta\sigma_p(t_q)$ is the final losses in prestressing BFRP bar.

In order to define the final prestress losses the time analysis of the cross section will use the age-adjusted effective modulus method (AEMM) together with a relaxation approach. The change of strain in the top fiber and the change of the curvature through the duration of prestressing are calculated using the equivalent properties of the age-adjusted transformed section.

Let us refine the Eq. (2.39) accordingly:

$$\begin{Bmatrix} \Delta\varepsilon_0^{top} \\ \Delta\dfrac{1}{r_0} \end{Bmatrix}_{t_q} = \frac{1}{\overline{E}_{c.eff}(t_p)\left(\overline{A}_{eff}\overline{I_{eff}^{top}} - \left(\overline{S_{eff}^{top}}\right)^2\right)} \begin{bmatrix} \overline{I_{eff}^{top}} & -\overline{S_{eff}^{top}} \\ -\overline{S_{eff}^{top}} & \overline{A}_{eff} \end{bmatrix} \begin{Bmatrix} -\Delta N \\ -\Delta M \end{Bmatrix}, \tag{2.41}$$

where $\overline{A}_{eff}$, $\overline{S_{eff}^{top}}$, $\overline{I_{eff}^{top}}$ are the area of the age-adjusted transformed section and its first and second moment about an axis through the top fiber. In the prestress losses

procedure, the strain state is assumed to be held constant through the prestressing time period.

If the total strain is held constant and the strain of creep and shrinkage of the concrete change, then the instantaneous component of strain shall also change by an equal and opposite amount. As the instantaneous strain varies, so the concrete stresses do too so. The concrete stresses on the cross-section are, therefore, allowed to vary due to relaxation. As a result, the internal actions vary, and equilibrium is not maintained. An axial force ΔN and bending moment ΔM as a sum of three terms shall be applied to the cross-section to restore equilibrium:

$$\begin{Bmatrix} \Delta N \\ \Delta M \end{Bmatrix}_{t_q} = \begin{Bmatrix} \Delta N \\ \Delta M \end{Bmatrix}_{c} + \begin{Bmatrix} \Delta N \\ \Delta M \end{Bmatrix}_{s} + \begin{Bmatrix} \Delta N \\ \Delta M \end{Bmatrix}_{r} . \tag{2.42}$$

If the creep were free to occur, the axial strain and curvature would increase over the prestressing time period ($t_q - t_p$) by the amounts $\varphi(t_q,t_p)\varepsilon(t_p)$ and $\varphi(t_q,t_p)1/r(t_p)$. The forces and moments necessary to prevent these deformations shall be determined by:

$$\begin{Bmatrix} \Delta N \\ \Delta M \end{Bmatrix}_{c} = -\left\{ \overline{E}_{c.eff}\varphi(t_q,t_p) \begin{bmatrix} A_c & S_c^{top} \\ S_c^{top} & I_c^{top} \end{bmatrix} \begin{Bmatrix} \varepsilon_0^{top} \\ \dfrac{1}{r_0} \end{Bmatrix}_{t_q} \right\}, \tag{2.43}$$

where A_c, S_c^{top}, I_c^{top} are the area of the concrete and its first and second moment about an axis through the top fiber. The forces and moments necessary to prevent shrinkage are:

$$\begin{Bmatrix} \Delta N \\ \Delta M \end{Bmatrix}_{s} = -\left\{ \overline{E}_{c.eff}\varepsilon_{cs} \begin{bmatrix} A_c \\ S_c^{top} \end{bmatrix} \right\}_{t_q} , \tag{2.44}$$

where ε_{cs} is the free shrinkage over the prestressing time period ($t_q - t_p$).

The forces and moments necessary to prevent the strain due to stress relaxation of prestressing BFRP bar are:

$$\begin{Bmatrix} \Delta N \\ \Delta M \end{Bmatrix}_{r} = \sum \begin{Bmatrix} A_{pi}\Delta\sigma_{pr} \\ A_{pi}y_{pi}\Delta\sigma_{pr} \end{Bmatrix}_{t_q} . \tag{2.45}$$

The change of both the strain and stresses in the top fiber as well as the change of the curvature through the duration of prestressing are calculated:

$$\Delta\varepsilon_0^{top}(t_\mathrm{q}) = \frac{-\overline{S_\mathrm{eff}^{top}}\Delta M(t_\mathrm{q}) + \overline{I_\mathrm{eff}^{top}}\Delta N(t_\mathrm{q})}{\overline{E}_\mathrm{c.eff}(t_\mathrm{q})\left(\overline{A}_\mathrm{eff}\,\overline{I_\mathrm{eff}^{top}} - \left(\overline{S_\mathrm{eff}^{top}}\right)^2\right)}\ ; \tag{2.46}$$

$$\Delta\frac{1}{r}(t_\mathrm{q}) = \frac{-\overline{S_\mathrm{eff}^{top}}\Delta N(t_\mathrm{q}) + \overline{A}_\mathrm{eff}\Delta M(t_\mathrm{q})}{\overline{E}_\mathrm{c.eff}(t_\mathrm{q})\left(\overline{A}_\mathrm{eff}\,\overline{I_\mathrm{eff}^{top}} - \left(\overline{S_\mathrm{eff}^{top}}\right)^2\right)}\ ; \tag{2.47}$$

$$\Delta\sigma^{top}(t_\mathrm{q}) = \frac{\overline{I_\mathrm{eff}^{top}}\Delta N(t_\mathrm{p}) - \overline{S_\mathrm{eff}^{top}}\Delta M(t_\mathrm{p})}{\left(\overline{A}_\mathrm{eff}\,\overline{I_\mathrm{eff}^{top}} - \left(\overline{S_\mathrm{eff}^{top}}\right)^2\right)}\ . \tag{2.48}$$

The resultants of the creep and shrinkage induced internal restraining forces on the concrete and stress relaxation on the BFRP bar are an increment of the axial force and an increment of the moment about the reference axis:

$$\Delta N(t_\mathrm{q}) = \Delta N_\mathrm{c} + \Delta N_\mathrm{s} + \Delta N_\mathrm{r} = \overline{E}_\mathrm{c.eff}[\varphi(t_\mathrm{q},t_\mathrm{p})\left(A_\mathrm{c}\varepsilon_0^{top}(t_\mathrm{p}) + S_\mathrm{c}^{top}\frac{1}{r_0}(t_\mathrm{p})\right) + \varepsilon_\mathrm{sh}(t_\mathrm{q})A_\mathrm{c}] + A_\mathrm{pi}\Delta\sigma_\mathrm{pr}(t_\mathrm{q})\ ; \tag{2.49}$$

$$\Delta M(t_\mathrm{q}) = \overline{E}_\mathrm{c.eff}[\varphi(t_\mathrm{q},t_\mathrm{p})\left(S_\mathrm{c}^{top}\varepsilon_0^{top}(t_\mathrm{q}) + I_\mathrm{c}^{top}\frac{1}{r_0}(t_\mathrm{q})\right) + \varepsilon_\mathrm{cs}(t_\mathrm{q})S_\mathrm{c}^{top}] + A_\mathrm{pi}y_\mathrm{pi}\Delta\sigma_\mathrm{pr}\ ; \tag{2.50}$$

$$\Delta\sigma(t_\mathrm{q}) = E_\mathrm{p}\left(\Delta\varepsilon_0^{top}(t_\mathrm{q}) + y_\mathrm{p}\Delta\frac{1}{r_0}(t_\mathrm{q})\right). \tag{2.51}$$

In case of *the third phase*, due to some applied load cross-section is cracked. Axial force of cracked cross-section equilibrium Eqs. (2.25, 2.26) can be re-written as:

$$N_\mathrm{i} = \left(A_\mathrm{cc}E_\mathrm{cm}\varepsilon_0 + S_\mathrm{cc}E_\mathrm{cm}\frac{1}{r_0}\right) + \left(\sum_{i=1}^{m_\mathrm{s}}A_\mathrm{si}E_\mathrm{si} + \sum_{j=1}^{m_\mathrm{p}}A_\mathrm{pj}E_\mathrm{pj}\right)\varepsilon_0 + \left(\sum_{i=1}^{m_\mathrm{s}}y_\mathrm{si}A_\mathrm{si}E_\mathrm{si} + \sum_{j=1}^{m_\mathrm{p}}y_\mathrm{pj}A_\mathrm{pj}E_\mathrm{pj}\right)\frac{1}{r_0} + \sum_{j=1}^{m_\mathrm{p}}A_\mathrm{pj}\Delta\sigma_\mathrm{pr}\ . \tag{2.52}$$

The internal moment M_i resisted by the cross-section at time t_q can be expressed n a similar manner.

Regarding this phase, it is assumed that the axial force and bending moment about the reference axis (N_{ext} and M_{ext}) produce tension in the bottom of the cross section and compression at the top of the section. From this standpoint Eq. (2.52) can be expressed as:

$$N_{\text{ext}} - \sum_{j=1}^{m_{\text{p}}} A_{\text{pj}} \Delta\sigma_{\text{pr}} = \int_{A_{\text{cc}}} E_{\text{cm}} \left(\varepsilon_0 + y \frac{1}{r_0} \right) \mathrm{d}A + \left(\sum_{i=1}^{m_{\text{s}}} A_{\text{si}} E_{\text{si}} + \sum_{j=1}^{m_{\text{p}}} A_{\text{pj}} E_{\text{pj}} \right) \varepsilon_0 + \left(\sum_{i=1}^{m_{\text{s}}} y_{\text{si}} A_{\text{si}} E_{\text{si}} + \sum_{j=1}^{m_{\text{p}}} y_{\text{pj}} A_{\text{pj}} E_{\text{pj}} \right) \frac{1}{r_0} . \tag{2.53}$$

With respect to bending moment cross section equilibrium it can be expressed:

$$M_{\text{ext}} - \sum_{j=1}^{m_{\text{p}}} y_{\text{pj}} A_{\text{pj}} \Delta\sigma_{\text{pr}} = \int_{A_{\text{cc}}} E_{\text{cm}} \left(\varepsilon_0 + y \frac{1}{r_0} \right) y \mathrm{d}A + \left(\sum_{i=1}^{m_{\text{s}}} y_{\text{si}} A_{\text{si}} E_{\text{si}} + \sum_{j=1}^{m_{\text{p}}} y_{\text{pj}} A_{\text{pj}} E_{\text{pj}} \right) \varepsilon_0 + \left(\sum_{i=1}^{m_{\text{s}}} (y_{\text{si}})^2 A_{\text{si}} E_{\text{si}} + \sum_{j=1}^{m_{\text{p}}} (y_{\text{pj}})^2 A_{\text{pj}} E_{\text{pj}} \right) \frac{1}{r_0} . \tag{2.54}$$

Dividing Eq. (2.54) by Eq. (2.53) it derives:

$$\frac{M_{\text{ext}} - \sum_{j=1}^{m_{\text{p}}} y_{\text{pj}} A_{\text{pj}} \Delta\sigma_{\text{pr}}}{0 - \sum_{j=1}^{m_{\text{p}}} A_{\text{pj}} \Delta\sigma_{\text{pr}}} = \frac{\int_{A_{\text{cc}}} E_{\text{cm}} \left(\varepsilon_0 + y \frac{1}{r_0} \right) y \mathrm{d}A + \left(\sum_{i=1}^{m_{\text{s}}} y_{\text{si}} A_{\text{si}} E_{\text{si}} + \sum_{j=1}^{m_{\text{p}}} y_{\text{pj}} A_{\text{pj}} E_{\text{pj}} \right) \varepsilon_0}{\int_{A_{\text{cc}}} E_{\text{cm}} \left(\varepsilon_0 + y \frac{1}{r_0} \right) \mathrm{d}A + \left(\sum_{i=1}^{m_{\text{s}}} A_{\text{si}} E_{\text{si}} + \sum_{j=1}^{m_{\text{p}}} A_{\text{pj}} E_{\text{pj}} \right) \varepsilon_0} + \frac{\left(\sum_{i=1}^{m_{\text{s}}} (y_{\text{si}})^2 A_{\text{si}} E_{\text{si}} + \sum_{j=1}^{m_{\text{p}}} (y_{\text{pj}})^2 A_{\text{pj}} E_{\text{pj}} \right) \frac{1}{r_0}}{\left(\sum_{i=1}^{m_{\text{s}}} y_{\text{si}} A_{\text{si}} E_{\text{si}} + \sum_{j=1}^{m_{\text{p}}} y_{\text{pj}} A_{\text{pj}} E_{\text{pj}} \right) \frac{1}{r_0}} . \tag{2.55}$$

Dividing the top and bottom of the right side of Eq. (2.55) by $1/r_0$ and also assuming that $y = y_{\text{n}} = -\varepsilon_0/1/r_0$, the equation above for rectangular cross-section of width b becomes:

$$\frac{M_{\text{ext}}-\sum_{j=1}^{m_{\text{p}}} y_{\text{pj}} A_{\text{pj}} \Delta\sigma_{\text{pr}}}{0-\sum_{j=1}^{m_{\text{p}}} A_{\text{pj}} \Delta\sigma_{\text{pr}}} = \frac{\int_{y=0}^{y=y_{\text{n}}} E_{\text{cm}}\left(-y_{\text{n}}+y\right) b y \mathrm{d}y - \left(\sum_{i=1}^{m_{\text{s}}} y_{\text{si}} A_{\text{si}} E_{\text{si}} + \sum_{j=1}^{m_{\text{p}}} y_{\text{pj}} A_{\text{pj}} E_{\text{pj}}\right) y_{\text{n}}}{\int_{y=0}^{y=y_{\text{n}}} E_{\text{cm}}\left(-y_{\text{n}}+y\right) b \mathrm{d}y + \left(\sum_{i=1}^{m_{\text{s}}} A_{\text{si}} E_{\text{si}} + \sum_{j=1}^{m_{\text{p}}} A_{\text{pj}} E_{\text{pj}}\right) y_{\text{n}}} + \frac{\left(\sum_{i=1}^{m_{\text{s}}} \left(y_{\text{si}}\right)^2 A_{\text{si}} E_{\text{si}} + \sum_{j=1}^{m_{\text{p}}} \left(y_{\text{pj}}\right)^2 A_{\text{pj}} E_{\text{pj}}\right)}{\left(\sum_{i=1}^{m_{\text{s}}} y_{\text{si}} A_{\text{si}} E_{\text{si}} + \sum_{j=1}^{m_{\text{p}}} y_{\text{pj}} A_{\text{pj}} E_{\text{pj}}\right)} . \tag{2.56}$$

In order to estimate y_{n}, Eq. (2.56) may be solved by the employment of simple trial and error search. Having solved y_{n}, the area, the first and the second moment of area of the compressive concrete above the neutral axis around the top surface of the cross-section shall be determined:

$$A_{\text{cc}} = b y_{\text{n}} + \sum_{i=1}^{m_{\text{s}}} (\alpha_{\text{si}} - 1) A_{\text{si}}^{top} + \sum_{i=1}^{m_{\text{s}}} (\alpha_{\text{si}}) A_{\text{si}}^{btm} + \sum_{i=1}^{m_{\text{p}}} (\alpha_{\text{pi}}) A_{\text{pi}} ; \tag{2.57}$$

$$S_{\text{cc}}^{top} = \frac{b y_{\text{n}}^2}{2} + \sum_{i=1}^{m_{\text{s}}} (\alpha_{\text{si}} - 1) A_{\text{si}}^{top} y_{\text{si}} + \sum_{i=1}^{m_{\text{s}}} (\alpha_{\text{si}}) A_{\text{si}}^{btm} y_{\text{si}} + \sum_{i=1}^{m_{\text{p}}} (\alpha_{\text{pi}}) A_{\text{pi}} y_{\text{pi}} ; \tag{2.58}$$

$$I_{\text{cc}}^{top} = \frac{b y_{\text{n}}^3}{12} + b y_{\text{n}} \left(\frac{y_{\text{n}}}{2}\right)^2 + \sum_{i=1}^{m_{\text{s}}} (\alpha_{\text{si}} - 1) A_{\text{si}}^{top} a_{\text{si}}{}^2 + \sum_{i=1}^{m_{\text{s}}} (\alpha_{\text{si}}) A_{\text{si}}^{btm} d^2 + \sum_{i=1}^{m_{\text{p}}} (\alpha_{\text{pi}}) A_{\text{pi}} y_{\text{pi}}^2 . \tag{2.59}$$

From notation point of view, the following sign convention were assumed in this chapter: 1) axial force N is positive when tensile; 2) according horizontal direction, a bending moment M that produces tension at the bottom fiber and the related curvature $1/r_0$ are positive; 3) tensile stress σ and strain ε are positive; 4) the shrinkage of concrete ε_{cs} is a negative quantity; 5) the loss of tension in the prestressed bar due to stress relaxation, creep and shrinkage of concrete is generally a negative quantity; 6) the number of prestressed bars (BFRP) and non-prestressed steel bars are denoted as m_{p} and m_{s}, respectively. The subscript "s" is used for steel bars and $i = 1, \ldots, m_{\text{s}}$. Likewise, the subscript "p" represents prestressed BFRP bar and $i = 1, \ldots, m_{\text{p}}$. All symbols are defined in the thesis where they first arized.

2.2.2. Calculation Algorithm

Herewith aforesaid calculation method for effective prestress force estimation including instantaneous and time-dependent losses by means of relaxation approach of BFRP is described in the flowchart as follows. This procedure forms the basis of analysis of prestress losses depending on the input data and actual phase considered: instantaneous losses due to stress relaxation of BFRP at stretching ($t_p - t_0$); time-dependent losses ($t_q - t_p$); and applied external short-term static service loading (t_q).

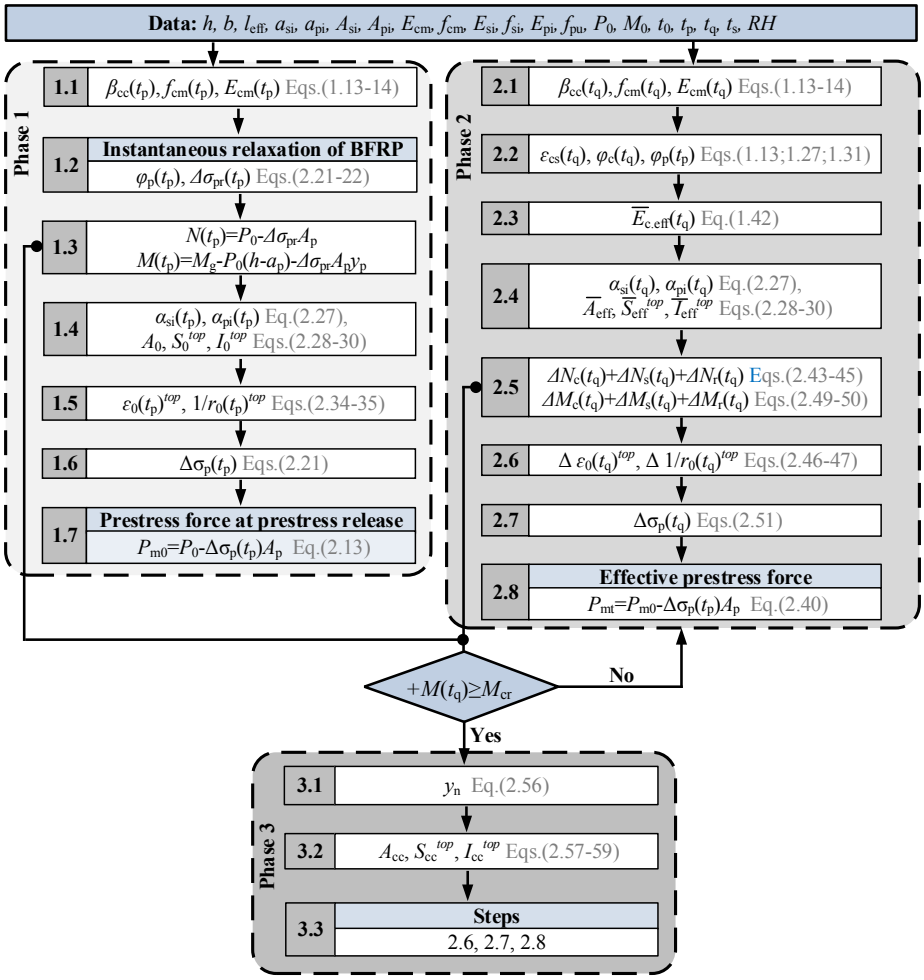

Fig. 2.6. Calculation algorithm for instantaneous losses of prestressed bars at prestress release from bulkheads to the concrete beam

2.3. Analysis of Serviceability Behaviour

2.3.1. Proposal for Deflection Analysis

In many PC structures, it is unlikely that the service load will be applied during the design life of the structural member. It is, therefore, reasonable to design PC members in such a way that cracking will occur under full-service load. The calculation of the deflection becomes a matter of practical importance due to a potential reduction of flexural stiffness after cracking that may result in an increase of deflection, but which still may be sufficient to exceed the acceptable serviceability limit state.

From a regulation point of view, the flexural stiffness of PC member can be taken into account in the estimation of deflection either by the well-known effective moment of inertia, originally developed by Branson (1968) (ACI 440.4R 2004) or by CEN 2004 and *fib* 2013 proposals based on effective elastic modulus of concrete approaches.

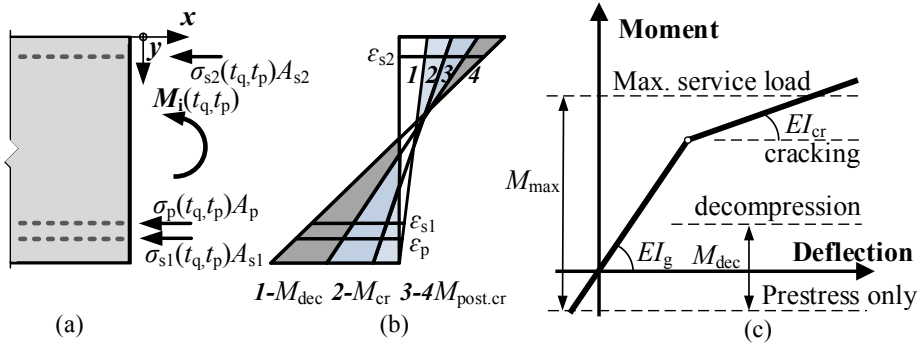

Fig. 2.7. Typical variables of components of flexural prestressed concrete member: elevation and forces induced on reinforcement (a); strain distribution depending on each stage (b); moment-deflection diagram (c)

From PC point of view, a major assumption that signifies the transition between the performance of the member complying with principles of PC and the principles of RC will be explained.

Let the parameters $\left\{\varepsilon_0^{top},\ 1/r_0\right\}$ define the initial strain distribution in a PC cross-section, and the section is subjected to a normal force N combined with a moment M at the top fiber producing cracking. At some point, the stress in concrete is zero at the extreme fiber, but not in prestressing reinforcement due to decompression effect (Fig. 2.7). Thus, the strain parameters due to $\{N, M\}$ are the sum of the strain parameters due to decompression forces $\{N, M\}_{\mathrm{dec}}$ and those due to cracking forces $\{N, M\}_{\mathrm{cr}}$. The values of former ones are equal and opposite to

the resultants of stresses $\sigma_c(t)$ on the concrete and α times this stress on prestressing reinforcement. The decompression forces are given by:

$$\begin{Bmatrix} N \\ M \end{Bmatrix}_{\text{dec}} = -\begin{bmatrix} A_0 & S_0^{top} \\ S_0^{top} & I_0^{top} \end{bmatrix} \begin{Bmatrix} \varepsilon_0^{top} \\ 1/r_0 \end{Bmatrix}_{t_p} . \tag{2.60}$$

Also, the cracking forces will be:

$$\begin{Bmatrix} N \\ M \end{Bmatrix}_{\text{cr}} = \begin{Bmatrix} N \\ M \end{Bmatrix}_{t_p} - \begin{Bmatrix} N \\ M \end{Bmatrix}_{\text{dec}} , \tag{2.61}$$

where $\{N, M\}_{t_p}$ is taken from Eq. (2.33).

Hence the total strain at the midlength cross–section is determined as the sum of strains due to decompression forces and the strain due to cracking forces:

$$\begin{Bmatrix} \varepsilon_0^{top} \\ 1/r_0 \end{Bmatrix}_{\text{mid}} = \begin{Bmatrix} \varepsilon_0^{top} \\ 1/r_0 \end{Bmatrix}_{\text{dec}} + \begin{Bmatrix} \varepsilon_0^{top} \\ 1/r_0 \end{Bmatrix}, \tag{2.62}$$

where $\{\varepsilon_0^{top}, 1/r_0\}$ is given by Eq. (1.54) (CEN 2004), but in the more general form:

$$\begin{Bmatrix} \varepsilon_0^{top} \\ 1/r_0 \end{Bmatrix} = \begin{Bmatrix} \varepsilon_0^{top} \\ 1/r_0 \end{Bmatrix}_{\text{I}} \cdot (1-\zeta) + \begin{Bmatrix} \varepsilon_0^{top} \\ 1/r_0 \end{Bmatrix}_{\text{II}} \cdot \zeta . \tag{2.63}$$

In general, taking into account such approach would lead to risk mitigation with respect to deflection analysis of BFRP-PC flexural members in order to avoid overestimation or underestimation of deflection values by design code provisions.

From proposed model point of view (Section 2.2.2), algorithm of deflection calculation would depend on the phase considered: 1) in case of decompression (t_p), curvature to be calculation from Eq.2.35 (step 1.5); 2) under applied load (t_q), the curvature to be calculated through the step 2.6 from Eq. 2.47. The final deflection shall be estimated as the sum of the members depending on actual phase (cf. Eq. 1.55). According to Gribniak *et al.* (2013) deflection shall be estimated with respect to curvature assessed and in general form:

$$\delta = k \cdot 1/r_0 \cdot l_0^2 , \tag{2.64}$$

where k is the factor due to the type of loading; l_0 is the effective span of the beam.

2.3.2. Proposal for Calculation of Crack Width

Cracking is an inevitable and natural phenomenon in RC and even in PC flexural members. The check of crack width can be performed either in a simplified way through the verification of the requirements stated in the appropriate design codes or through a direct calculation.

In general, the calculation of crack width for PC structural members follows the procedure and the formulas given for RC members in Chapter 1.5, but this approach might not reflect to the prestress force effect. Basically, the crack width could be determined from the difference between the strain in the reinforcement and the strain in the concrete between cracks:

$$w_k = \int_{S_r} (\varepsilon_{sx} - \varepsilon_{cx}) dx \,, \tag{2.65}$$

where s_r is the distance between the adjacent cracks while ε_{sx}, ε_{cx} are the real strains in the reinforcement and concrete along the length x, respectively.

From PC element point of view, let us assume that $\varepsilon_{sx} = \varepsilon_p(t_q)$ having assessed $\Delta\sigma_{c+s+r}(t_q)$ as per Eq. (2.51). Also, due to decompression force effect $\varepsilon_{cx} = \varepsilon_{p.dec}$. In this case, $\varepsilon_{p.dec}$ is the strain in prestressing tendon starting from the state of decompression immediately prior to initiation of the first crack.

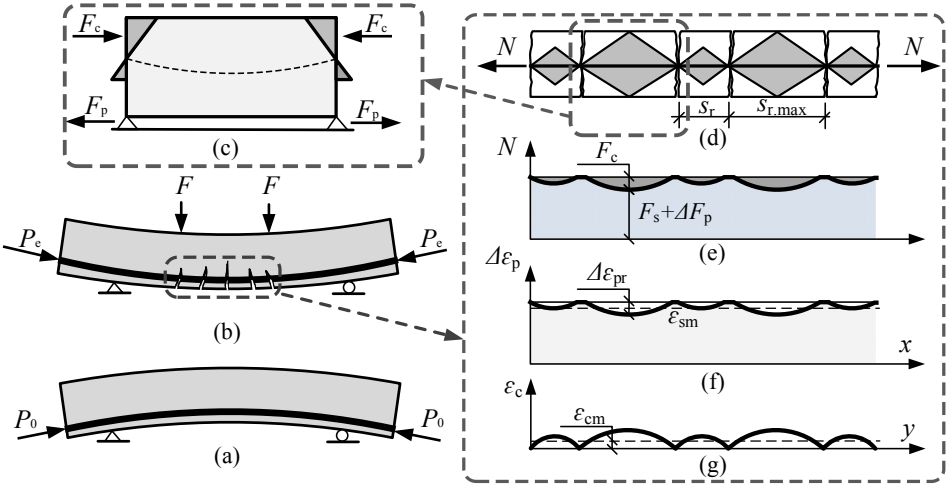

Fig. 2.8. Force and strain distribution at the stabilized cracking phase: under initial prestress (a); under service load (b); force resultant distribution (c); flexural element subjected to axial tension (d); transfer of load (e); strain in reinforcement (f); strain in concrete (g)

In order to perform as much as the realistic behavior of flexural PC element, the last but not least parameter in Eq. (2.66) shall be taken into account is the strain of the concrete due to shrinkage $\varepsilon_{cs}(t_q)$. Therefore, Eq. (2.65) shall be rewritten as:

$$w_k = s_{r.max} \cdot \left(\varepsilon_p(t_q) - \varepsilon_{p.dec}(t_p) - \varepsilon_{cs}(t_q)\right), \tag{2.66}$$

where $\varepsilon_{p.dec}(t_p)$ shall be estimated considering Eqs. (2.34, 2.35):

$$\varepsilon_{p.dec}(t_p) = \varepsilon_0^{top}(t_p) + y_p \cdot \frac{1}{r_0}(t_p). \tag{2.67}$$

Free shrinkage strain $\varepsilon_{cs}(t_q)$ shall be estimated based on Eq. (1.27).

With regard to crack width estimation, the most critical issue is to calculate maximum cracking spacing, because existing regulation formula (Eq. 1.61) belong mostly on many empirical constants. In this case, due to decompression over the cross-section, the maximum crack spacing will be given by:

$$s_{r.max} = 1/3(h - y_n), \tag{2.68}$$

where y_n is going to be estimated from Eq. (2.56).

In order to use Eq. (1.61) for maximum crack spacing estimation, factor k_b shall be known since bond performance plays a key role in determining the crack width and, however, a mentioned factor might be necessary to account for the different bond characteristics of the different FRP materials. Based on experimental work by Atutis *et al*. (2017). Analysis of the impact of the factor that accounts for the degree of the bond at the interface (contact) of FRP bars and concrete. According to Eq. (1.61) this coefficient varies from 0.8 to 1.6 due to the type of reinforcement and is recommended for steel reinforcement but not taking into account FRP. In regard to Eq. (1.59) this factor varies between 0.8 and 1.4 and shall be used for FRP applications depending on the type of FRP material. Once the GFRP is used, the width of crack values are in a good agreement with experimental results when k_b is equal to 0.3 based Eq. (1.61). Good agreement was found among calculated and experimental values of crack widths as well taking into account Eq. (1.59) when coefficient k_b is equal to 0.85. In regard to BFRP, this factor should be determined experimentally due to lack of information within scientific literature and design codes.

2.4. Conclusions of Chapter 2

Within this Chapter, the following conclusions can be drawn:

1. The constitutive equation was proposed in order to perform an evaluation of stress relaxation history at loading under ε = constant. It was observed that stress relaxation in BFRP is a manifestation of viscoelasticity and based on Maxwell's rheological model can be mathematically approximated by a sum of exponentials. Unlike design code provisions, proposed equation produces the more realistic character of stress relaxation curve by having an increasing downward slope over the times, while empirical formulas from design codes provide the straight line of FRP stress relaxation curves. Therefore, it cannot estimate even the instantaneous stress relaxation accurately. In order to prove the proposed approach, experimental tests of BFRP stress relaxation are utmost important.
2. In the present work, the prestress losses (instantaneous and time-dependent), cross-sectional stress-strain, deflection and cracking behavior of PC members reinforced with BFRP bars are described as an interrelated process. This complex approach allows to avoid disappearing of prestressing effect, such as camber or strain of decompression, as a base point and the principle of serviceability analysis of PC members.
3. The proposed calculation method for effective prestress force takes into account stress relaxation behavior of BFRP prestressing bars that allow to evaluate prestress losses accurately depending on certain consecutive stage: BFRP stretching at the bulkhead (reaction frame); release of prestressing from the bulkhead to concrete; at external loading applied, etc. The proposed method shall be verified by experimental measurements.
4. The proposed calculation method for deflection estimation of PC members with BFRP tendons is based on the major assumption that signifies the transition between the performance of the member complying with principles of PC and RC members. This method provides a technique that allows to expand existing design code equations by taking into account decompression effect. Unlike this approach, proposed calculation method based on stress relaxation approach might be used as an alternative one due to aforesaid considerations. The analytical analysis shall be proved by experimental tests.
5. The proposed method for crack width analysis allows performing realistic cracking behavior of flexural PC members considering the effect of decompression and shrinkage of concrete: a strain in prestressing tendon starting from the state of decompression immediately prior to initiation of

the first crack and strain of the concrete due to free shrinkage. This would allow to avoid calculation errors caused by many empirical constants used in a manner similar to that for formulas applicable for RC members. This analytical approach shall be granted by experimental test.

3

Experimental Tests and Validation of Theoretical Models of Prestressed Elements

This chapter provides information on detailed experimental program with a major focus to perform the tests of stress relaxation of BFRP and PC beams internally prestressed with BFRP bars. A few designs of anchorage have been used, and preliminary experiments were employed in order to find a successful grip and, finally, to determine the actual tensile strength of BFRP bars. Experimental results on tests of PC beams having a certain degree of prestressing level are reported. In general, a major interest of experimental investigation was to evaluate serviceability conditions of PC beams internally prestressed with BFRP bars.

An experimental program was split in two parts: 1) full-scale PC beams tested under static four-point load; 2) and stress relaxation of BFRP bars with respect to the constant strain. Three levels of prestress 40%, 45% and 55% of the tensile strength was selected. Twelve PC beams (three groups of four specimens) and nine (three groups of three specimens) were examined and the results are presented in the text below.

This chapter includes the material presented in journal publications by Atutis *et al*. (2017), Atutis *et al.* (2018a), Atutis *et al.* (2018b).

3.1. Experimental Test of Basalt Fiber Reinforced Polymers Anchorage

In general, the design of suitable anchorage system either temporary or permanent presents a major difficulty for FRP bars, as the brittle reinforcement, is able to fail in the grip itself due to the combined effects of shear and compressive stress added to the tensile strength. In order to use FRP bars properly, the stress that occur in the interface between the anchorage and the bar has to be suitably managed. Considering the behavior of the FRP bar, the anchorage must be durable enough. An ideal anchorage solution shall be based on gradually transmitted tension stress from the bar to grip system. Thus further experiments are utmost necessary.

Tests on three concepts were made with respect to: 1) composite grip commercially known as Blocking system carbo (Fig 3.1a, b). This mechanical anchorage relies on the friction between the reinforcing bar and the inner anchorage surface, where compressive stress perpendicular to the bar is applied. Blocking system carbo is composed by steel barrel (class C40) (∅ = 60 mm) and gripping longitudinally constant cone wedges of technopolymer reinforced with glass fibers (density 1.64 g/cm^3, tensile strength 200 MPa); 2) conical grip system (Fig. 3.1c). This system consists of longitudinally curved wedges which transfer compressive stress to the back of the anchorage, where the tensile stresses are less; and 3) straight steel tube-sleeve system (Fig. 3.1e). In this bonded anchor an outer sleeve tube surrounds a resin by bonding it to anchor the FRP bar.

The first system was delivered by the company *Sireg S.p.A.* (Italy), and the remaining two systems were designed and manufactured by the author at the laboratory of Vilnius Gediminas Technical University (VGTU). Conical grip system was designed of two steel elements composed by threated parts in order to turn off steel cones without interface to the surface of BFRP specimen. Turning arm was constructed in order to maintain the anchorage prior to and after the test. Steel tube system was designed and constructed based on the required anchorage length of the specimen. The system was composed of ∅ = 33.7 mm and 300 mm length steel tube (class S355) and end plates in order to keep epoxy resin and to avoid any leakage of it.

Static tension-tension tests were performed according to ACI440 (2004) requirements (Fig. 3.1d). Experiments have shown that considering the 1st and the 2nd concepts it was not possible to determine the tensile strength of BFRP bars due to its slippage out from griped carbon and steel wedges or failure at the anchorage – bar interface. The shear fracture was initiated and observed. While considering the 3rd concept, the tensile strength of BFRP was determined by rupture of the bars without any epoxy debonding (Fig. 3.2 g, h). In this case, failure occurred through plastic instability, and the fracture pattern took place in the central portion of the BFRP bar with necking of the fibers.

Fig. 3.1. Anchorage types for basalt fiber reinforced polymer bars tensile strength test: blocking system carbo (Sireg S.p.A) (a) and (b); conical grip system (Atutis *et. al.* 2015) (c); trial assembly of conical grip system (d); sleeve anchor (Atutis *et al.* 2015) (e); bar specimens (f); tensile-tensile test of bar specimen (g); fracture pattern of the bar (h)

3.2. Experimental Test of Prestressed Concrete Beams

In general, considering previously discussed prestressing methods (Section 1.1.1), and based on experimental work regarding the anchorage above a new internal prestressing system was designed in order to construct the beams for experimental

tests with respect to maintenance of the effective prestress of flexural concrete beams prestressed with BFRP bars. The principle of the system was to conduct a certain level of prestressing by means of control of prestressing force reduction and its impact to the flexural stiffness of PC beams in particular to cambers, deflections, crack widths and expected fracture pattern (failure type).

3.2.1. Jacking Setup

Firstly, BFRP tendons were connected with pretensioning steel rebars through special coupling type mounting details with internal threads, where ends of the BFRP are anchored in the steel tubes with external threads for locknut and passes fixed reaction frame supports, casting bed and formwork on the top (Atutis *et al.* 2018b). Later, BFRP were jacked to the certain level of prestress by a hydraulic jack, then measured by dynamometer and released from external reaction frame to the beams. Prior to release, beam specimens have to observe minimum 70 percent of the concrete compressive strength and the epoxy adhesive has to be fully cured in BFRP anchors due to prestress is transferred to the RC beam based on the adhesive bond of FRP bar and anchor tube interfaced by epoxy resin. Prestressing force is measured and controlled by dynamometers at the end of the reaction frame. The principle of preparation of PC beams and main consecutive phases are shown in Figures 3.2 and 3.3. Specimens are divided into certain series depending on different prestress levels 40%, 45%, and 55% of the ultimate strength f_{fu} of the BFRP bars. Later, all PC BFRP beams are to be tested based on static four-point bending scheme and results are presented further in this paper.

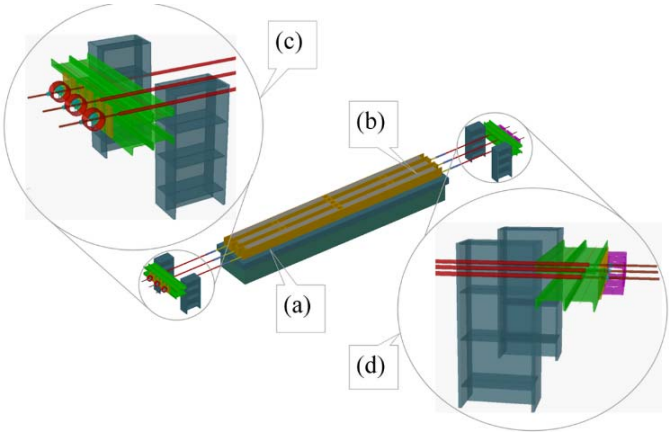

Fig. 3.2. Principle of fabricated beam specimens based on prestressing bed (bulkheads): prestressing bed L = 7000 mm (a); beam specimen $H \times B$ = 300×150 mm, L = 3200 mm (b); fixed end support – bulkhead for measurement of applied load (c); jacking support – bulkhead support frame for application of the initial prestress (d)

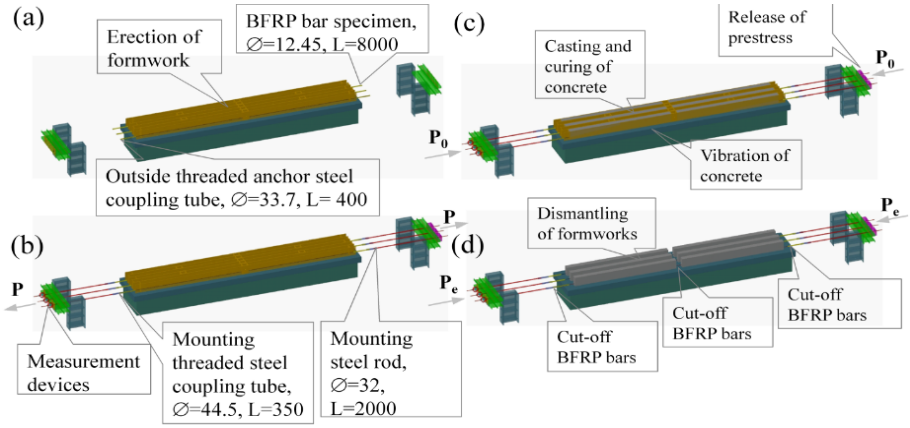

Fig. 3.3. The main consecutive phases of prestress concrete beams: erection and installation of basalt fiber reinforced polymer bars (a); stretching of the bars into bulkheads (b); casting and curing of concrete (c); prestress release to concrete (d)

3.2.2. Beam Specimens

A total of twelve large-scale PC beams (denoted as SSI–1 to SSI–12), and one control RC beam (denoted as S-1) were designed, cast and tested by the static load. One concrete composition was assumed in the experimental program (Table 3.1). In regard to the reinforcement of the beams, BFRP reinforcement, commercially known as *RockBar Composite* bars were used (Fig. 3.1f). Mechanical characteristics of the bars were estimated by static tension – tension test (Fig. 3.4a). Concrete cylinders (∅150 mm, h = 300 mm) cubes (100×100×100 mm) and prisms (100×100×400 mm) were cast for each concreting patch and were tested at the day PC beams static bending tests (Figs. 3.4b–3.4c). Elastic modulus, as well as tensile and compressive strengths, were evaluated. In regard to local laboratory premises beams were specified by original notations. The letter "S" refers to the type of member ("Sija"="Beam") and letters "SSI" refers to the reinforcing method ("sija įtemptoji bandoma statine apkrova" = "prestressed beam tested by static load"). Experimental program is introduced in Tables 3.1 and 3.2.

Table 3.1. Concrete mixture composition for 1 m^3

Ingredients	Amount, kg/ m^3
Sand (0–4)	730
Crushed aggregate (5–8, 11–16)	1100
Cement CEM I 42.5 N	595
Water	220

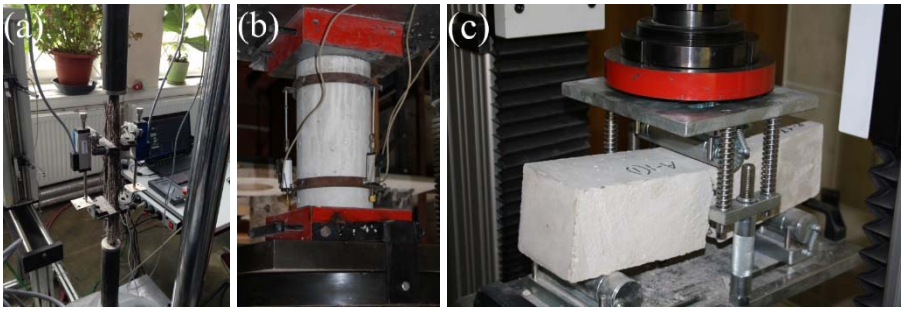

Fig. 3.4. Experimental tests of material properties: tension – tension test of basalt fiber reinforced polymer bars (a); cylinder compressive strength test of concrete (b); tensile strength test of concrete prisms (c)

At the beginning of experimental program, reinforcement cages were designed and constructed as well as the appropriate concrete mixture was calculated. Due to the high tensile strength of BFRP bars, concrete mixture was designed for concrete strength above 40 MPa. (Table 3.1). The concrete had a 16 mm maximum aggregate size. The water/cement ratio was about 0.37, and the cement content was 450 kg/m^3. Each beam series was split in 2 concrete batches. Twelve concrete cylinders were cast from each batch. 6 cylinders were tested in compression prior release of the prestressing stress and six on the day of testing, according to CEN (2004) requirements. The elastic modulus of the concrete was evaluated on the day of testing of the beams. The average compressive strength of the concrete ranged from 40.21 to 46.01 MPa among the beams tested.

At first, formwork and constructive steel reinforcement cages were erected (Fig. 3.5a). In order to ensure health and safety (HSE) requirements real scale testing beams were lifted from casting bed to the testing equipment place by installed lifting lugs. Later, the main BFRP prestressing bars were installed, and connection details were calibrated (Fig. 3.5b). The prestressing force was applied using a hydraulic screw jack of 25-tons capacity until the required prestress level was achieved (Fig. 3.5c). The force was maintained constant after prestressing by locking nuts. The load was applied in increments using a hydraulic air pump. After prestressing, the readings of the strain gauges and the load cell were continuously recorded until the release of the prestressing force at a rate of 1 reading every 5 minutes. After prestressing of BFRP bars by a time approximately 24 hours, the concrete was cast for 6 beams at the same time. After pouring of concrete into formworks of the beams, certain concrete prisms were cast to measure shrinkage strain of the concrete (Fig. 3.5d, Table 3.3). 15 days after casting, the prestressing force was released by releasing the pressure of the hydraulic jack POWER TEAM.

Fig. 3.5. Preparatory works prior experimental tests: mounting of the formworks and reinforcement cages (a); installation of prestressing reinforcement (b); mounting of hydraulic jack (c); casting of concrete (d); visual quality inspection due to honeycombing (e); cut-off prestressing reinforcement, lifting and storage (f)

PC beams were taken out and precisely inspected in case of honeycombing, etc. After quality inspection (QA) beams were lifted by overhead crane to testing equipment place (Figs. 3.5e–3.5f).

No cracks were observed at the surface of the beams due to the lifting process. It should be mentioned that all beam series were fabricated and tested under the same loading conditions. Prestress force was released at $t_p = 15^{th}$ day, and static four-point loading was applied at $t_q = 48^{th}$ day after casting.

Table 3.2. Main material properties of the beams

Beam	h, mm	b, mm	l, mm	a_1, mm	f_u, MPa	ε_{fu}	E_f, GPa	ρ, %	f_{ck}, MPa
Control									
S-1	301	149	3200	50	1098.3	0.0246	45	0.32	46.01
Series 1									
SSI-1	303	150							
SSI-2	300	149	3200	50	1098.3	0.0246	45	0.33	44.47
SSI-3	301	150							
SSI-4	299	149							
Series 2									
SSI-5	300	150							
SSI-6	303	152	3200	50	1098.3	0.0246	45	0.32	40.21
SSI-7	301	148							44.29
SSI-8	303	147							
Series 3									
SSI-9	301	151							
SSI-10	302	150	3200	50	1098.3	0.0246	45	0.32	46.01
SSI-11	302	150							
SSI-12	300	149							

3.2.3. Experimental Test Scheme

Experimental beams were instrumented Novotechnik's T50 linear voltage displacement transducers (LVDTs) with an accuracy of ±0.02% as shown in Figure 3.6, respectively. Also, LVDTs T50 were placed at the BFRP bar location of both ends of the beam to monitor any slippage during the experiment. The LVDTs and dynamometer were connected to a laptop within automation processing equipment ALMEMO 25, and the readings were taken every 2 seconds.

The beams were tested under a static four-point loading scheme using 2 static concentrated loads, 0.96 m apart. (Fig. 3.6). The test was performed with increments (5 kN) and paused for short periods to take readings of gauges and to measure crack spacing and growth. Measurement base of all inductive sensors was 200 mm.

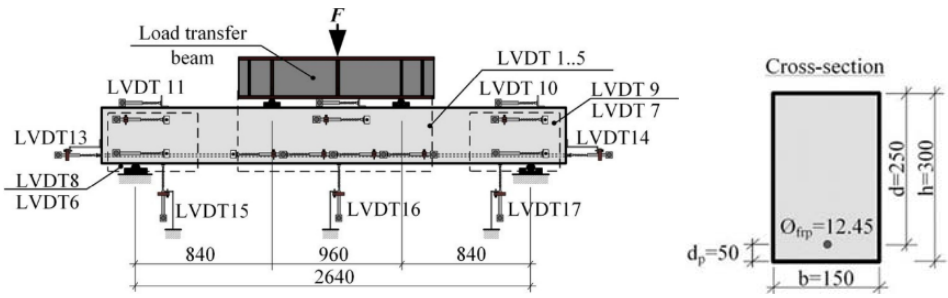

Fig. 3.6. Principal test scheme of the experimental work

3.2.4. Discussion of the Test Results

In general, there is a difference of deflection measurement of PC beams in comparison with regular RC beams. Prior load is applied PC beams exhibit camber due to initial prestress force effect (Fig. 3.7a). Increasing the load deflection varies from upwards to downwards up to failure (Fig. 3.7b). Comparative load-deflection responses for the all beams with different prestress level 40, 45 and 55 percent of f_u appear in Figure 3.8 and Table 3.4. Inspection of these figures shows that the response of the BFRP prestressed beams is initially linear and tend to be identical. The linear part corresponds to the uncracked section and departures in this region due to differences in prestressing (jacking) level with respect to all beams. Once the applied load overcome the cracking load, the stiffness of the beams is being decreased.

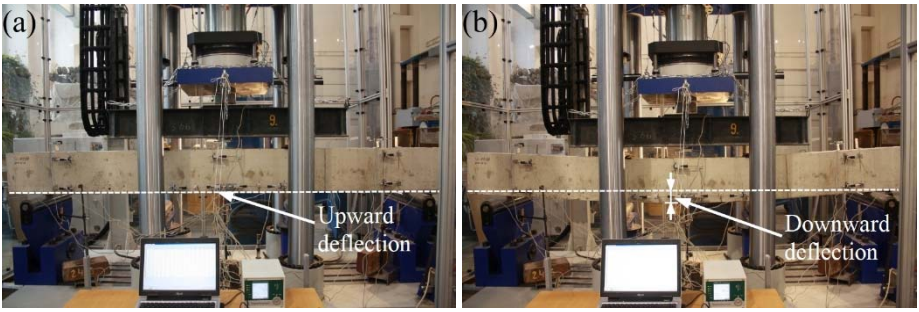

Fig. 3.7. Deflection variation of tested prestressed concrete beams: prior loading (a); at ultimate loading (b)

The comparaison of the experimental free shrinkage strains against the predicted ones by the Eurocode 2 (CEN 2004) method are compared in Table 3.2 below.

Table 3.3. Shrinkage strains of 100×100×400 mm prisms

Beam	Time	Predicted by CEN (2004)	Experimental
Series (1)	t_0	-1.401×10^{-4}	-1.310×10^{-4}
SS-1÷4	t_p	-2.090×10^{-4}	-1.954×10^{-4}
Series (2a)	t_0	-1.364×10^{-4}	-1.275×10^{-4}
SS-5,6	t_p	-2.072×10^{-4}	-1.937×10^{-4}
Series (2b)	t_0	-1.394×10^{-4}	-1.309×10^{-4}
SS-7,8	t_p	-2.081×10^{-4}	-1.953×10^{-4}
Series (3)	t_0	-1.425×10^{-4}	-1.323×10^{-4}
SS-9÷12	t_p	-2.110×10^{-4}	-1.961×10^{-4}

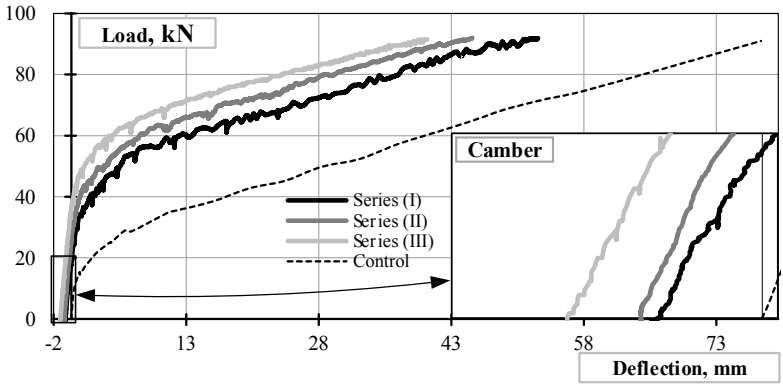

Fig. 3.8. Experimental load-deflection curves of the series of prestressed concrete beams due to initial prestress level

Considering failure mode, all prestressed BFRP beams failed due to the rupture of the BFRP bars. Control beam S–1 failed in the compression zone due to the crushing of concrete. No slip of the BFRP bars was observed in any of the beams. Regarding beam Series 1 specimens SSI–1, SSI–2, SSI–3 and SSI–4 a midspan downward deflection at ultimate load ranged between 50.62 and 52.82 mm and it was about 1/50 of the span. Prior static loading average measured camber value was – 0.72 mm. Variation of measured cambers among beam Series 1, 2 and 3 is shown in Fig. 3.8. As it was expected no major variations regarding ultimate load neither of prestressed BFRP beams nor of beam S–1 were observed.

In case of series 2 specimens SSI–5, SSI–6, SSI–7, SSI–8 ultimate deflections at midspan ranged between 43.60 to 51.15 mm, and it was about 1/55 of the member's span. Average measured camber value was – 0.78 mm. With respect to beam Series 3 specimens SSI–9, SSI–10, SSI–11, SSI–12 ultimate deflections at midspan ranged between 36.96 and 46.05 mm or in other words, average deflection of beam Series 3 was about 12 percent less in comparison with beam Series 2 specimens and 21 percent less than deflections of beam Series 1 specimens. Average measured camber value of beam Series 3 was – 0.91 mm. Interestingly enough that the increase of prestressing force or jacking stress by 5 and 15 percent, correspondingly decrease ultimate deflection at midspan by 12 and 26 percent, respectively.

In regard to the type of the beam reinforcement, beam Series 1, 2 and 3 had 33, 40 and 47 percent lower midspan deflection at ultimate load than control beam S-1, respectively. This confirms the fact that prestress load released to the flexural concrete member effects member stiffness (*EI*), and an increase of the member stiffness can be achieved only by increasing prestressing, correspondingly

Table 3.4. Experimental values of the ultimate and serviceability limit states

Beam	Cracking load, kN	Ultimate load, kN	Ultimate deflection, mm	Failure mode
Control				
S-1	12.60	91.70	78.04	Crushing of concrete
Series (1)				
SSI-1	34.50	93.22	52.82	
SSI-2	34.40	89.51	53.46	Rupture of tendon
SSI-3	36.20	94.17	52.16	
SSI-4	34.00	93.27	50.62	
Series (2)				
SSI-5	39.10	93.73	45.25	
SSI-6	38.60	96.77	51.15	Rupture of tendon
SSI-7	39.30	93.39	43.60	
SSI-8	39.10	93.01	46.58	
Series (3)				
SSI-9	43.50	93.23	40.28	
SSI-10	43.00	101.1	46.05	Rupture of tendon
SSI-11	42.50	93.62	36.96	
SSI-12	43.50	99.81	41.65	

decreasing of deflection of midspan of the uncracked and cracked sections either at serviceability or ultimate loads.

From the prestress level point of view, a midspan downward deflection at 60 percent of ultimate load ($P_{u.exp}$) of specimens SSI–1, SSI–5 and SSI–9 ranged between 7.48 mm, 4.12 mm and 2.68 mm and it was less than 1/200 of the span. Similarly, specimens SSI–2, SSI–6 and SSI–10 contained 8.61 mm, 5.6 mm and 2.85 mm deflections, respectively. Beams SSI–3, SSI–7 and SSI–11 provided 9.15 mm, 5.25 mm and 3.14 mm deflections. Considering beams SSI–4, SSI–8 and SSI–12, those deflected to 6.75 mm, 5.35 mm and to 2.91 mm, accordingly whereas beam S–1 achieved 34.5 mm deflection at the same value of the load. Considering mentioned above, beams prestressed to 40, 45 and 55 percent of f_u produced 4.6, 7 and 12 times less average deflection in comparison with control beam S–1.

From cracking point of view, beams prestressed to 40 percent of f_u SSI–1, SSI–2, SSI–3, SSI–4 had a cracking load ($P_{cr.exp}$) and ultimate load ratios – 0.370, 0.384, 0.384, 0.364 whereas $P_{cr.exp}/P_{u.exp}$ of control beam S–1 was 0.137. Further, $P_{cr.exp}/P_{u.exp}$ of series 2 specimens SSI–5, SSI–6, SSI–7, SSI–8 were 0.417, 0.398, 0.420, 0.380, respectively. Then, $P_{cr.exp}/P_{u.exp}$ of Series 3 beams SSI–9, SSI–10, SSI–11, SSI–12 were 0.467, 0.425, 0.454, 0.436, accordingly. Particularly, the average stiffness of the group 1, 2 and 3 beams was 2.66, 2.47 and 2.24 times higher than the stiffness of beam S–1, correspondingly. This confirms the finding

that such difference on the stiffness of the beams is caused due to compression stresses occurred in the tension zone of the beams by prestressing force. Hence, the increase of prestressing force by 5 and 15 percent provides 7 and 19 percent higher flexural stiffness of the beam.

The crack pattern of the tested beams is presented in Figures 3.9–3.12 where the failure cracks at the poor bending zone of each beam are visible. The crack distributions is given at the load 60 percent of $P_{u.exp}$ and prestressing of 40 percent of f_{fu} is producing a maximum crack width of 0.5 mm, and the number of cracks was not increased by increasing the rest of the load up to the failure. This stage is defined as stabilization of cracks when the number of cracks does not increase by increasing the load. Normally, at this stage 60 percent $P_{u.exp}$ provides crack width 0.4 mm, and further crack width development is not in line with serviceability requirements. In regard to the rest of the beam groups, stabilization of cracks occur at higher than 60 percent of $P_{u.exp}$ due to higher degree of prestressing. Increasing prestress level to 45 and 55 percent of f_u it delivers consequently less number of cracks and 21 and 30 percent larger average spacing between cracks, accordingly.

It should be mentioned that the crack width was measured within the constant moment zone, and at the level of the bottom BFRP bars, 50 mm from the bottom surface of the concrete.

Table 3.5. The measured response of cracks at 60% of the ultimate load

Beam	**No of cracks**	**Maximum crack width, mm**	**Average crack spacing, mm**	**Maximum crack spacing, mm**
Control				
S-1	4	2.0	313	360
Series 1				
SSI-1	7	0.4	170	290
SSI-2	8	0.5	159	225
SSI-3	7	0.4	166.5	220
SSI-4	7	0.4	175	210
Series 2				
SSI-5	6	0.2	203	245
SSI-6	6	0.25	200	245
SSI-7	6	0.2	208	270
SSI-8	6	0.2	200	305
Series 3				
SSI-9	4	0.1	283	340
SSI-10	5	0.1	221.5	275
SSI-11	4	0.15	295	330
SSI-12	5	0.1	256	340

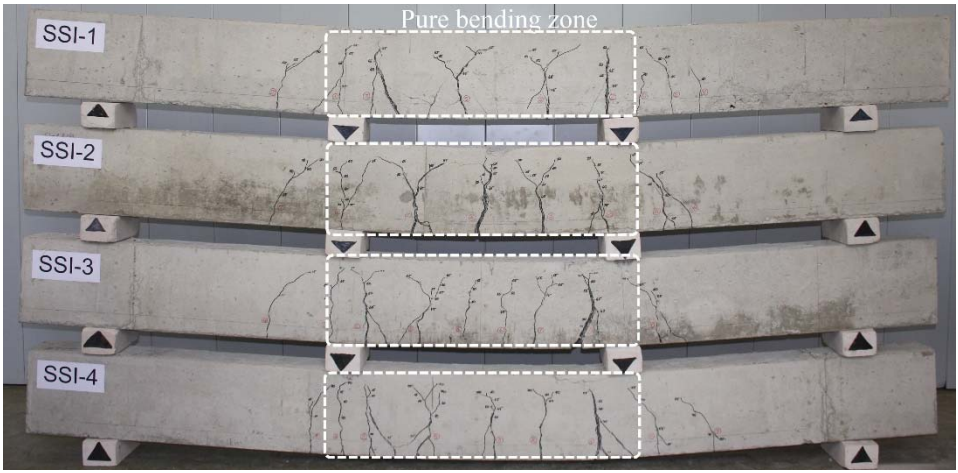

Fig. 3.9. Cracking pattern of beam Series 1

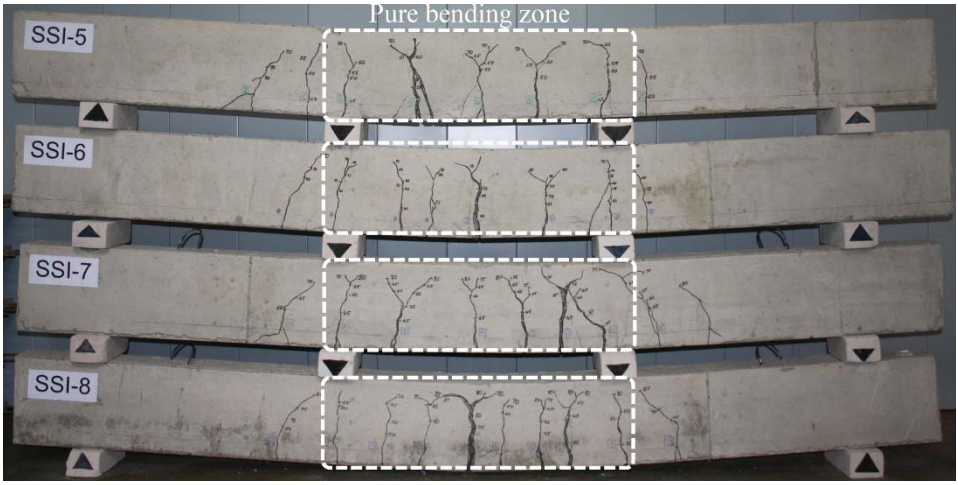

Fig. 3.10. Cracking pattern of beam Series 2

The relationship of the maximum, minimum and average crack widths (hereinafter – w_{max}, w_{min}, w_{avg}) for all the cracks at 60 percent of $P_{u.exp}$ are shown in Figure 3.13a. The average values of the ratios w_{min}/ w_{avg} and w_{max}/ w_{avg} were 0.36 and 1.77, 0.76 and 1.33, 0.9 and 1.20 for the beam group 1, 2, 3, respectively. With respect to control beam S–1, ratios w_{min}/ w_{avg} and w_{max}/ w_{avg} were 0.72 and 1.21 and were close to the average values of the beams of Series 2. Cracking pattern was monitored in terms of crack width and height.

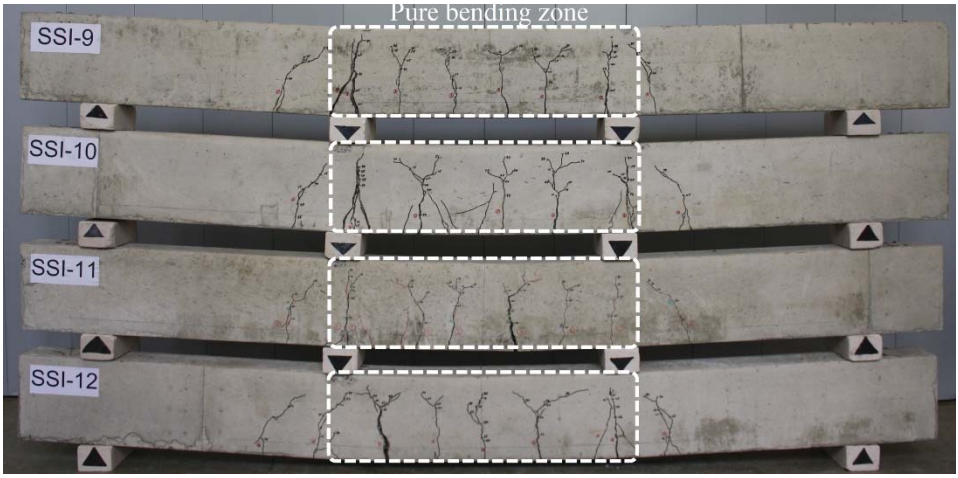

Fig. 3.11. Cracking pattern of beam Series 3

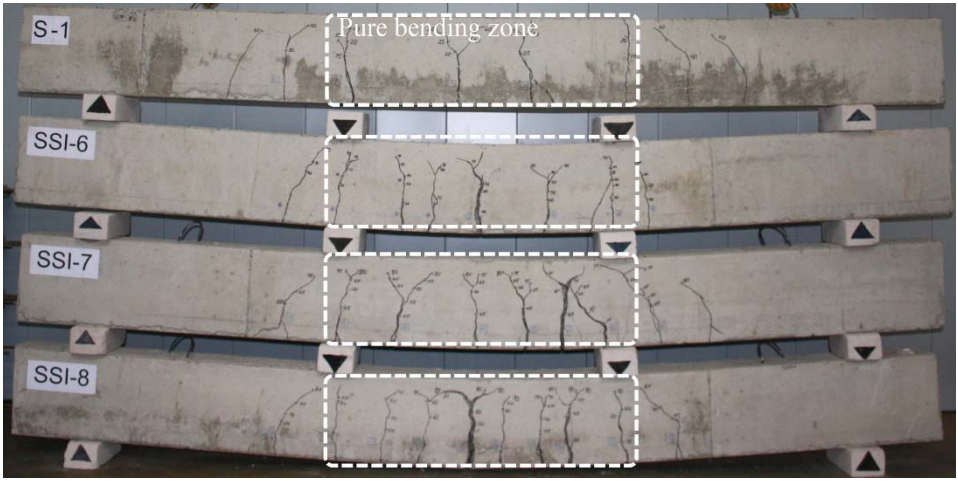

Fig. 3.12. Cracking pattern of Series 2 versus control beam

At load level assumed to be 60 percent of $P_{u.exp}$ which shall be considered a limit of the service load, the ratios of crack spacing and average cracking spacing (s and s_{avg}) were computed for each beam and are given in Figure 3.13b. The average ratios of s_{min}/s_{avg} and s_{max}/s_{avg} were 0.56 and 1.41 for series 1 specimens, 0.59 and 1.31 for Series 2 specimens and 0.76 and 1.22 for Series 3 beams, respectively.

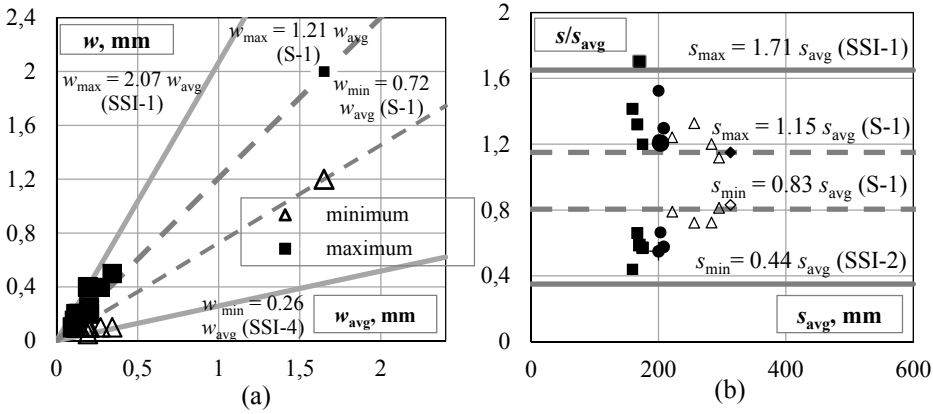

Fig. 3.13. Variation of maximum and minimum values at serviceability state: crack width (a); crack spacing (b)

Regarding the mentioned ratios above of control beam S–1 were 0.83 and 1.15, accordingly. A control beam S–1 had consequently larger spacing between the cracks and less variation of the crack spacing than PC (Series 1, 2 and 3).

3.3. Experimental Test of Stress Relaxation of Basalt Fiber Reinforced Polymer Bars

Once the anchorage of BFRP bars was solved, it was also possible to start with stress relaxation experimental works. As it was mentioned above, BFRPs have excellent resistance to creep, but for a prestressing tendon, relaxation is more important than a creep, since relaxation reduces the available prestressing force. Estimation of the prestress loss over time requires that stress relaxation of the tensile element shall be known. Matrix resin and fibers can be assumed as viscoelastic materials and due to time exhibit stress relaxation. BFRP is not yet included in design codes. Thus none of the codes provide significant information in order to determine the prestress losses due to stress relaxation and mechanical properties belong to scientist's interpretation and various prognosis. Further, the author has proposed an experimental program and implemented an innovative equipment capable to sustain stress reduction under constant strain. Experimental data and results are explained below.

3.3.1. Experimental Program of Testing Bars

Stress relaxation tests were conducted on modular prestress transfer system (Fig. 3.14) capable of resisting constant strain for 1000 h and more. Three sets of direct tension tests were carried out on 9 BFRP bar specimens (BP-1÷BP-9), commercially known as *RockBar Composite bars*, comprising three types of prestress force (40, 45, and 55 %) and one type of diameter (∅ = 12.45 mm). Each bar was provided with anchors at each end to ensure no breakage of the bar at the jaws or slippage from the grips. The anchors consisted of a threaded steel pipe filled with epoxy resins and designed according to ACI 440.3R-04 (2004). For the sake of these experiments, each specimen had separate prestress reaction frame (R-1 to R-9) as for the uniform conditions (Fig. 3.15). All tests were carried out at room temperature (20 °C±3 °C), and 40–45% relative humidity using a proposed universal prestress transfer system. Most of the test specimens were exposed to a predefined environment for a period of 1000 h, which is considered long enough for stress reduction processes to stabilized and is recommended by ACI 440.4R-04 (2004) and JSCE-E 531(1995).

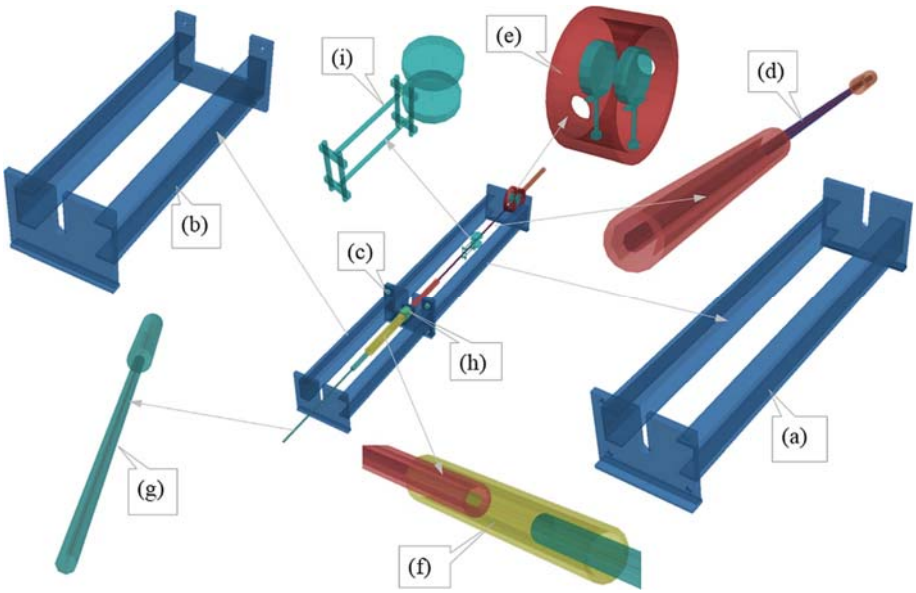

Fig. 3.14. Principle of stress relaxation test: reaction frame $H \times B$ = 256×310 mm, L = 1200 mm (a); stress transfer frame $H \times B$ = 256×310 mm, L = 800 mm (b); bolts 4×M18 (c); BFRP specimen ∅ = 12.55 mm, L = 2000 mm and end anchors ∅ = 33.7 mm, L = 350 mm (d); dynamometer ring ∅ = 170 mm (e); stress transfer rod ∅ = 12/16 mm, L = 850 mm (g); nuts 2×M33 (h); mechanical watch-type extensometer with base 200 mm (i)

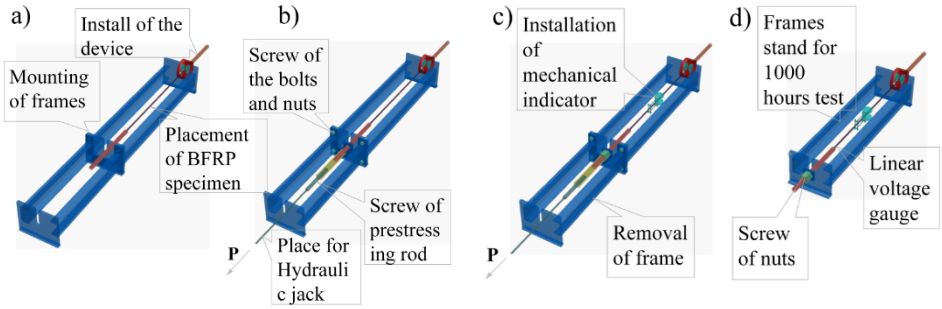

Fig. 3.15. Main phases of the experimental test: connection of frames and installation of basalt fiber reinforced polymer bar specimen (a); fixed connection and installation of transfer rod (b); prestress transfer and installation of extensometer (c); screwed nuts and removal of the transfer frame

3.3.2. Test Specimens

All the specimens have constant ∅ = 12.45 mm and a length of 2000 mm. BFRP bars were treated by sandblasting over the length and anchored with seamless steel tubes (details "D-3" and "D-6") with an outer ∅ = 33.7 mm and a thickness of 5 mm (Fig. 3.16). Epoxy resin was used to fill the gap between the steel tube and the BFRP bar, and the specimen was allowed to be cured for 3 (three) days to ensure that sufficient bond strength is achieved. Remaining details of prestress system are shown in Figures 3.14 and 3.16.

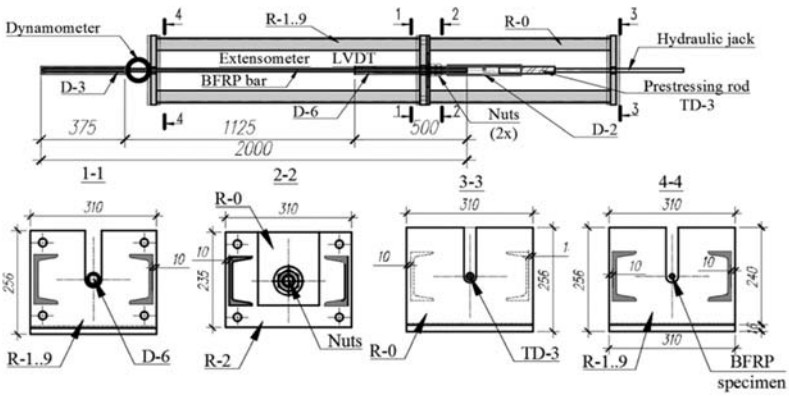

Fig. 3.16. Workshop details of relaxation test equipment

3.3.3. Instrumentation

A new system was developed in order to measure the load loss when strain is fixed. The prestressing load is applied through a hydraulic jack, but the jack did

not prestress the specimen/anchor directly. Instead, a prestress rod which was attached to the anchor through the anchor connector threaded both sides seamless steel tube (detail D-2, Fig. 3.16). Further, major phases of prestress transfer were followed: mounting of flange type connection by transfer frame (R-0) and reaction frames (R-1÷R-9); installation of the BFRP specimen; screwing bolts and nuts; hydraulic jack attached, and the specimen prestressed; once actual prestress is transferred, the bolts and nuts were screwed, and transfer frame was removed. Reaction frame remains for 1,000 h test regime.

The hydraulic jack was manually controlled approximately at 5 kN/min. Then, the force was unloaded with the hydraulic jack, and the force was transferred to the specimen (Figs 3.15 and 3.17).

It was very inportant to apply initial force without subjecting the specimen to any shock or vibration. The rate of loading was 200±50 N/mm^2. Fixed strain after the prestress is applied to the specimen and maintaind for 120±2 sec. Records after the following times elapsed: 1, 3, 6, 15, 30, 45 minutes; 1, 1.5, 2, 4, 10, 24, 48, 72, 96, 120 hours; later, every 24 hours subsequently.

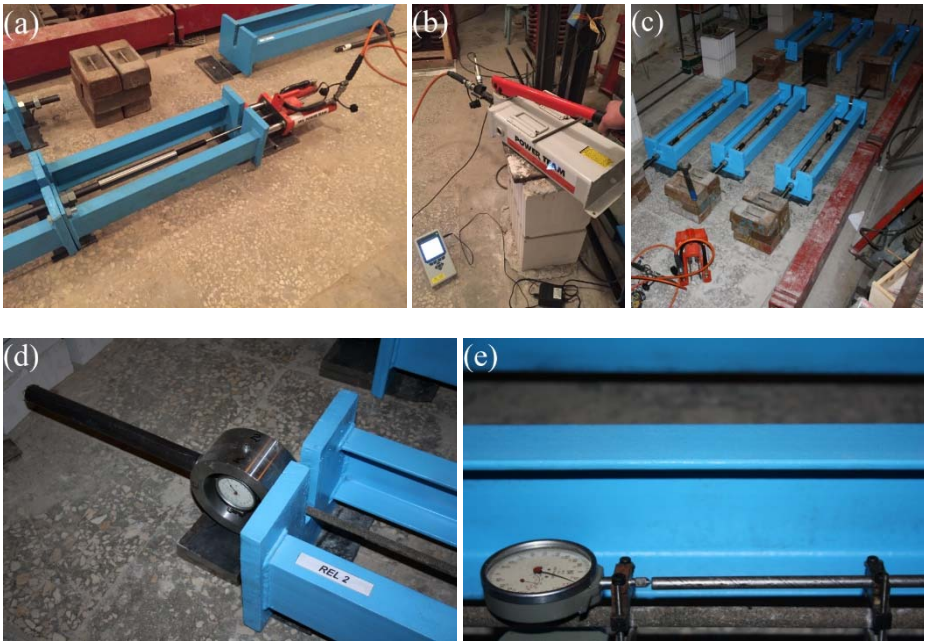

Fig. 3.17. Process of stress relaxation test: installation of hydraulic jack (a); hydraulic jack pump (b); test specimens after removal of prestressing frame (c); measurement of prestress decrement from mechanical extensometer at dynamometer ring (d); measurement of strain by mechanical extensometer at midspan of the bar (e)

3.3.4. Results of the Experimental Work

In principle, stress relaxation was not a common task because of difficulties that the strain of the specimen shall remain constant over the prestress of the specimen. In this study, experimental equipment was designed in order to measure key deliverables: initial load at mechanical extensometer on dynamometer ring (P_{dyn}) and deformation of BFRP bar specimen (ε_b) which allows to eliminate auxiliary deformation of reaction frame and to determine the base point of pure stress relaxation (Fig 3.18a).

Mutual relaxation was estimated by the following expression:

$$\frac{\Delta P_e}{P_0} = \frac{P_0 - P_{dyn}(t)}{P_0}, \tag{3.1}$$

where P_0 is initial prestress load; ΔP_e is effective prestress force after elimination of prestress decrement at mechanical extensometer on dynamometer ring at the end of reaction frame.

Then stress relaxation rate of bar specimen was calculated:

$$\frac{\Delta P_e - \Delta P_f}{P_0} = \frac{P_0 - P_{dyn}(t) - \Delta\varepsilon_b \cdot E_b \cdot A_b}{P_0}, \tag{3.2}$$

where ΔP_f is the loss of prestress force due to the strain of the testing frame (stress relaxation equipment) due to initial prestress; $\Delta\varepsilon_b$ is a measured strain of the BFRP bar after deformation of reaction frame; E_b is the elastic modulus of BFRP bar; A_b is a cross section of BFRP bar.

The results presented in Figure 3.18 have been obtained, highlighting a marked regression of the strength retention of the bar axial stress over the experimental time interval [0, 1000 hours]:

$$\frac{P_0 - \Delta P_e}{P_0} = \frac{P_0 - (P_0 - P_{dyn}(t))}{P_0}. \tag{3.3}$$

According to JSCE (1995) the relaxation curve shall be plotted on a semi-logarithmic graph where the relaxation value (%) is presented on an arithmetic scale on the vertical axis, and test time in hours is represented on a logarithmic scale on the horizontal axis. An approximation line shall be derived from the graph data using the least-square method:

$$Y_r = a - b\log t, \tag{3.4}$$

where Y is relaxation rate (%); a, b are empirical constants; and t is time (in hours).

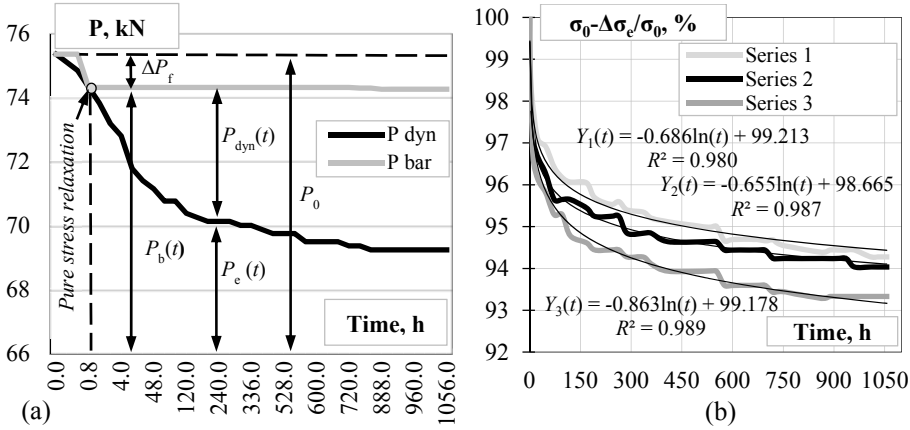

Fig. 3.18. Experimental test results: the principle of stress relaxation estimation (Series 3) (a); Stress relaxation curves due to initial prestress (b)

It is also recommended that the relaxation rate after 1 million hours (approximately 114 years) shall be evaluated from the approximation line; this value represents the million hours relaxation rate. Where the service life of the structure in which the FRP is to be used is determined in advance, the relaxation rate for the number of years of service life ("service life relaxation rate") shall be determined. It is shown in Fig. 3.18b that the logarithm fitting curves might well represent the relation of strength reduction to aging time, in which the R^2 values of the fitted curves are 0.9808, 0.9877 and 0.9896 for the BFRP bars under prestressing of $0.4f_u$, $0.45f_u$, and $0.45f_u$, respectively.

Table 3.6. Predicted values of the stress relaxation rate at 1000 hours

Initial stress	Series	Specimen No.	Mean a	Mean b	Predicted load retention, %	Predicted relaxation rate, %	Mean value of relaxation rate, %
		BP-1				5.42	
$0.4f_u$	Series 1	BP-2	98.665	0.655	94.28	5.76	5.72
		BP-3				5.98	
		BP-4				6.01	
$0.45f_u$	Series 2	BP-5	99.213	0.686	93.96	6.09	6.04
		BP-6				6.02	
		BP-7				6.5	
$0.55f_u$	Series 3	BP-8	99.178	0.863	93.33	7.1	6.67
		BP-9				6.4	

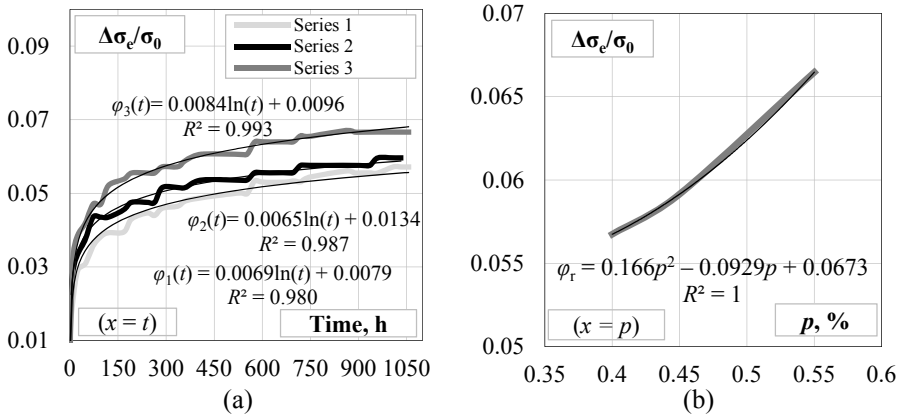

Fig. 3.19. Experimental curves of relaxation factor: depending on instantaneous relaxation time at certain prestress level (a); depending on prestress level at 1000 h (b)

Because the usual requirement for reliable fitting curves is that R^2 should be greater than 0.95, the current fitting relationships shall be treated as acceptable. In regard to prestress force effect on the stress degradation rate, the relation of the prestressing ratios to the parameters before ln(x) is represented in Figure 3.18b. A logarithm equation is adopted to describe the relation accurately, which shows a good fit to the existing experimental data.

Relaxation curves shown in Figure 3.18b can be approximated by relaxation factor that would be used in order to verify calculation algorithm described in Section 2.2.2. In this case, it can be assumed that:

$$\varphi_{\mathrm{r}} = \frac{\Delta\sigma_{\mathrm{e}}}{\sigma_0}. \tag{3.5}$$

Having this ratio from experimental data (Fig. 3.19a) general form depending on prestressing ratio at certain loading shall be expressed:

$$\varphi_{\mathrm{r}} = (0.166p^2 - 0.0929p + 0.0673)\ln(t) + 1, \tag{3.6}$$

where p is the prestress ratio, and t is the time period (hours). A polynomial equation is adopted to describe the relation accurately, which shows a good fit to the existing experimental data (R^2 is equal to 1). Eq. (3.6) allow to estimate relaxation factor that would be used in order to calculate prestress losses of PC beams based on prestress level taking into account that instantaneous stress relaxation may occur within the first 1000 h of prestressing.

3.4. Validation of Theoretical Predictions

This Chapter serves comparison analysis of prestress losses, deflection and cracking based on verification of theoretical assumptions taking into account experimental results of real scale PC beams and relaxation tests of BFRP specimens. The focus is to validate the accuracy of proposed calculation algorithms leading to the adequate prediction of the prestress losses and serviceability.

3.4.1. Prestress Losses

This Section considers a comparative analysis of the calculated and experimental results. The difference between the methods capable to predict prestress losses is described and compared with experimental data (Fig 3.20).

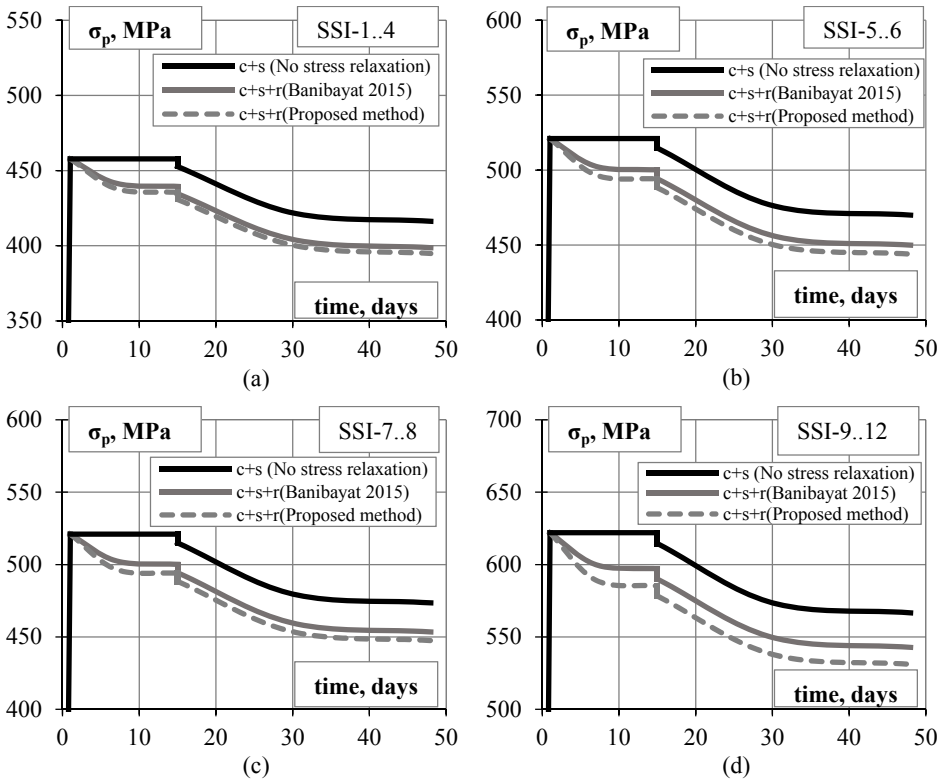

Fig. 3.20. Stress distribution in prestressed basalt fiber reinforced polymer bars based on theoretical and experimental values of stress relaxation: series 1 (a); series 2 due to the different compressive strength of concrete (b) and (c); series 3 (d)

Table 3.7. Comparison of loss in stress due to calculated and experimental values of φ_r

Beam Series	σ_{p0}, MPa	$\Delta\sigma_p$, MPa			$\Delta\sigma_p/\sigma_{p0}$, %		
		c+s	c+s+r	c+s+r$_{(exp)}$	c+s	c+s+r	c+s+r$_{(exp)}$
SSI-1÷ SSI-4 (1)	457.8	41.44	59.05	62.91	9.05	12.89	13.74
SSI-5, SSI-6 (2)	521.0	50.97	70.97	76.98	9.78	13.62	14.78
SSI-7, SSI-8 (2)	521.0	47.45	67.50	73.50	9.10	12.96	14.11
SSI-9÷SSI-12 (3)	622.0	55.26	72.20	90.91	8.88	11.61	14.62

Note: c – concrete creep; s – concrete shrinkage; r – stress relaxation of BFRP according to Banibayat 2015; r$_{(exp)}$ – stress relaxation of BFRP according to present experiments

To start with, analysis on estimation of losses in stress was based on comparison of different calculation approach of prestress losses: 1) major focus on losses due to concrete creep and shrinkage (Zamblauskaitė 2005, Balevičius 2010, Balevičius 2018); and 2) focusing on full range of prestress losses due to concrete creep and shrinkage and stress relaxation of prestressing reinforcement. Moreover, in regard to latter, the impact of instantaneous relaxation of BFRP for time-dependent losses is described further on.

From prestess point of view, Series 1 beams (prestressed to 40 percent of f_u) contained 9.05% prestress losses considering concrete creep and shrinkage and 3.84% higher losses in stress including stress relaxation of BFRP based on Banibayat's (2015) relaxation factor and 4.69% higher losses due to experimental value of φ_r (Atutis *et al.* 2018). Effective prestress force ranged from initial prestress force 55.73 kN to 50.69 kN, 48.54 kN, and 48.07 kN, accordingly. Due to mentioned above the decrease of stress in BFRP bars is shown in Figure 3.20a. Further, Series 2 beams (prestressed to 45% of f_u) posse difference in losses of stress due to unlike compressive concrete strength: beams SSI-5, SS-6 contained 9.78% losses ignoring stress relaxation and 3.84% to 5% higher losses including assumed (Banibayat 2015) and experimentally gained values of φ_r, while beams SSI-5, SS-6 considering mentioned factors produced 3.86% to 5.01% higher losses, respectively and lead to decrease of initial stress from 521 MPa to 470 MPa with no relaxation included, from 450 MPa to 444 MPa including relaxation factors, accordingly (SSI-5, SSI-6) and to 473 MPa not included relaxation, but from 453.5 MPa to 447.5 MPa including relaxation factors of BFRP in case of beams SSI-7 and SSI-8, respectively (Figs 3.20b, c). Finally, considering beam Series 3 (prestressed to 55 percent of f_u) it is visible that the difference of losses in stress taking into account φ_r as assumed based on Banibayat's (2015) proposal and experimentally gained φ_r expands to 3.01%, while considering beam Series 1 and 2 it varies from 0.85% (SSI-1÷ SSI-4) to 1.16% (SSI-5, SSI-6) and 1.15% (SSI-7, SSI-8), respectively (Table 3.7). It shall be explained based on experimental results.

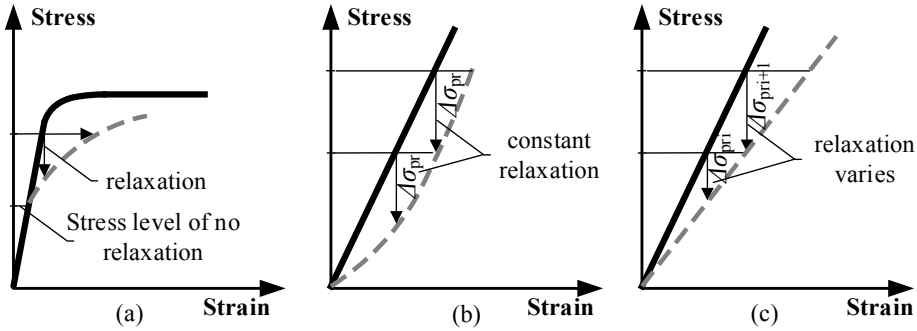

Fig. 3.21. Schematic relaxation behavior at different initial stress levels: regular prestressed steel (a); theoretical relation (Banibayat 2015) (b); experimental relation (Atutis *et al.* 2018) (c)

Having assessed that increasing prestress level (from 40 to 45% and 55%) stress relaxation of prestressed BFRP increase and varies (depending on time) from 0.049 (at stretching) and 0.057 (at load applied) to 0.052 (at stretching) and 0.059 (at load applied), and 0.059 (at stretching) and 0.069 (at load applied), respectively (Fig. 3.21c), while φ_r proposed by Banibayat (2015) remains constant due prestress level and belongs to 0.04 (at stretching) and 0.047 (at load applied) (Fig. 3.21b). Lastly, in regard to beam Series 3 effective prestress force ranged from an initial value of 75.72 kN to 68.96 kN, 66.08 kN and 64.66 kN based on the same manner of comparison above.

Further, strain distribution over the cross section of beams is to be analyzed by means of comparison of calculated and experimentally measured strains of flexural PC beams described in Section 3.2. The key criteria was assumed that stress relaxation of BFRP is included into theoretical calculations. The proposed algorithm based on stress relaxation approach (Section 2.2) was applied for strain analysis of the experimental results. Average values of the strain at the top and the bottom of the cross section obtained based on effective modulus method (EMM) that was used by Zamblauskaitė (2005), and average stress-strain approach (ASSA) proposed by Balevičius (2010) were assumed in the calculations. The calculated average strain of all beams have been compared with the experimental results and are presented in Figure 3.22 and Table 3.8.

The results of the average strain of PC beams cross-section show that the proposed algorithm (Section 2.2.2) based on stress relaxation of BFRP approach assures adequate estimation of the strain and good agreement with experimental values was attained.

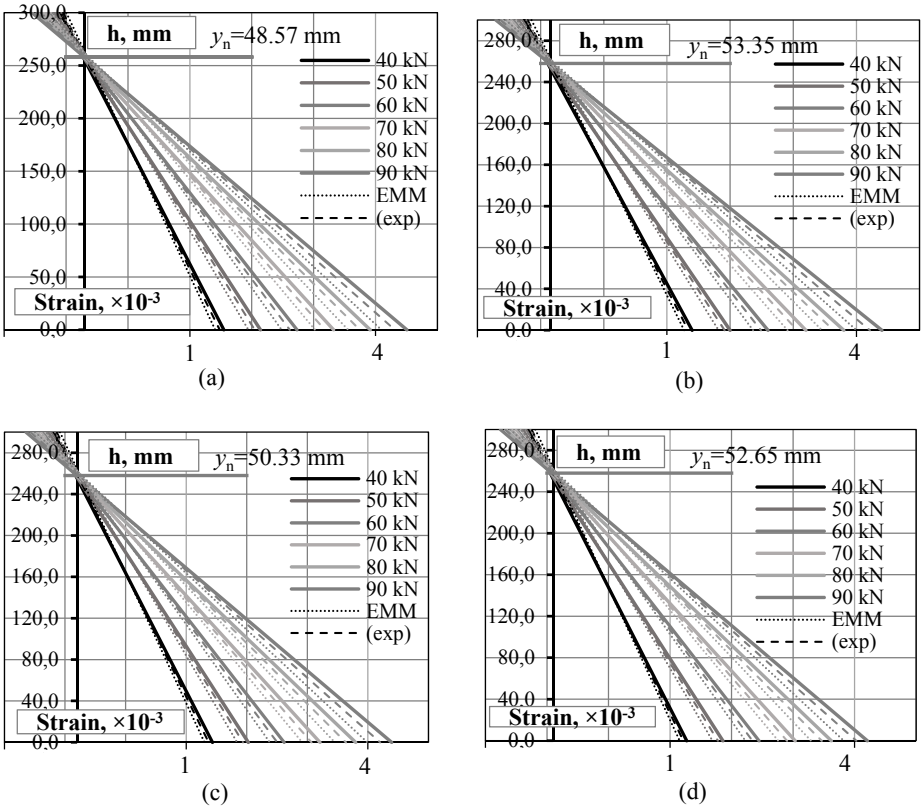

Fig. 3.22. Strain distribution over cross section: beam Series 1 (a); beam Series 2 (b) and (c); beam Series 3 (d)

Table 3.8. Strain over the beam cross-section based on calculated and experimental values

Beam (Series)	*F*, kN	$\varepsilon_{top}\times10^{-3}$				$\varepsilon_{btm}\times10^{-3}$			
		Exp.	EMM	ASSA	Author	Exp.	EMM	ASSA	Author
SSI-1÷	40	–1.076	–1.036	–1.094	–1.094	1.497	1.465	1.548	1.548
SSI-4	60	–1.232	–1.208	–1.276	–1.276	2.638	2.588	2.730	2.730
(1)	80	–1.408	–1.381	–1.458	–1.458	3.780	3.709	3.913	3.913
SSI-5,	40	–1.218	–1.195	–1.261	–1.261	1.349	1.324	1.397	1.397
SSI-6	60	–1.391	–1.364	–1.440	–1.440	2.511	2.463	2.599	2.599
(2)	80	–1.564	–1.534	–1.619	–1.619	3.672	3.602	3.801	3.801
SSI-7,	40	–1.151	–1.128	–1.128	–1.191	1.383	1.357	1.432	1.432
SSI-8	60	–1.325	–1.300	–1.300	–1.372	2.526	2.478	2.615	2.615
(2)	80	–1.499	–1.471	–1.471	–1.552	3.669	3.601	3.798	3.798
SSI-9÷	40	–1.266	–1.242	–1.242	–1.311	1.227	1.203	1.270	1.270
SSI-12	60	–1.439	–1.497	–1.497	–1.490	2.362	2.317	2.454	2.454
(3)	80	–1.611	–1.581	–1.581	–1.668	3.498	3.431	3.622	3.621

It was noticed that calculated strain values based on proposed algorithm assure from 1.6 to 3.5% higher than experimental values, while average strain estimated by EMM vary from 5% to 6.5% less than experimental values and thus might be underestimated that would lead to not anticipated errors. Also, the analysis of strain distribution shown that average strain based on proposed algorithm is equal to the values calculated by ASSA (2010) approach, thus this prove the adequacy of the viscoelastic laws used for the concrete and BFRP reinforcement behavior.

3.4.2. Load-Deflection Response

Figures 3.23a–3.23d show the values of experimental and analytical deflection values ($\delta_{calc}/\delta_{exp}$) of beam Series 1, 2 and 3. Average values of deflections were obtained based on the effective moment of inertia (I_e) derived by ACI (2004) and including decompression moment effect, Eurocode 2 (CEN 2004), Toutanji *et al.* (2000) and author's proposal (Sections 1.4 and 2.3.1). At the service load equivalent to 60% of ultimate load beam Series 1 (SSI-1÷SSI-4) produced average deflection 7.2 mm that is 11.6% higher than calculated using traditional ACI (2004) equation for I_e (δ_{calc} = 6.45 mm) and from 21.9% to 64% less than calculated by Toutanji's *et al.* (δ_{calc}=9.22 mm), authors's (δ_{calc} = 15.59 mm) and CEN (2004) (δ_{calc} = 20.02 mm). It is evident from Fig. 3.23a that deflections derived by ACI (2004) without taking into consideration the decompression moment are underestimated theoretical values ($\delta_{calc}/\delta_{exp}$ = 0.90) in comparison with experimental results (Fig. 3.24a). According to Toutanji *et al.* (2000), author's and Eurocode 2 (CEN 2004) equations, the ratios $\delta_{calc}/\delta_{exp}$ are 1.28, 2.17 and 2.78, respectively that lead structural engineers to overestimation of deflections with quite sufficient safety margin. Increasing prestress level to 45% beam Series 2a, 2b contained less average deflections from 5.31 mm, 4.38 mm, accordingly. At the same time deflection ratios $\delta_{calc}/\delta_{exp}$ according to equations by Toutanji *et al.* (2000), the author's proposal and Eurocode 2 (CEN 2004) decreased to 1.17, 2.0 and 2.24 (Series 2a) and 1.17, 1.93 and 2.06 (Series 2b), respectively (Fig. 3.23b,c). With respect to decompression moment effect, it leads to overestimated deflections (ratios $\delta_{calc}/\delta_{exp}$ equal to 1.28 and 1.22) while taking into account no decompression, deflections still remain underestimated (ratios $\delta_{calc}/\delta_{exp}$ equal to 0.89 and 0.88). In regard to beam Series 3, deflections remain to decrease due to higher prestress level (55%) that lead to decreasing of the ratios $\delta_{calc}/\delta_{exp}$ to 1.50 and 1.81 according to equation by author's proposal and Eurocode 2 (CEN 2004) while ratios $\delta_{calc}/\delta_{exp}$ increased to 1.29, 1.39 and 1.10 according to formulas by Toutanji *et al.* (2000), ACI (2004) including decompression and without its consideration. This could be explained that due to no direct relation of power m and coefficient β_d and prestress level.

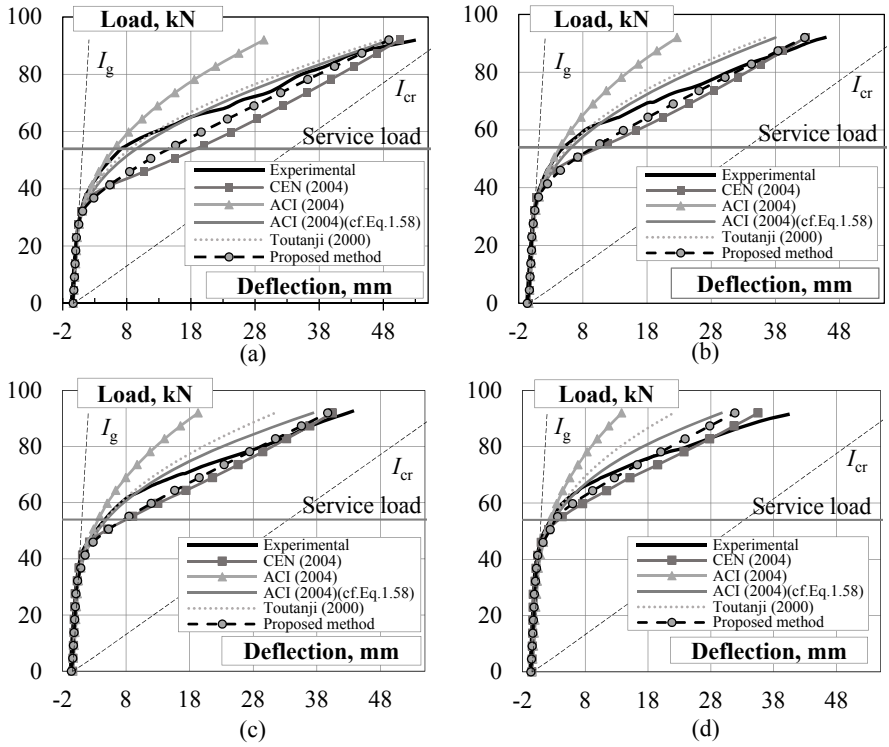

Fig. 3.23. Load-deflection curves: beam Series 1 (a); beam Series 2 (b) and (c); beam Series 3 (d)

Those parameters shall be evaluated and proved experimentally in the future. With regards to post-cracking behavior, the assessment of the decompression effect is also more visible (Fig. 3.23 and Fig. 3.24b). At the ultimate load, all mentioned methods underestimate deflection of experimental PC beams. In the case of beam Series 1 ratio $\delta_{calc}/\delta_{exp}$ varies from 0.91, 0.93 to 0.96 based on Toutanji *et al.* (2000), author and Eurocode 2 (CEN 2004), accordingly. In case of formulae by ACI (2004), even decompression is assesed, it poses to underestimation of deflections ($\delta_{calc}/\delta_{exp}$ = 0.93), while no decompression leads to 56% higher underestimation of deflections ($\delta_{calc}/\delta_{exp}$ = 0.56). Further, according to the author's proposal and Eurocode 2 (CEN 2004) it delivers the analytical curves that have very similar character to experimental diagrams and increasing prestress level to 45%, and 55% produce deflection close to experimental values ($\delta_{calc}/\delta_{exp}$ varies from 0.93 to 0.79 and 0.93 to 0.88), respectively (Fig. 3.24b).

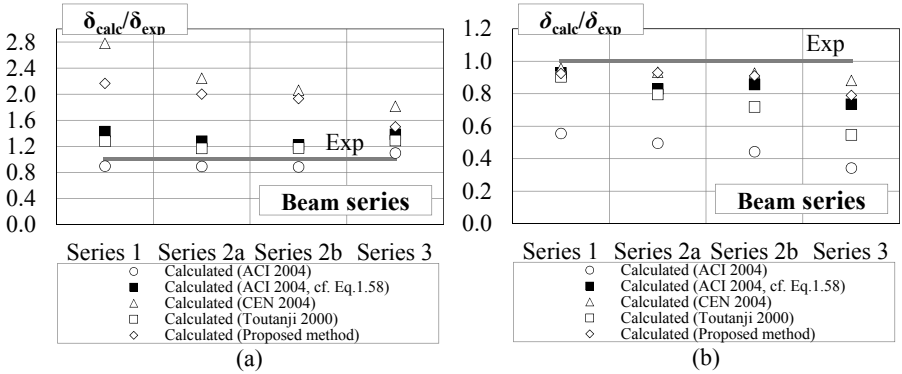

Fig. 3.24. Comparison of the ratios of theoretical and experimental deflections: at service load (a); at ultimate load (b)

Regarding ACI (2004) code, taking into account decompression effect, due to an increase of prestressing to 45% and 55% deflection ratios $\delta_{calc}/\delta_{exp}$ slightly decrease from 0.83 to 0.74, however having no decompression assessed deflection ratios $\delta_{calc}/\delta_{exp}$ increase considerably from 0.50 to 0.34, respectively. This is mainly due to the effect of power m and coefficient β_d that are empirical constants proposed originally for particular cases.

3.4.3. Cracking Control

In regard to cracking analysis, average values of crack width were derived by methods proposed by ACI (2004), Eurocode 2 (CEN 2004) and author's proposal based on decompression moment effect included but not limited to early relaxation of BFRP and shrinkage of concrete. The proposed method is described in Section 2.3.2. Figures 3.25–3.28 compare the values of experimental and analytical crack width values of beam Series 1, 2 and 3. At the service load equivalent to 60% of ultimate load beam Series 1 (SSI-1÷SSI-4) produced average crack width 0.4 mm that is 77.3% less than calculated CEN (2004) equation ($w_{k.calc}$ = 1.76 mm) and 67% less than based on ACI (2004) recommendations ($w_{k.calc}$ = 1.22 mm) (Fig. 3.25a–3.25b). Such difference is caused due to recommended values of the factor k_b that normally used for steel reinforcement and based on CEN (2004) and ACI (2004) it belongs to 0.8 and 1.2, respectively. In order to improve analytical values mentioned factor was assumed as 0.05 for CEN (2004) and 0.3 for ACI (2004) equations and this lead to less overestimation of crack width, $w_{k.calc}/w_{k.exp}$ = 1.85 and $w_{k.calc}/w_{k.exp}$ = 1.30, accordingly. However, the least difference of w_{calc}/w_{exp} obtained by calculated crack width based on author's proposal (Eq. 2.67) and was 1.25 (Table 3.9).

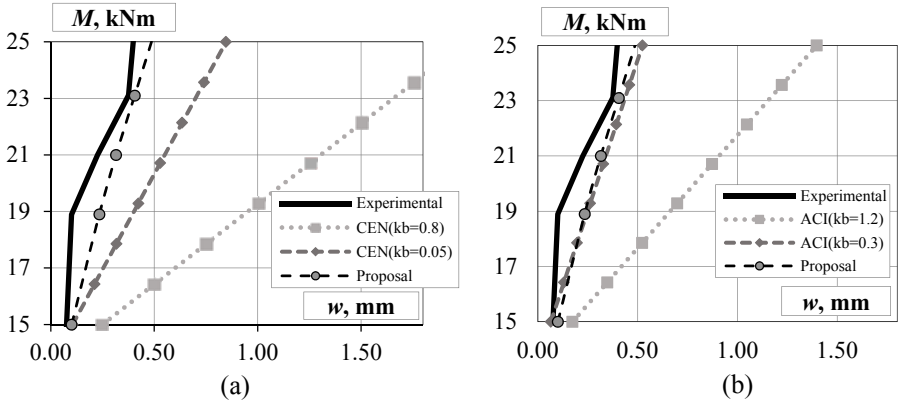

Fig. 3.25. Distribution of crack width of beam Series 1: according to CEN (2004) (a); according to ACI (2004) (b)

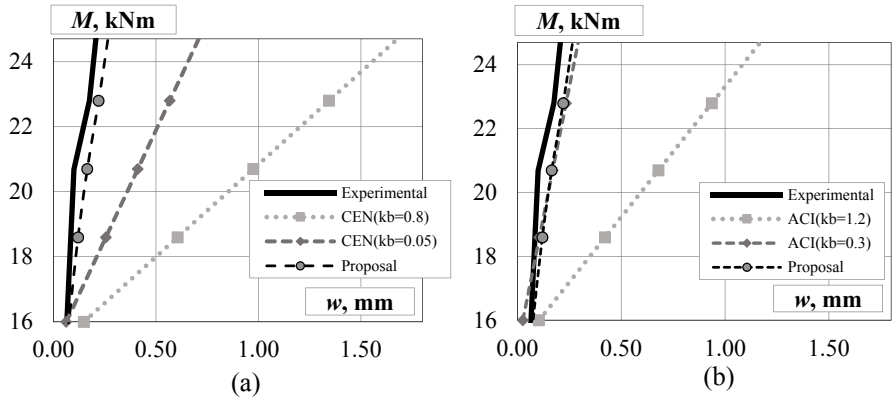

Fig. 3.26. Distribution of crack width of beam Series 2a: according to CEN (2004) (a); according to ACI (2004) (b)

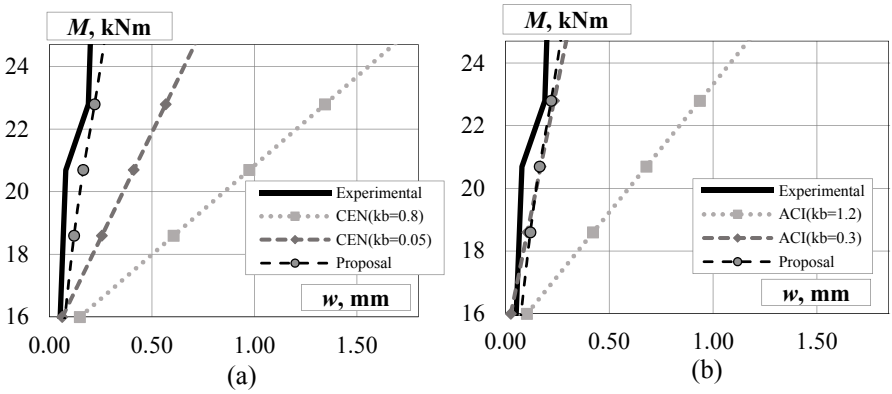

Fig. 3.27. Distribution of crack width of beam Series 2b: according to CEN (2004) (a); according to ACI (2004) (b)

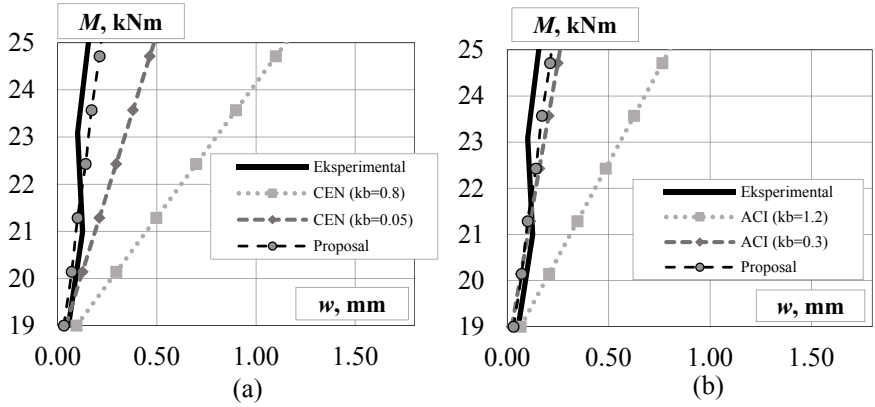

Fig. 3.28. Distribution of crack width of beam Series 3: according to CEN (2004) (a); according to ACI (2004) (b)

Up to 45% of prestress level, beam Series 2a contained 0.20 mm average crack width that was 30% overestimated by authors proposal while changing k_b from 0.8 to 0.05 it reduced overestimation from 8.55 times to 3.6 times based on CEN (2004) and varying k_b from 1.2 to 0.3 overestimation of crack width decreased from 5.95 times to 1.5 times according to ACI (2004) approach. Author‘s proposal gave the closest form of analytical curve to the experimental diagram by having $w_{k.calc}/w_{k.exp}$ = 1.30 (Figs. 3.26a–3.26b) and average $w_{k.calc}/w_{k.exp}$ = 1.25 for beam Series 2b due to higher compressive strength (Figs. 3.27a–3.27b).

Table 3.9. Calculated and experimental values of crack width at service load

Beam Series	Experimental $w_{k.exp}$, mm	Proposed by author $w_{k.calc}$, mm	CEN k_b = 0.8 (recommended) $w_{k.calc}$, mm	ACI k_b = 1.2 (recommended) $w_{k.calc}$, mm	CEN k_b = 0.05 (assumed) $w_{k.calc}$, mm	ACI k_b = 0.30 (assumed) $w_{k.calc}$, mm
Series 1 SSI-1÷SSI-4	0.40	0.50	1.760	1.220	0.74	0.52
Series 2a SSI-5, SSI-6	0.20	0.26	1.710	1.190	0.72	0.30
Series 2b SSI-7, SSI-8	0.20	0.25	1.680	1.170	0.71	0.29
Series 3 SSI-9÷SSI-12	0.12	0.15	1.300	0.90	0.55	0.23

In particular to beam Series 3, based on author's prediction, ratio $w_{k.calc}/w_{k.exp}$ = 1.25 while considering CEN (2004), $w_{k.calc}/w_{k.exp}$ = 10.8 (k_b = 0.8) and $w_{k.calc}/w_{k.exp}$ = 4.5 (k_b = 0.05). Finally, $w_{k.calc}/w_{k.exp}$ = 7.5 (k_b = 1.2) and $w_{k.calc}/w_{k.exp}$ = 1.92 (k_b = 0.3) were predicted using equation by ACI(2004) (Figs. 3.28a–3.28b). It is evident that among design codes used for this analysis, ACI (2004) provides the closest characteristic values to experimental results with assumption k_b = 0.3.

3.5. Conclusions of Chapter 3

1. The experimental investigation of 13 full-scale beams has shown that BFRP reinforcement can be successfully employed for linear internal prestressing by using the appropriate anchor and prestress transfer system capable to undertake a certain level of prestress. Beam Series 1, 2 and 3 had 33%, 40%, and 47% less deflection of midspan at ultimate load than RC (control) beam. This confirms that prestress effects member flexural stiffness and increasing initial prestressing, deflections of midspan are decreasing correspondingly. The increase of prestressing force by 5% and 15%, deflection at midspan decreases by 12% and 26%, respectively.
2. The experimental investigation of stress relaxation of 9 BFRP specimens has shown that BFRP exhibit low relaxation under constant strain up to relaxation time. The increment of the level of prestressing to 40%, 45%, and 55% produce a loss in stress due to relaxation by 5.72%, 6.04% and 6.67%, respectively. Investigation shows that an increase of initial stress level stress relaxation increases proportionally exactly from the beginning of prestress. Moreover, the increase of initial stress produces increasing not constant, but increasing stress relaxation percentages.
3. Based on experimental results, assumed constant stress relaxation percentages based on Banibayat's (2015) model underestimate the results of prestress losses analysis. In order to improve the adequacy of the developed prestress losses stress relaxation behavior shall be evaluated based on present experimental results.
4. Stress-strain values defined by the author‘s proposed calculation method based on stress relaxation approach assures adequate calculation of the average strain over the cross-section. Calculated strain values based on the proposed method were from 1.6 to 3.5% higher than experimental ones.
5. According to the author's proposed method based on stress relaxation approach of BFRP, it delivers the analytical load-deflection curves that have

a similar character to experimental diagrams and remains with safety margin under service load.

6. From design codes point of view, the analysis of deflections based on a comparison of calculated and experimental values confirms the necessity to take into account the decompression moment effect in particular to the estimation of effective moment of inertia. In case of design code formula with no consideration of decompression could lead to 56% higher underestimation of deflections.
7. Using the proposed calculation method in the cracking analysis, calculated crack widths were in good agreement with experimental results (greater 1.23 to 1.36 times than experimental ones) depending on the increase of prestressing level from 5% to 15%.

General Conclusions

Summarizing the findings of the dissertation, the following conclusion could be drawn:

1. The literature review showed that there are no particular values of stress relaxation of BFRP reinforcement for analysis of prestress losses. Calculation of prestress losses due to stress relaxation in a manner similar to that for steel or other FRPs would lead to inaccurate estimation results.
2. In contrary to prestressed steel bars, where an increase of stress relaxation appears at the higher choice of the initial stress level with an increase of initial stress level in BFRP prestressing bars, stress relaxation increases proportionally at low prestress level.
3. The proposed calculation method for effective prestress force takes into account stress relaxation behavior of BFRP prestressing bars that allow to evaluate prestress losses accurately depending on the certain consecutive stage of PC members.
4. Stress-strain values defined by the author‘s proposed method based on stress relaxation approach assures adequate calculation of the average strain over the cross-section. Calculated strain values were up to 3.5% higher than the experimental results. It means that predictions by the proposed method were more accurate than using other authors technique.

5. Analysis has shown that deflections were underestimated by 56% in comparison with experimental results having no decompression moment considered in the estimation of effective moment of inertia from design code provisions. In the present work, it was proposed to perform with decompression moment considered in regard to the principles of PC behavior.
6. Unlike this design code approach, proposed calculation method based on stress relaxation of BFRP might be used as an alternative one. It delivers the analytical load-deflection curves with similar character to experimental diagrams.
7. The proposed method for crack width analysis allows to perform realistic cracking behavior of PC beams prestressed with BFRP bars considering the effect of decompression and shrinkage of concrete. Based on this method calculated crack widths were in good agreement with experimental results. Experimental values were overestimated by 25–30% by theoretical ones.
8. The experimental results showed that the increase of prestress level significantly impact the stiffness of the beams. Beams prestressed with 40%, 45% and 55% of the ultimate tensile strength of BFRP produced 33%, 40%, and 47% less deflection that in comparison with RC beam. The increase of prestressing force by 5% and 15%, deflection at midspan decreases by 12% and 26%, respectively.
9. Unique experimental investigation of stress relaxation of BFRP bars showed that BFRP exhibit stress relaxation rates 5.72%, 6.04% and 6.67% depending on prestressing level 40%, 45%, and 55%, respectively. With an increase of initial stress level stress relaxation increases proportionally from low prestress level.
10. Based on experimental results, the stress relaxation coefficient is proposed for BFRP reinforcement. A polynomial equation is evaluated to describe the relationship of prestress ratio, relaxation time and the mechanical properties of BFRP.

References

Abdelrahman, A.; Rizkalla, S.1997. Serviceability of concrete beams prestressed by carbon fiber-reinforced-plastic bars. *ACI Structural Journal* 94(4): 447–454.

Abdelrahman, A.; Rizkalla, S. 1999. Deflection control of concrete beams pretensioned by CFRP reinforcements. *ASCE Journal of Composites for Construction* 3(2): 55–62.

Abhijit, M.; Gopal, L. R. 2009. Performance of reinforced concrete beams externally prestressed with fiber composites. *Construction and Building Materials* 23(2): 822–828.

ACI Committee 440. 2006. *Guide Test Methods for Fiber-Reinforced Polymers (FRPs) for Reinforcing or Strengthening Concrete Structures, ACI 440.3R-04*. Farmington Hills, Michigan: ACI. 40 p.

ACI Committee 440.2004. *Guidelines for prestressing concrete structures with FRP tendons*, ACI–440.4R–04. Farmington Hills, Michigan: ACI. 35 p.

Arockiasamy, M.; Sowrirajan, R.; Zhuang, M. 1995. Behaviour of beams prestressed or strengthened with fiber reinforced plastic composites. *IABSE Reports V*: 997–1002.

Balaguru, P.; Nanni, A.; Giancaspro, J. 2009. *FRP Composites for Reinforced and Prestressed Concrete Structures. A Guide to Fundamentals and Design for Repair and Retrofit*. New York: Tailor&Francis 348 p.

Balafas, I.; Burgoyne, C.J. 2012. Economic design of beams with FRP rebar or prestress, *Magazine of Concrete Research* 64(10): 885–898.

Balevičius, R. 2010. An average stress strain approach to creep analysis of RC uncracked elements, *Mechanics of Time-Dependent Materials* 14: 69–89.

Balevičius, R.; Augonis, M. 2018. The effects of bond, shrinkage anf creep on cracking resistance of steel and GFRP RC members, *Composite Structures* 187: 85–101.

Banibayat, P.; Patnaik, A. 2015. Creep rupture performance of basalt fiber-reinforced polymer bars, *ASCE Journal of Aerospace Engineering* 28(3): 1–9.

Bažant, Z.; Buyukozturk, O. 1988. *Mathematical Modeling of Creep and Shrinkage of Concrete*. New York: Wiley. 459 p.

Bažant, Z.; Yu, Q. 2013. Relaxation of prestressing steel at varying strain and temperature: viscoplastic constitutive relation, *ASCE Journal of Engineering Mechanics* 139(7): 814–823.

Bischoff, P. 2005. Reevaluation of deflection prediction for concrete beams reinforced with steel and fiber reinforced polymer bars. *ASCE Journal of Composites for Construction* 131(5): 752–767.

Bischoff, P.; Gross, S. 2011. Design approach for calculation deflection of FRP-reinforced concrete, *ASCE Journal of Composites for Construction* 15(4): 490–499.

Bhatt, P. 2011. *Prestressed Concrete Design to Eurocodes*. London: Spon Press. 617 p.

Buyukozturk, O.; Hearing, B. 1998. Failure behaviour of precracked concrete beams retrofitted with FRP, *ASCE Journal of Composites for Construction* 2(3): 138–144.

Borosnyói, A. 2002. *Serviceability of CFRP Prestressed Concrete Beams*. PhD thesis. Budapest University of Technology and Economics. 285 p.

Brinson, H.F.; Brinson, L.C. 2015. *Polymer Engineering Science and Viscoelasticity. An Introduction*. New York: Springer. 488 p.

Bryan, P. E.; Green, M. F. 1996. Low temperature behaviour of CFRP prestressed concrete beams, *Canadian Journal of Civil Engineers* 23(2): 464–470.

Canadian Network of Centres of Excellence on Intelligent Sensing for Innovative Structures (ISIS). 2008. *Prestressing concrete structures with fibre-reinforced polymers. Design Manual No. 5*. Winnipeg: ISIS Canada Corporation. 149 p.

Collins, M. P; Mitchell, D. 1991. *Prestressed Concrete Structures*. New Jersey: Englewood Cliffs. 766 p.

Comité Euro-International du Béton (CEB). 1984. *Structural Effects of Time-Dependent Behaviour of Concrete. Bulletin No. 142*. Saint-Saphorin: Georgi Publishing Company. 393 p.

Creazza, G.; Mele, M. 1991. *Advanced Problems in Bridge Construction*. New York: Springer–Verlag Wien. 298 p.

Diab, H.; Iwashita, K. 2009. Short and long-term bond performance of prestressed FRP sheets anchorage, *Engineering Structures* 31(5): 1241–1249.

Det Norske Veritas. 2012. *Offshore Concrete Structures, DNV–OS–C502*.Høvik:102 p.

Dolan, C. W.; Hamilton, H. R.; Bakis, C. E.; Nanni, A. 2000. Design recommendations for concrete structures prestressed with FRP tendons, Draft Final Report, University of Wyoming, Department of Civil and Architectural Engineering*, Report DTFH61-96-C-00019*, Laramie Wyoming: 133 p.

European Committee for standardization (CEN). *Design of concrete structures. Part 1-1: General rules and rules for buildings. Eurocode 2, EN 1992–1–1*. Brussels: 230 p.

El Refai, A. 2013. Durability and fatigue of basalt fiber-reinforced polymer bars gripped with steel wedge anchors, *ASCE Journal of Composites for Construction* 17(6): 1–11.

El-Hacha, R.; Wight, R. G.; Green, M. F. 2001. Prestressed carbon fiber reinforced polymer sheets for strengthening structures, *Progress in Structural Engineeringand Materials* 3: 111–121.

El-Hacha, R.; Green, M. F.; Wight, R. G. 2003. Innovative system for prestressing fiber-reinforced polymer sheets, *ACI Structural Journal* 100(3): 305–313.

Fam, A. Z.; Rizkalla, S. H.; Tadros, G. 1997. Behavour of CFRP for prestressing and shear reinfrocements of concrete highway bridges, *ACI Structural Journal* 94(1): 77–86.

Fédération Internationale du Béton (*fib*). 2007. *FRP reinforcement in RC structures, fib Bulletin No.40*. Lausanne: EPFL. 160 p.

Fédération Internationale de la précontrainte. 1978. *Recommendations for the Design of Prestressed Concrete Oil Storage Tanks. FIP Report*. London. 44 p.

Fédération Internationale de la précontrainte. 1982. *Cryogenic Behavior of Materials for Prestressed Concrete.FIP Report*. London: Wexham Springs. 84 p.

Fico, R. 2004. *Limit States Design of Concrete Structures Reinforced with FRP Bars*. PhD Thesis. University of Naples Federico II, Naples, Italy, 167 p.

fib (International Federation for Structural Concrete). 2013. *Model Code for Concrete Structures 2010*, Berlin: Ernst & Sohn, 245 p.

Fornůsek, J; Konvalinka, P; Sovják, R; Vítek, J. L. 2009. Long-Term Behaviour of Concrete Structures Reinfroced with Prestressed GFRP Tendons, *Cumputation Methods and Experimental Measurements XIV*, 18: 535–545.

Freudenthal, A. M.; Roll, F. 1958. Creep and Creep Recovery of Concrete under High Compressive Stress, *ACI Concrete Journal*, 1111–1142.

Gaythwaite, J. W. 2004. *Design of Marine Facilities for the Berthing, Mooring and Repair of Vessels*. ASCE Press. 524 p.

Gaythwaite, J. W. 2016. *Design of Marine Facilities. Engineering for Port and Harbour Structures*, Reston, Virginia: ASCE Press. 734 p.

Garden, H. N.; Hollaway, L. C. 1998. An experimental study of the failure modes of reinforced concrete beams strengthened with prestressed carbon composite plates, *Composites Part B: Engineering* 29(4): 411–424.

GangaRao, H. V. S; Vijay. P. V.1997. Aging of structural composites under varying environmental conditions. Proc. 3rd Int Symp. Non-Metallic (FRP) Reinforcement for Concrete Structures, JCI.

Gerwick, B.1992. *Construction of Prestressed Concrete Structures*, New York: John Wiley & Sons. 591 p.

Gilbert, I. R.; Mickleborough, N. C. 1988. *Design of Prestressed Concrete*, London: Spon Press. 547 p.

Gilbert, I. R.; Ranzi, G. 2011. *Time-Dependent Behaviour of Concrete Structures*, London: Spon Press. 447 p.

Gilbert, I. R.; Mickleborough, N. C.; Ranzi, G. 2017. *Design of Prestressed Concrete to Eurocode 2*, Boca Raton: CRC Press. 665 p.

Ghali A. 1993. Deflection of reinforced concrete members: a critical review. *ACI Structural Journal* 90(4):364–373.

Ghali, A.; Favre, R.; Eldbadry, M. 2012. *Concrete Structures. Stresses and Deformations*, London: Spon Press. 637 p.

Ghali, A. 2017. *Circular Storage Tanks and Silos*, CRC Press. 387 p.

Grace, N.; Singh, S. B. 2003. Design approach for carbon fiber-reinforced polymer prestressed concrete bridge beams, *ACI Structural Journal* 100(3): 365–376.

Grace, N.; Enomoto, T.; Baah, P.; Bebawy, M. 2012. Flexural behaviour of CFRP precast prestressed decked bulb T-beams, *ASCE Journal of Composites for Construction* 16(3): 225–234.

Grace, N.; Ushijima, K.; Matsagar, V.; Wu, C. 2013. Performance of AASHTO-type bridge model prestressed with carbon fiber-reinforced polymer reinforcement, *ACI Structural Journal* 110(3): 491–501.

Gribniak, V.; Cervenka, V.; Kaklauskas, G. 2013. Deflection prediction of reinforced concrete beams by design codes and computer simulation, *Engineering Structures* 56: 2175–2186.

Harding, J. E.; Parke, G. E. R.; Ryall, M. J. 2010. *Bridge Management. Inspection, Maintenance, Assessment and Repair.* New York: Tailor&Francis. 888 p.

Heo, S.; Shin, S.; Lee, C. 2013. Flexural behavior of concrete beams internally prestressed with unbonded carbon-fiber-reinforced polymer tendons, *ASCE Journal of Composites for Construction* 17(2): 167–175.

Issa, M. A. 1995. Prestress losses in fiberglass pretensioned concrete compression members, *Materials and Structures* 28: 330–339.

Jakubovskis, R.; Kaklauskas, G.; Gribniak, V.; Weber, A.; Juknys, M. 2014. Serviceability analysis of concrete beams with different arrangements of GFRP bars in the tensile zone, *ASCE Journal of Composites for Construction* 18(5): 1–10.

Japan Society of Civil Engineers (JSCE). 1995. *Test Method for Tensile Properties of Continous Fiber Reinforced Materials, JSCE-E 531*. Tokyo: JSCE Concrete Committee: 77 p.

Jirásek, M.; Bažant, Z. 2001. *Inelastic Analysis of Structures*. Chichester: Wiley&Sons. 758 p.

Jokūbaitis, V.; Kamaitis, Z. 2000. *Cracking and Repair of Reinforced and Prestressed Concrete Structures*. Monograph. Vilnius: Technika. 155 p.

Jokūbaitis, A.; Marčiukaitis, G.; Valivonis, J. 2016. Influence of technological and environmental factors on the behaviour of the reinforcement anchorage zone of prestressed concrete sleepers, *Construction and Building Materials* 121: 507–518.

Kaklauskas, G. 2001a. *Integral Flexural Constitutive Model for Deformational Analysis of Concrete Structures*. Monograph.Vilnius: Technika.140 p.

Kaklauskas, G.; Bačinskas, D.; Zamblauskaitė, R. 2001b. *Deformations of Reinforced Concrete Members*. Vilnius: Technika. 206 p.

Kaklauskas, G. 2004. Flexural layered deformational model of reinforced concrete members, *Magazine of Concrete Research* 56(10): 575–584.

Karbhari, V. M.; Youakim S. A. 2007. An approach to determine long-term behaviour of concrete members prestressed with FRP tendons, *Construction and Building Materials* 21: 1052-1060.

Kim, Y. J.; Green, M. F.; Wight, R. G. 2007. Flexural behavior of reinforced and prestressed concrete beams including strengthening with prestress carbon fibre reinforced polymer sheets: Application of a fracture mechanics method, *Canadian Journal of Civil Engineering* 34(5): 664–677.

Kim, Y. J. 2014. *Advanced Composites in Bridge Construction and Repair*, Cambridge: Woodhead Publishing (Elsevier). 351 p.

Kostikov, V. I. 1995. *Fibre Science and Technology. Soviet Advances Composites Technology Series. Russian Academy of Sciences*. Dordrecht: Springer. 694 p.

Lees, J. M.; Burgoyne, C. J. 1999. Experimental study of influence of bond on flexural behavior of concrete beams pretensioned with aramid fiber reinforced plastics, *ACI Structural Journal*96 (3): 377–385.

Leonhardt, F.1977. Crack Control in Concrete Structures. *IABSE Surveys S-4*(77): 26 p.

Lemini, D. G. 2014. *Engineering Viscoelasticity*. New York: Springer. 359 p.

Lin, T. Y.; Burns, N. H. 1981. *Design of Prestressed Concrete Structures*. New York: Wiley&Sons. 646 p.

Malkin, A. Y. 1994. *Rheology Fundamentals*. Moscow: Reasearch Institute of Plastics. ChemTec Publishing. 326 p. (in Russian).

Marčiukaitis, G.; Jonaitis, B.; Papinigis, V.; Valivonis, J. 2007. *Design of Reinforced Concrete Structures According to Euronorms*, Vilnius: Technika. 340 p. (in Lithuanian).

Marčiukaitis, G. 2012. *Prestressed Concrete*, Vilnius: Technika. 296 p. (in Lithuanian).

Marčiukaitis, G. 2013. *Influence of Technological Factors on the Behavior of Concrete and Reiforced Concrete*, Vilnius: Technika. 284 p. (in Lithuanian).

McConnell, K.; Allsop, W.; Cruikshank, I. 2004. *Piers, Jetties and Related Structures Exposed to Waves. Guidelines for Hydraulic Loadings*, London: ICE (Thomas Telford). 133 p.

Meier, U. 1987. Proposal for a carbon fiber reinforced composite bridge across the strait of Gibraltar at its narrowest site. *Proceedings of the Institution of Mechanical Engineers*, 201(2):73–78.

Meiswinkel, R.; Meyer, J.; Schnell, J. 2013. *Beton Kalender. Design and Construction of Nuclear Power Plants*, Berlin: Wiley. 150 p.

Meier, U. 1995. Strengthening of structures using carbon fibre/epoxy composites, *Construction and Building Materials* 9(6): 341–351.

Mertol, H. C.; Rizkalla, S. H.; Scott, P.; Lees, J. M.; El-Hacha, R. 2007. Durability and fatigue behaviour of concrete beams prestressed with CFRP, *Proceedings of the 3rd International Conference on Durability and Field Applications of Fiber-Reinforced Polymers (FRP) Composites for Construction*: 17–24.

Mias, C.; Torres, L.; Turon, A.; Barris, C. 2013. Experimental study of immediate and time-dependent deflections of GFRP reinforced concrete beams. *Composite Structures* 96(2): 279–285.

Mias, C.; Torres, L.; Guadagnini, M.; Turon, A. 2015. Short and long-term cracking behavior of GFRP reinforced concrete beams. J Compos Part B: Eng 77(8): 223–231.

Mota, C.; Alminar, S.; Svecova, D. 2006. Critical review of deflection formulas for FRP-RC members, *ASCE Journal of Composites for Construction* 10(3):183-194.

Mousavi, S. R.; Esfahani, M. R. 2012. Effective moment of inertia prediction of FRP-reinforced concrete beams based on experimental results. *ASCE Journal of Composites for Construction* 16(5): 490–498.

Navrátil, J. 2006. *Prestressed Concrete Structures*, Brno: Akademicke Nakladatelstvi. 184 p.

Nanni, A.; Tanigaki, M. 1992. Pretensioned prestressed concrete members with bonded fiber reinforced plastic tendons: development and flexural bond length (Static), *ACI Structural Journal* 89: 433–441.

Nanni, A. 1993. *Fiber-Reinforced-Plastic (FRP) Reinforcement for Concrete Structures. Properties and Applications*. Elsevier Science Publishers. 436 p.

Nawy, E. G. 2003. Prestressed concrete. A fundamental approach. Prentice Hall. 939 p.

Notkus, A. J. 2010. *Fundaments of Bridges Design*, Vilnius: Technika. 256 p. (in Lithuanian).

Noël, M. Soudki, K. 2013. Effect of prestressing on the performance of GFRP-reinforced concrete slab bridge strips, *ASCE Journal of Composites for Construction* 17(2): 188–196.

Noël, M. Soudki, K. 2014. Fatigue behavior of full-scale slab bridge strips with FRP reinforcement, *ASCE Journal of Composites for Construction* 19(2): 1–9.

Odagiri, T.; Matsumoto, K.; Nakai, H. 1997. Fatigue and relaxation characteristics of continuous aramid fiber reinforced plastic rods, *Proceedings of the 3rd International Symposium on FRP reinforcement for concrete structures*, Sapporo, Japan: 227–234.

Park, S. Y.; Naaman, A. E. 1999. Dowel behaviour of tensioned fiber reinforced polymer (FRP) tendons, *ACI Structural Journal* 96(5): 799–807.

Pallegrino, C.; Modena, C. 2009. Flexural strengthening of real scale RC and PRC beams with end-anchored pretensioned FRP laminates. *ACI Structural Journal* 106(3): 319–328.

Pearson, M.; Donchev, T.; Salazar, J. 2013. Long – term behaviour of prestressed basalt fibre reinforced polymer bars, *Procoedia Engineering* 54: 261–269.

Pisani, M.A. 2000. Long-term behaviour of beams prestressed with aramid fibre cables Part 1: a general method, *Engineering Structures* 22:1641–1650.

Reddy, J. N. 2013. *An Introduction to Continuum Mechanics*. New York: Cambridge University Press. 479 p.

Rosenboom, O. A.; Rizkalla, S. H. 2005. Fatigue behavior of prestressed concrete bridge girders strengthened with various CFRP systems, FRPRCS-7597-612.

Rubinsky I. A.; Rubinsky A. 1954. A preliminary investigation of the use of fiberglass for prestressed concrete, *Magazine of Concrete Research* 6(17): 71–78.

Saadatmanesh, H.; Tannous, F. E. 1999. Long-term behaviour of aramid fiber reinforced plastic (AFRP) tendons, *ACI Materials Journal* 96(3): 291–299.

Sen, R.; Issa, M.; Mariscal, D. 1992. *Feasibility of Fiberglass Pretensioned Piles in a Marine Environment. Report*. Florida: The University of South Florida. 320 p.

Sen, R.; Shahawy, M.; Rosas, J.; Sukumar, S. 1998. Durability of Aramid Pretensioned Elements in a Marine Environment, *ACI Structural Journal* 95(5): 578–586.

Sen, R.; Shahawy, M.; Rosas, J.; Sukumar, S. 1999. Durability of aramid fiber reinforced plastic pretensioned elements under tidal/thermal cycles, *ACI Structural Journal* 96(1): 95–104.

Serbescu, A.; Guadagnini, M.; Pilakoutas, K. 2014. Mechanical characterization of basalt FRP rebars and long-term strength predictive model, *ASCE Journal of Composites for Construction* 19(2): 1–13.

Sim, J.; Park, C.; Moon, D.Y. 2005. Characteristics of basalt fiber as a strengthening material for concrete structures. *Composites Part B: Engineering* 36(7): 504–12.

Shi, J; Wang, X; Wu, Z; Zhu, Z. 2015. Creep behavior enhancement of a basalt fiber-reinforced polymer tendon, *Construction and Building Materials* 94: 750–757.

Shi, J.; Wang, X.; Huang, H.; Wu, Z. 2016. Relaxation behaviour of prestressed fiber-reinforced polymer tendons considering anchorage slippage, *Journal of Composite Materials* 51(9): 1275–1284.

Sovják, R.; Konvalinka, P. 2012. Creep behavior and residual flexural capacity of GFRP and CFRP prestensioned concrete slabs, Asian Review of Civil Engineering (ARCE) 1(1): 30–37.

Stanley, T. K. N.; Soudki, K. 2010. Shear behaviour of externally prestressed beams with carbon fiber-reinforced polymer tendons, *ACI Structural Journal* 107(4): 443–450.

Toutanji, H. A.; Saafi, M. 2000. Flexural behavior of concrete beams reinforced with glass fiber – reinforced polymer (GFRP) bars, *ACI Structural Journal* 97(5): 712–719.

Thien, N. P. 2013. *Understanding Viscoelasticity. An Introduction to Rheology*. Heidelberg: Springer. 207 p.

Tsinker G. 1995. *Marine Structures Engineering: Specialized Applications*. Springer. 566 p.

Tsinker G. 1997. *Handbook of Port and Harbor Engineering.Geotechnical and Structural Aspects*, Springer. 1054 p.

Torres, L.; Sharaky, I.; Barris, C.; Baeba, M. 2013. Experimental study of the influence of adhesive properties and bond length on the bond of NSM FRP Bars in Concrete. *Journal of Civil Engineering and Management* 22(6): 808–817.

Triantafillou, T. C.; Deskovič, N. 1991. Innovative prestressing with FRP sheets: Mechanics of short –term behaviour, *ASCE Journal of Engineering Mechanics* 117(7): 1652–1672.

Triantafillou, T. C.; Deskovič, N.; Deuring, M. 1992. Strengthening of concrete structures with prestressed fiber reinforced plastic sheets, *ACI Structural Journal* 89(3):235–244.

Valivonis, J; Jurkša, A. 1995. Obobshchionyj metod raszheta izgibajemych zhelezobetonnych elementov s dopolnytelnym wneshnym nemetalitsheskim armrovanijem, *Zhelezobetonnyje konstrukciji* 17(1): 43–38. (in Russian).

Wang, X; Wu, Z; Wu, G; Zhu, H; Zen, F. 2013. Enhancement of basalt FRP by hybridization for long-span cable-stayed bridge, *Composites: Part B*, 44: 184–192.

Wang, X; Shi, J; Liu, S; Yang, L; Wu, Z. 2014a. Creep behavior of basalt fiber reinforced polymer tendons for prestressing application, *Materials and Design*, 59: 558–564.

Wang, X; W, G; Wu, Z; Dong, z; Xie, Q. 2014b. Evaluation of prestressed basalt fiber and hybrid fiber reinforced polymer tendons under marine environment, *Materials and Design*, 64: 721–728.

Wang, X; Shi, J; Wu, Z; Zhu, Z.2016a. Fatigue Behavior of Basalt Fiber-Reinforced Polymer Tendons for Prestressing Applications, *ASCEJournal of Composites for Construction*20 (3): 1–10.

Wang, X; Shi, J; Wu, Z; Zhu, Z. 2016b. Creep strain control by pretension for basalt fiber-reinforced polymer tendon in civil applications, *Materials and Design*, 89: 1270–1277.

Wight, R. G.; Green, M. F.; Erki, M. A. 2001. Prestressed FRP sheets for post strengthening reinforced concrete beams, *ASCE Journal of Composites for Construction* 5(4): 214–220.

Woo, S. K.; Nam, J. W.; Kim, H. J.; Han, S. H.; Byun, K. J. 2008. Suggestion of flexural capacity evaluation and prediction of prestress CFRP strengthened design. *Engineering Structures*, 30(12): 3751–3763.

Xue, W.; Tan, Y.; Zeng, L. 2010. Flexural response predictions of reinforced concrete beams strengthened with prestressed CFRP plates, *Composite Structures* 92(3): 612–622.

Yang, D. S.; Park, S. K.; Neale, K. W. 2009. Flexural behavior of reinforced concrete beams strengthened with prestressed carbon composites, *Composite Structures* 88(4): 497–508.

Yost, J. R.; Gross, S. P.; Dinehart, D. W. 2003. Effective moment of inertia for glass fiber-reinforced polymer reinforced concrete beams, *ACI Structural Journal* 100(6): 732–739.

Zavadskas, E.; Kamaitis, Z.; Kudzys, A. 1974. Study of prestress losses in composite laminated timber elements, *Beton i Zelezobeton (Concrete Structures)* 6: 115–124 (in Russian).

Zhuo, J.; Wang, F.; Li, T. 2009. Application of FRP Strap in an Innovative Prestressed Method, *ASCE Journal of Materials in Civil Engineering* 21(4): 176–180.

Zoghi, M. 2014. *The International Handbook of FRP Composites in Civil Engineering*, CRC Press. 692 p.

Zou, P. X. W. 2003a. Long-term properties and transfer length of fiber-reinforced polymers, *ASCE Journal of Composites for Construction* 7(3): 10–19.

Zou, P. X. W. 2003b. Long-term deflection and cracking behaviour of concrete beams prestressed with carbon fiber-reinforced polymer tendons, *ASCE Journal of Composites for Construction* 7(3): 187–193.

Zou, P. X. W. 2003c. Theoretical study on short-term and long-term deflections of fiber reinforced polymer prestressed concrete beams, *ASCE Journal of Composites for Construction* 7(3): 285–291.

List of Scientific Publications by the Author on the Topic of the Dissertation

Publications in the Reviewed Scientific Journals

Atutis, M; Valivonis, J.; Atutis, E. 2018a. Experimental study of concrete beams prestressed with basalt fiber reinforced polymers. Part II: Stress relaxation phenomenon, *Composite Structures* 202:344–354. Oxford: Elsevier. ISSN 0263-8223. [Clarivate Analytics Web of Science, IF: 4.193].

Atutis, M.; Valivonis J.; Atutis, E. 2018b. Experimental study of concrete beams prestressed with basalt fiber reinforced polymers. Part I: Flexural behavior and serviceability, *Composite Structures* 183:114–123. Oxford: Elsevier. ISSN 0263–8223. [Clarivate Analytics Web of Science, IF: 4.193].

Atutis, M; Valivonis J; Atutis, E. 2015. Analysis of serviceability limit state of GFRP prestressed concrete beams. *Composite Structures* 134: 450–459. Oxford: Elsevier. ISSN 0263-8223. [Clarivate Analytics Web of Science, IF: 4.193].

Atutis, E.; Budvytis, M.; Atutis, M. 2013a. Experimental study on the flexural and shear analysis of concrete beams reinforced with glass fiber-reinforced (GFRP) bars, *Science – future of Lithuania: civil and transport engineering, aviation technologies* 5(5): 467–473. Vilnius: Technika. ISSN 2029-2341. http://dx.doi.org/10.3846/mla.2013.73

Atutis, E.; Valivonis, J.; Atutis, M. 2013b. Experimental analysis on flexural behaviour of concrete beams with GFRP reinforcement, *Engineering Structures and Techniques*, 5(2): 76–81. Vilnius: Technika. ISSN 2029-2317.

Atutis, M.; & Valivonis, J. 2011. Anchorage characteristics of non-metallic reinforcement for concrete, *Engineering Structures and Techniques* 3(2): 72–78. Vilnius: Technika. ISSN 2029-2317.

Atutis, M. 2010a. Calculating the carrying capacity of flexural prestressed concrete beams with non-metallic reinforcement, *Science – future of Lithuania: civil and transport engineering, aviation technologies* 2(6): 5–13. Vilnius: Technika. ISSN 2029-2341. http://dx.doi.org/ 10.3846/mla.2010.104

Atutis, M.; & Valivonis, J. 2010b. Reinforcement cahracteristics of prestressed concrete beams with fiber-reinforced polymer tendons, *Engineering Structures and Techniques* 2(2): 71–78. Vilnius: Technika. ISSN 2029-2317.

Publications in Other Editions

Atutis, E.; Atutis, M.; Budvytis, M.; Valivonis, J. 2017. Serviceability and Shear Response of RC beams prestressed with various types of FRP bars, *Procedia Engineering* 172: 60–67. Modern Building Materials, Structures and Techniques (MBMST 2016). Amsterdam: Elsevier Ltd. ISSN 1877-7058.

Atutis, M.; Atutis, E.; Valivonis, J. 2017. Prestress losses due to relaxation of basalt fiber reinforced polymers. *Proceedings of the Third International Conference on Mechanics of Composites (MECHCOMP3)*. Bologna: Societa' Editrice Esculapio. ISSN 2421-2822. 110–111.

Atutis, M.; Valivonis, J.; Atutis, E. 2016. Experimental study of flexural behaviour of concrete beams prestressed with basalt fiber reinforced plastics. *Proceedings of the 19th International Conference on Composite Structures (ICCS19).* Porto: Societa' Editrice Esculapio. ISSN 2421-2822. 177–178.

Atutis, M.; Valivonis, J.; Atutis, E. 2015. The issues related to flexural behaviour of FRP prestressed concrete beams. *Proceedings of the 18th International Conference on Composite Structures (ICCS18)*. June 15-18, 2015, Lisbon, Portugal. 74–75.

Summary in Lithuanian

Įvadas

Problemos formulavimas

Iš anksto įtemptas gelžbetonis yra vienas iš ekonomiškai efektyviausių gelžbetoninių konstrukcijų tipų. Šio tipo konstrukcijos vis plačiau naudojamos energetikos, transporto infrastruktūros statiniuose. Skaičiuojant iš anksto įtemptuosius gelžbetoninius elementus yra svarbu žinoti išankstinės įtempimo jėgos dydį, kuris priklauso nuo įvairių reiškinių, sukeliančių įtempių nuostolius armatūroje ir taip mažinančius išankstinio įtempimo jėgos didumą priklausomai nuo elemento apkrovimo stadijos (armatūros įtempimo į atsparas, elemento sandėliavimas be išorinės apkrovos poveikio, elemento apkrovimo išorine apkrova). Išankstiniai armatūros įtempių nuostoliai turi didelę įtaką armatūros išankstiniams įtempiams, betono apgniuždymui, gelžbetoninių konstrukcijų įtempių ir deformacijų būviui bei priklauso nuo armatūros rūšies ir jos įtempimo būdo. Įtempus armatūrą į atsparas įtempiai armatūroje laikui bėgant mažėja. Pagrindinės išankstinių įtempių nuostolių priežastys yra greitai pasireiškiantis betono valkšnumas, betono traukumas, iš anksto įtemptosios armatūros relaksacija ir kt. Išankstinės įtempimo jėgos kitimą laike lemia gamybos metu atsirandantys nuostoliai (iškart patiriami arba trumpalaikiai) ir nuostoliai, kurių atsiranda atleidus armatūrą, vadinami nuo laiko priklausantys (antriniais) arba ilgalaikiais. Skaičiuojant išankstinių įtempių nuostolius didelę įtaką turi pasirinktas betono įtempių ir deformacijų matematinis modelis. Įvarių šalių projektavimo normos rekomenduoja analogiškus medžiagų fizinių ir mechaninių rodiklių vertinimo modelius, tačiau skirtingus įtempių nuostolių vertinimo bei skaičiavimo metodus. Nepriklausomai nuo gelžbetoninių

konstrukcijų tipo bei armatūros įtempimo būdo atsparumas korozijai vis dar lieka pagrindine kliūtimi, apribojančia šių konstrukcijų eksploataciją agresyvioje aplinkoje, o tai gali lemti papildomus eksploatacijos kaštus statinių naudotojams jas remontuojant. Tokiu atveju, kaip alernatyva, gali būti taikomos naujos ir inovatyvios kompozitinės medžiagos, tokios kaip, neplieninės kompozito arba polimerų pluošto armatūros strypai (angl. *FRP*), kurie pasižymi didesniu nei plieno tempiamuoju stipriu, antimagnetinėmis savybėmis, atsparumu korozijai, pakankamu atsparumu nuovargiui, mažu šilumos laidumu, didesniu nei plieno stiprio ir masės santykiu bei galimai mažesniais išankstinio įtempimo nuostoliais dėl armatūros relaksacijos lyginant su plienine armatūra. Anglies, stiklo, aramido pluošto kompozitai, naudojami aviacijos ir kosmoso bei automobilių pramonėje iš dalies pakeičia tradicines natūralias medžiagas. Naujų konstrukcinių medžiagų poreikis nuolat auga, kuriama vis daugiau kompozitinių medžiagų rūšių ir labai dažnai stokojama informacijos apie jų savybes. Viena tokių – bazalto pluošto kompozitas. Tai neorganinis cheminis pluoštas, kurio žaliava – vulkaninė uoliena – pigesnė už stiklo. Bazalto pluoštas turi visus teigiamus anksčiau minėtų kompozitų požymius, ir remiantis eksperimentiniais tyrimais, yra atsparesnis aukštoms temperatūros bei šarmams, o tempiamasis medžiagos stipris gali būti išnaudojamas suteikiant išankstinį įtempimą.

Nepasaint vis didėjančio mokslininkų susidomėjimo pritaikyti naujas kompozitines medžiagos statybos pramonėje, praktinį šių medžiagų panaudojimą riboja tiek projektavimo normų reikalavimų, tiek naujų eksperimentinių tyrimų rezultatų stoka. Suteikus armatūrai išankstinius įtempius, pasikeičia visos konstrukcijos įtempių ir deformacijų būvis, laikui bėgant įtempiai joje mažėja, tačiau deformacija lieka pastovi. Armatūros įtempių relasakcijos elgsenai didelę įtaka turi medžiagos struktūra bei pradiniai jos įtempiai. Tokių tyrimų trūksta, todėl svarbu nustatyti bazalto pluošto armatūros įtempių relaksacijos reikšmes priklausomai nuo pradinių jos įtempių, siekiant įvertinti efektyvų išankstinio armatūros įtempimo dydį ir jo įtaką betoninių sijų armuotų iš anksto įtemptais bazalto pluošto strypais tinkamumo ribiniam būviui.

Darbo aktualumas

Bazalto pluošto kompozitai gali būti taikomi iš anksto įtemptoms betoninėms konstrukcijoms armuoti. Tačiau, dauguma iš anksto įtemptų gelžbetininių konstrukcijų tyrimų buvo skirta tradicine plienine armatūra armuotiems elementams. Norint tinkamai suprojektuoti ir pagaminti betonines konstrukcijas, armuotas iš anksto įtemptais bazalto pluošto strypais, tradicinių gelžbetoninių konstrukcijų skaičiavimo metodai gali nevisiškai atspindėti realią šių konstrukcijų elgseną veikiant išorinei apkrovai. Tai ypač aktualu norint tiksliai apskaičiuoti išankstinio įtempimo jėgos dydį ir jos nuostolius, kuriuos aprašantys inžineriniai metodai apytiksliai atspindi sudėtingą konstrukcinės medžiagos elgseną. Naudojant kompozitines medžiagas ir jas iš anksto įtempiant, kompozito armatūros relaksacijos elgsena yra itin svarbi išankstinių įtempių nuostolių priežastis nustatant efektyviąją išankstinio įtempimo jėgą. Adekvatus bazalto pluošto armatūros įtempių relaksacijos įvertinimas leidžia tiksliau įvertinti iš anksto įtemptų betoninių konstrukcijų pleišėjimo pobūdį ir deformacijas.

Remiantis konstrukcinių medžiagų kontinuumo mechanikos (reologinių) modelių, išankstinių įtempių nuostolių, pleišėtumo ir įlinkių metodikų analizės rezultatais buvo pasiūlytas efektyviosios išankstinio įtempimo jėgos vertinimo modelis ir sudarytas skaičiavimo algoritmas atsižvelgiant į įtemptosios bazalto pluošto armatūros įtempių relaksacijos nuostolius bei jų pasireiškimo eiliškumą. Pasiūlytos įlinkių ir pleišėjimo skaičiavimo metodikos, tinkančios iš anksto įtemptais bazalto pluošto strypais armuotų betoninių konstrukcijų skaičiavimui.

Tyrimo objektas

Darbe nagrinėjama išankstinių armatūros įtempių ir jos įtempių relaksacijos įtaka betoninių elementų, armuotų iš anksto įtemptais bazalto pluošto strypais, elgsenai.

Darbo tikslas

Šios disertacijos tikslas – pasiūlyti naujus bazalto pluošto armatūros įtempių relaksacijos bei efektyviosios išankstinio įtempimo jėgos nustatymo modelius, kuriais remiantis būtų galima vertinti iš anksto įtemptųjų betoninių elementų deformacijas ir pleišėjimą.

Darbo uždaviniai

Darbo tikslui pasiekti sprendžiami šie uždaviniai:

1. Išanalizuoti empyrinius ir analitinius išankstinių įtempių nuostolių skaičiavimo metodus atsižvelgiant į konstrukcinių medžiagų klampiai tamprią (armatūros relaksacijos, betono valkšnumo bei susitraukimo) elgseną.
2. Pasiūlyti analitinį armatūros įtempių nuostolių dėl įtempių relaksacijos vertinimo modelį, atsižvelgiant į bazalto pluošto mechanines savybes.
3. Pasiūlyti iš anksto įtemptų betoninių elementų armuotų bazalto pluošto armatūra ir veikiamų statine apkrova įlinkių bei plyšio pločio vertinimo modelius.
4. Atlikti bazalto pluošto armatūros įtempių relaksacijos nuostolių eksperimentinius tyrimus veikiant skirtingiems išankstiniams įtempiams.
5. Eksperimentiškai ištirti iš anksto įtemptais bazalto pluošto strypais armuotų betoninių sijų, veikiamų statine apkrova, įlinkius ir pleišėjimą.
6. Lyginant eksperimentinius ir apskaičiuotus įlinkių ir pleišėjimo rezultatus, atlikti pasiūlytų analitinių modelių adekvatumo analizę.

Tyrimų metodika

Darbe taikomi teoriniai kontinuumo mechanikos, analiziniai ir eksperimentiniai metodai. Siūlomas bazalto pluošto armatūros relaksacijos elgsenos vertinimas pagrįstas deformacijos proceso diferencialine lygtimi, o įtempių relaksacijos kitimo funkcijos aproksimacija pagrįsta Maksvelo reologiniu modeliu. Armatūros įtempių nuostolių dėl bazalto pluošto

armatūros įtempių relaksacijos vertinimo modelis pagrįstas esamų betoninių ir gelžbetoninių elementų įtempių bei deformacijų būvio metodų trūkumų analize. Eksperimentinių tyrimų metu bazalto pluošto strypų bandiniams nustatytos įtempių relaksacijos nuostolių reikšmės, pagrįstos įtempių relaksacijos funkcijomis. Eksperimentiniai tyrimai taip pat skirti betoninių sijų, armuotų iš anksto įtemptais bazalto pluošto strypais standumo analizei, įvertinant skirtingus pradinius armatūros įtempius. Atlikta teorinių ir eksperimentinių rezultatų analizė.

Mokslinis naujumas

1. Pasiūlytas naujas bazalto pluošto armatūros išankstinių įtempių relaksacijos nuostolių skaičiavimo metodas, pagrįstas bazalto pluošto kompozito elgsena.
2. Kaip alternatyva praktikoje taikomiems tinkamumo ribinio būvio charakteristikų apskaičiavimo metodams, pasiūlytos iš anksto įtemptais bazalto pluošto strypais armuotų betoninių elementų įlinkių it plyšio pločio vertinimo modeliai.
3. Pasiūlytas inovatyvus bazalto pluošto armatūros įtempių relaksacijos nuostolių eksperimentinių tyrimų metodas.
4. Gauti nauji bazalto pluošto įtempių relaksacijos nuostolių eksperimentinių tyrimų rezultatai.
5. Gauti nauji trumpalaike apkrova veikiamų iš anksto įtemptais bazalto pluošto strypais armuotų betoninių elementų eksperimentinių tyrimų rezultatai.

Darbo rezultatų praktinė reikšmė

Disertacijoje pasiūlyti išankstinių bazalto pluošto armatūros įtempių nuostolių skaičiavimo metodas, paremtas bazalto pluošto relaksacijos elgsena. Taip pat pasiūlyti iš anksto įtemptais bazalto pluošto strypais armuotų lenkiamų betoninių elementų įlinkių ir pleišėtumo analitiniai skaičiavimo metodai, paremti išankstinio apgniuždymo vertinimu. Skirtingai nuo daugelio teorinių modelių, remiantis pasiūlytais algoritmais galima apskaičiuoti liekamąjį išankstinės įtempimo jėgos dydį įvertinant bazalto pluošto armatūros įtempių nuostolių dėl relaksacijos reikšmes kartu arba atskirai nuo betono valkšnumo ir susitraukimo, tiksliau apskaičiouti įlinkius ir prognozuoti plyšių vystymąsi, atsižvelgiant į išankstinį apgniuždymą. Pasiūlytas bazalto pluošto armatūros įtempių relaksacijos koeficientas gali būti universaliai taikomas įvairiems išankstinio įtempimo dydžiams nustatyti.

Ginamieji teiginiai

1. Pasiūlytas analitinis išankstinių armatūros įtempių nuostolių skaičiavimo metodas, paremtas bazalto pluošto kompozito (BFRP) relaksacijos elgsena, leidžiai tiksliau apskaičiuoti efektyviąją išankstinio armatūros įtempimo jėgą.
2. Bazalto pluošto armatūros įtempių dėl relaksacijos nuostolio reikšmė (%) yra kintamas dydis ir didėjant pradiniams išankstiniams įtempiams proporcingai didėja.

3. Pasiūlyti įlinkių ir plyšio pločio skaičiavimo metodai, paremti išankstinio apgniuždymo bei BFRP armatūros įtempių relaksacijos elgsena, leidžia vertinti lenkiamų betoninių elementų tinkamumo ribinį būvį, kuris atitinka išankstinio įtempimo koncepciją.

Darbo rezultatų aprobavimas

Disertacijos tema paskelbti 9 moksliniai straipsniai, iš kurių 3 – žurnaluose turinčiuose cituojamumo rodiklį, o 1 – konferencijų rinkiniuose, referuojamuose *Clarivate Analysis Web of Science* duomenų bazėje. Disertacijoje atliktų tyrimų rezultatai buvo paskelbti 5 pranešimuose 5 konferencijose Lietuvoje ir užsienyje:

- 17-oji Jaunųjų mokslininkų konferencijoje *Lietuva be mokslo – Lietuva be ateities*, Vilnius, Lietuva, 2014.
- 18-oji tarptautinė konferencija *18th International Conference on Composite Structures,* Lisabona, Portugalija, 2015.
- 19-oji tarptautinė konferencija *19th International Conference on Composite Structures*, Porto, Portugalija, 2016.
- 11-oji tarptautinė konferencija „Modern Building Materials, Structures and Techniques“, Vilnius, Lietuva, 2016.
- 3-ioji tarptautinė konferencija *3rd International Conference on Mechanics of Composites MECHCOMP3*, Bolonija, Italija, 2017.

Disertacijos struktūra

Disertaciją sudaro įvadas, 3 skyriai, bendrosios išvados, autoriaus mokslinių publikacijų disertacijos tema sąrašas (9 publikacijos), santrauka lietuvių kalba ir 3 priedai.

Disertacijos apimtis – 126 puslapiai. Tekste panaudoti 61 paveikslai, 19 lentelių ir 135 literatūros šaltiniai.

Padėka

Autorius nuoširdžiai dėkoja savo mokslinio darbo vadovui, Gelžbetoninių konstrukcijų ir geotechnikos katedros vedėjui prof. dr. Juozui Valivoniui už puikią lyderystę, motyvaciją, vertingas žinias ir patarimus rengiant disertaciją. Disertacijos autorius dėkoja doc. dr. Algirdui Jonui Notkui, doc. dr. Broniui Jonaičiui, prof. dr. Charles Dolan, prof. dr. Oral Büyüköztürk, prof. dr. Vytautui Vaičaičiui, kurių patirtis ir kompetencija padėjo reikšmin-gai pagerinti disertacinio darbo kokybę. Autorius taip pat dėkoja dr. Aidui Jokūbaičiui bei doc. dr. Arnoldui Šneideriui už geranorišką pagalbą atliekant eksperimentinius tyrimus.

Autorius nuoširdžiai dėkoja savo tėvams, Audrutei ir Petrui, broliui Edgarui, uošviams Irenai ir Visvaldui bei mylimai žmonai Eglei už nuolatinį palaikymą, kantrybę ir paramą rengiant disertaciją. Disertacinio darbo autorius dėkoja Lietuvos mokslo tarybai už suteiktą paramą, finansuojamą pagal Europos Sąjungos struktūrinių fondų projektą Nr. 09.3.3-LMT-K-712-04-0118.

1. Klampiai tamprių medžiagų fizinių modelių ir konstrukcijų tipų apžvalga

Pirmajame disertacijos skyriuje pateikiama neplieninės armatūros savybių, iš anksto įtempto gelžbetonio konstrukcijų probleminių sričių (eksploatacija agresyvioje aplinkoje) išankstinių įtempių nuostolių bei tinkamumo ribinio būvio nustatymo metodų literatūros šaltinių apžvalga. Aptartos neplieninės armatūros ir betono fizinės ir mechaninės savybės, kurios lemia išankstinės įtempimo jėgos mažėjimą. Pristatyti bazalto pluošto armatūros privalumai ir perspektyvos. Analizuojami išankstinio įtempimo būdų privalumai ir trūkumai. Aprašomi neplieninės armatūros įtempių relaksacijos elgsenos įpatumai bei jos įtaka nustatant iškart patiriamus ir nuo laiko priklausomus nuostolius. Skyriuje apibūdintos pagrindinės iš anksto įtempto gelžbetoninių lenkiamų elementų pagrindinės apkrovimo stadijos. Aptarti tradiciniai metodai – efektyviojo modulio (McMillan 1916, Faber 1927), senėjančios medžiagos efektyviojo modulio (Trost 1967) bei nauji ir inovatyvūs metodai – bendrasis (Pisani 2000) bei vidutinių ekvivalentinių įtempių ir deformacijų (Balevičius 2010) metodai lenkiamų elementų įtempių ir deformacijų būviui nustatyti. Apžvelgti projektavimo normų reglamentuojami išankstinių įtempių nuostolių, įlinkių ir pleišėjimo prognozavimo metodai.

Parodyta, kad neplieninės (polimerinės) armatūros relaksacijos elgsena skiriasi nuo tradicinio plieno armatūros, todėl norint tinkamai įvertinti relaksacijos nuostolio reikšmę (%) yra reikalinga atlikti sudėtingus inžinerinius skaičiavimus arba aproksimuoti relaksacijos kreivę remiantis eksperimentiniai tyrimais. Pastaruoju atveju yra būtinas bandymo įrenginys, galintis išlaikyti pastovią bandinio deformaciją per visą relaksacijos laiką. Taip pat buvo parodyta, kad norint tiksliai apskaičiuoti iš anksto įtemptų betoninių lenkiamų elementų tarpatramio įlinkį ir vidutinį plyšio plotį, tiesioginis paprastojo gelžbetonio skaičiavimo formulių taikymas nebūtinai atspindi realią iš anksto įtemptos konstrukcijos elgseną. Tinkamumo ribinio būvio analizei įtakos turi tikslus išankstinės įtempimo jėgos bei jos sukelto išankstinio apspaudimo nustatymas.

2. Lenkiamųjų iš anksto įtemptųjų betoninių elementų išankstinių armatūros įtempių nuostolių ir tinkamumo ribinio būvio analizė

Antrajame skyriuje pasiūlytas analitinis skaičiavimo metodas išankstinių įtempių nuostoliams nustatyti, atsižvelgiant į bazalto pluošto armatūros įtempių relaksaciją. Ši metodika leidžia nustatyti kokią įtaką išankstinės įtempimo jėgos dydžiui turi armatūros įtempių relaksacija priklausomai nuo elemento apkrovimo stadijos (S2.1 pav.). Autoriaus pasiūlytoje armatūros įtempių nuostolių skaičiavimo metodikoje nagrinėjami šie pagrindiniai apkrovimo etapai: 1) bazalto pluošto armatūros įtempimas į atsparas (laiko momentu t_0). Laikoma, kad šioje stadijoje iš karto pasireiškia bazalto pluošto armatūros įtempių relaksacija ir kinta proporcingai nuo apkrovos pradžios; 2) elemento apspaudimas (laiko momentu t_p). Šioje stadijoje atleidus atsparas elementui perduodamas išankstinis įtempimas. Skaičiuojant armatūros įtempių nuostolius vertinami bazalto pluošto armatūros įtempių relaksacija, betono susitraukimas ir valkšnumas; 3) elemento apkrovimas išorine apkrova (laiko momentu t_q).

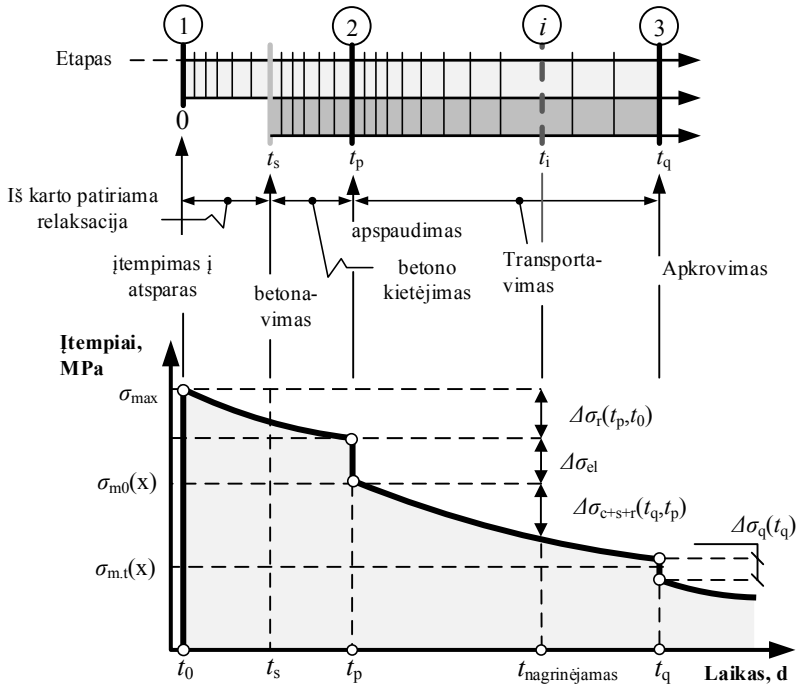

S2.1 pav. Išankstinių įtempių nuostolių modelis atsižvelgiant į elemento gamybos ir apkrovimo etapus

Nuo šio momento elementas be išankstinio apspaudimo papildomai apkraunamas išorine apkrova. Skaičiuojant išankstinių įtempių nuostolius taikomos tokios prielaidos: 1) iškart patiriami išankstiniai įtempių nuostoliai dėl bazalto pluošto armatūros relaksacijos pasireiškia vos tik armatūrai suteikus išankstinė įtempimo jėgą; 2) elemento skerspjūvis yra vienalytis prieš ir po supleišėjimo; 3) armatūros įtempių ir deformacijų diagramos yra tiesinės; 4) taikoma plokščiųjų pjūvių hipotezė t.y. deformacijos elemento skerspjūvio aukštyje kinta tiesiškai; elemento skerspjūvis yra vienalytis prieš ir po supleišėjimo; skaičiavimuose vertinami armatūros ir betono vidutiniai įtempiai bei vidutinės deformacijos; 5) armatūros ir betono sukibtis laikomas idealiu; 6) tempiamo betono darbas nėra vertinamas; 7) ilgalaikių įtempių nuostolių atveju, betono savybių įtaka elemento įtempių ir deformacijų būviui vertinama taikant senėjančios medžiagos efektyvųjį (AEMM) modelį (1.42 formulė).

Toliau pateikiamas išankstinių armatūros įtempių nuostolių skaičiavimo metodo algoritmas (S2.2 pav.). Ši metodika leidžia vertinti iš anksto įtemptais bazalto pluošto strypais armuotų lenkiamų betoninių elementų išankstinius armatūros nuostolius, pleišėjimą ir įlinkius kaip tarpusavyje susijusius procesus. Toks skaičiavimo būdas leidžia išvengti rezultatų prieštaravimų, kurie dažnai būdingi empyriniams metodams: pastovios armatūros įtempių relaksacijos bėgant laikui.

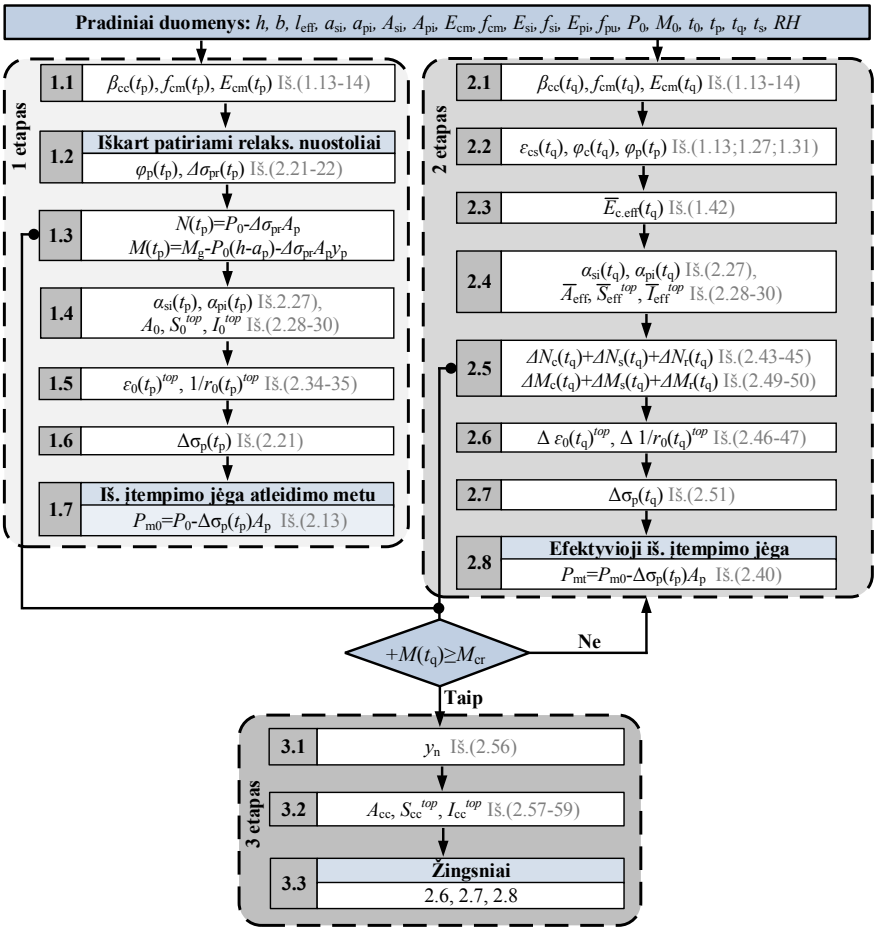

S2.2 pav. Išankstinių armatūros įtempių nuostolių skaičiavimo algoritmas

Atsižvelgiant į iškarto patiriamos bazalto pluošto armatūros įtempių relaksacijos svarbą, pasiūlyta įtempių relaksacijos kitimo funkcijos aproksimacija, pagrista Maksvelo reologiniu modeliu. Šiuo atveju galima aprašyti relaksacijos funkcijos formą eksponentine diagrama. Norint gauti tinkamą rezultatų tikslumą, reikalinga atlikti eksperimentinius tyrimus, kurie pagrįstų eksponentinės arba kitos (logaritminės) diagramos taikymą. Remiantis literatūros analize, autoriaus pasiūlytame skaičiavimo algoritme taikoma Banibayat (2015) pasiūlyta relaksacijos koeficiento išraiška iškart patiriamai bazalto pluošto armatūros relaksacijai nustatyti:

$$\varphi_{\mathrm{p}}(t) = 0{,}006\ln(t) + 0{,}0465\,, \tag{S1.1}$$

čia t ir t_0 – atitinkamai, nagrinėjamas ir išankstinio įtempimo laikas, valandomis.

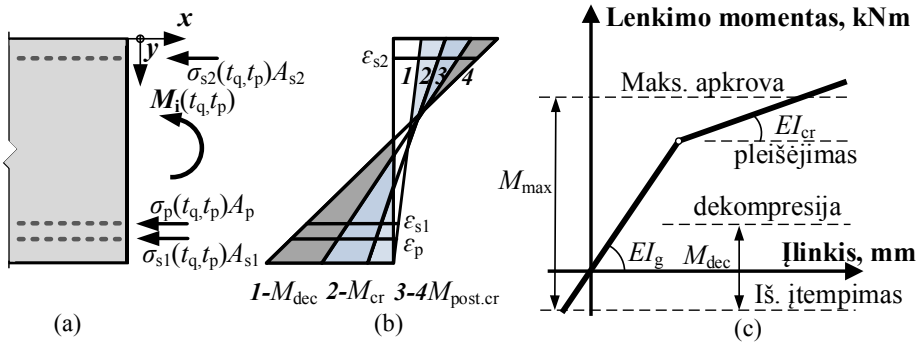

S2.2 pav. Iš anksto įtemptojo lenkiamojo gelžbetoninio elemento: veikiančios įrąžos (a); deformacijų pasiskirstymas priklausomai nuo ribinio būvio stadijos (b); lenkimo momento ir įlinkio priklausomybės diagrama (c)

Tinkamumo ribinio būvio analizei buvo pasiūlyta patikslinti JAV projektavimo normų įlinkių skaičiavimo metodiką. Šiuo atveju skaičiuojant efektyvųjį inercijos momentą siūloma papildomai vertinti dekompresijos efektą (S2.3 pav.). Šio efekto vertinimas buvo pagrįstas eksperimentinių tyrimų rezultatais. Tam tikru laiko momentu, iš anksto įtemptų betoninių elementų įlinkis priklauso nuo elemento apkrovimo stadijos. Lyginant su įprasto gelžbetinio lenkiamais elementais, papildomai reikalinga vertinti įšlinkį nuo išankstinio apgniuždymo.

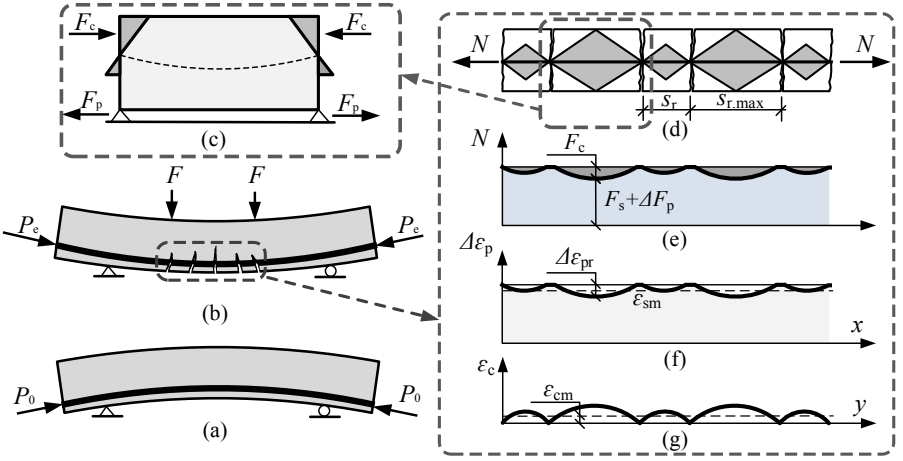

S2.3 pav. Elemento įrąžų ir deformacijų pasiskirstymas ruože tarp plyšių: išankstinio įtempimo suteikimas (a) išorinės apkrovimas (b); įrąžų pasiskirstymas (c); plyšių formavimasis (d); apkrovos pasiskirstymas (e); armatūros deformacijų pasiskirstymas (f); betono deformacijų pasiskirstymas (g)

Tokiu atveju, skaičiuojant iš anksto įtemptais bazalto pluošto strypais armuotų lenkiamų betoninių sijų įlinkius siūloma įvertinti išankstinio apspaudimo įtemptąja armatūra ribinį būvį eliminuojant dekompresijos momentą (2.62 formulė):

$$M_{\mathrm{dec}} = P_{\mathrm{e}} \cdot e + \frac{P_{\mathrm{e}} \cdot I_{\mathrm{g}}}{A_{\mathrm{g}} \cdot y_{\mathrm{g}}}, \tag{S1.2}$$

čia P_{e} – efektyvioji išankstinio įtempimo jėga; e – ekscentricitetas; A_{g} ir I_{g} – atitinkamai, nesupleišėjusio skerspjūvio plotas ir inercijos momentas; y_{g} – atstumas nuo nesupleišėjusio skerspjūvio svorio centro iki skerspjūvio viršutinio krašto.

Disertaciniame darbe taip pat pasiūlytos plyšio pločio ir deformacijų priklausomai nuo elemento apkrovimo stadijos bei atstumo tarp plyšių priklausomybės (S2.3 pav.). Skaičiuojant plyšio plotį įvertinamos išankstinio apspaudimo įtemptąja armatūra bei susitraukimo deformacijos:

$$w_{\mathrm{k}} = s_{\mathrm{r.max}}(\varepsilon_{\mathrm{p}}(t_{\mathrm{q}}) - \varepsilon_{\mathrm{p.dec}}(t_{\mathrm{p}}) - \varepsilon_{\mathrm{cs}}(t_{\mathrm{q}}))\,; \tag{S1.3}$$

$$s_{\mathrm{r.max}} = 1/3(h - y_{\mathrm{n}}), \tag{S1.4}$$

čia $\varepsilon_{\mathrm{p}}(t_{\mathrm{q}})$ – iš anksto įtemptosios armatūros deformacija nagrinėjamu apkrovimo metu; $\varepsilon_{\mathrm{p.dec}}(t_{\mathrm{p}})$ – išankstinio apspaudimo įtemptąja armatūra elemento deformacija nagrinėjamu išorinės apkrovos metu (2.67 formulė); $\varepsilon_{\mathrm{cs}}(t_{\mathrm{q}})$ – betono traukumo deformacija.

3. Iš anksto įtemptųjų elementų eksperimentiniai tyrimai ir teorinių prielaidų tikrinimas

Trečiajame skyriuje aprašomi atlikti natūralaus dydžio iš anksto įtemptų lenkiamų gelžbetoninių sijų eksperimentiniai tyrimai ir jų rezultatai. Šių bandinių eksperimentinę programą sudarė 12 iš anksto įtemptų sijų, kurios buvo suskirstytos į 3 serijas priklausomai nuo išankstinio įtempimo dydžio, atitinkamai 40 %, 45 % ir 55 % nuo tempiamojo bazalto pluošto armatūros tempiamojo stiprio. Viena neįtemptoji sija, buvo panaudota, kaip kontrolinė išankstinio įtempimo efekto lenkiamajam standumui palyginti. Sijų bandymams buvo panaudota bazalto pluošto armatūra RockBar Composite, kurios tempiamasis stipris f_{u} = 1098,3 MPa, tamprumo modulis E_{f} = 45 GPa. S3.1 paveiksle parodyta bandomųjų sijų apkrovimo schema.

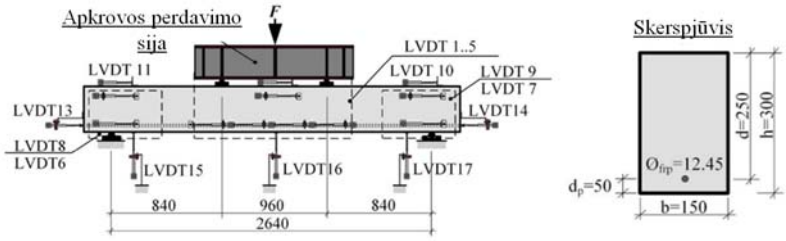

S3.1 pav. Sijų bandymų ir matavimų schema

S3.1 lentelė. Eksperimentinių sijų pagrindinės charakteristikos

Sija (Serija)	h, mm	b, mm	l, mm	a_1, mm	f_u, MPa	ε_{fu}	E_f, GPa	ρ, %	f_{ck}, MPa
S-1	301	149	3200	50	1098,3	0,0246	45	0,32	46,01
Serija 1									
SSI-1	303	150							
SSI-2	300	149	3200	50	1098,3	0,0246	45	0,33	44,47
SSI-3	301	150							
SSI-4	299	149							
Serija 2									
SSI-5	300	150							
SSI-6	303	152	3200	50	1098,3	0,0246	45	0,32	40,21
SSI-7	301	148							44,29
SSI-8	303	147							
Serija 3									
SSI-9	301	151							
SSI-10	302	150	3200	50	1098,3	0,0246	45	0,32	46,01
SSI-11	302	150							
SSI-12	300	149							

S3.2a–S3.2d paveiksluose palygintos eksperimentinės ir apskaičiuotos įlinkių reikšmės pagal Europos (CEN) ir JAV (ACI) projektavimo, Toutanji (2000) rekomendacijas efektyviajam inercijos momentui I_e nustatyti, bei pagal autoriaus pasiūlytą metodiką, atsižvelgiant į BFRP armatūros įtempių relaksaciją (žr. skyrių 2.3.1). Atliekant rezultatų analizę pastebėta, kad teoriniuose skaičiavimuose neįvertinant išankstinio apgniuždymo pagal JAV projektavimo normas apskaičiuoti įlinkiai yra 56 % mažesni nei eksperimentiniai. Iš pateiktų grafikų (S3.2 pav.) taip pat yra matyti, kad pagal siūlomą metodiką ir Europos projektavimo normas apskaičiuotų apkrovos ir įlinkių priklausomybių charakteris atitinka eksperimentinius rezultatus, atitinkamai, o apskaičiuotų ir eksperimentinių įlinkių santykiai $\delta_{calc}/\delta_{exp}$ sumažėja nuo 2,17 iki 1,50 ir nuo 2,24 iki 1,81, kai išankstinis įtempimas padidėja nuo 5% iki 15 %.

S3.3–S3.5 paveiksluose pateiktos pleišėjimo parametrų teorinės ir eksperimentinės reikšmės. Šiuo atveju buvo lyginamos vidutinės eksperimentinių ir apskaičiuotų pagal Europos, JAV projektavimo normas bei autoriaus pasiūlytas metodikas vidutinių plyšio pločio reikšmės. Buvo pastebėta, kad taikant koeficiento k_b reikšmes, naudojamas tradicinio plieno armatūros atveju, iš anksto įtemptų gelžbetoninių sijų armuotų bazalto pluošto armatūra apskaičiuotasis vidutinio plyšio plotis gali būti iki 77,3 % didesnis nei eksperimentinis. Atsižvelgiant į eksperimentinius matavimus ir keičiant koeficiento k_b vertes, kaip pavaizduota S3.3–S3.5 paveiksluose, esant 40 % išankstinio įtempimo dydžiui santykis w_{calc}/w_{exp} ženkliai sumažėja, atitinkamai, iki $w_{k.calc}/w_{k.exp}$ = 1,85 ir $w_{k.calc}/w_{k.exp}$ = 1,30. Remiantis autoriaus pasiūlyta metodika (2.67 formulė) teorinių ir eksperimentinių plyšio pločių santykis buvo $w_{k.calc}/w_{k.exp}$ = 1,25. Kai išankstinio įtempimo dydis yra 55 % armatūros tempiamojo stiprio, remiantis autoriaus pasiūlyta išraiška gauta, kad $w_{k.calc}/w_{k.exp}$ = 1,25. Tuo tarpu remiantis Europos bei JAV projektavimo normomis, minėtos santykinės reikšmės yra didesnės, atitinkamai, $w_{k.calc}/w_{k.exp}$ = 10,8 (k_b=0,8) ir $w_{k.calc}/w_{k.exp}$ = 4,5 (k_b = 0,05) bei $w_{k.calc}/w_{k.exp}$ = 7,5 (k_b = 1,2) ir $w_{k.calc}/w_{k.exp}$ = 1,92 (k_b = 0,3).

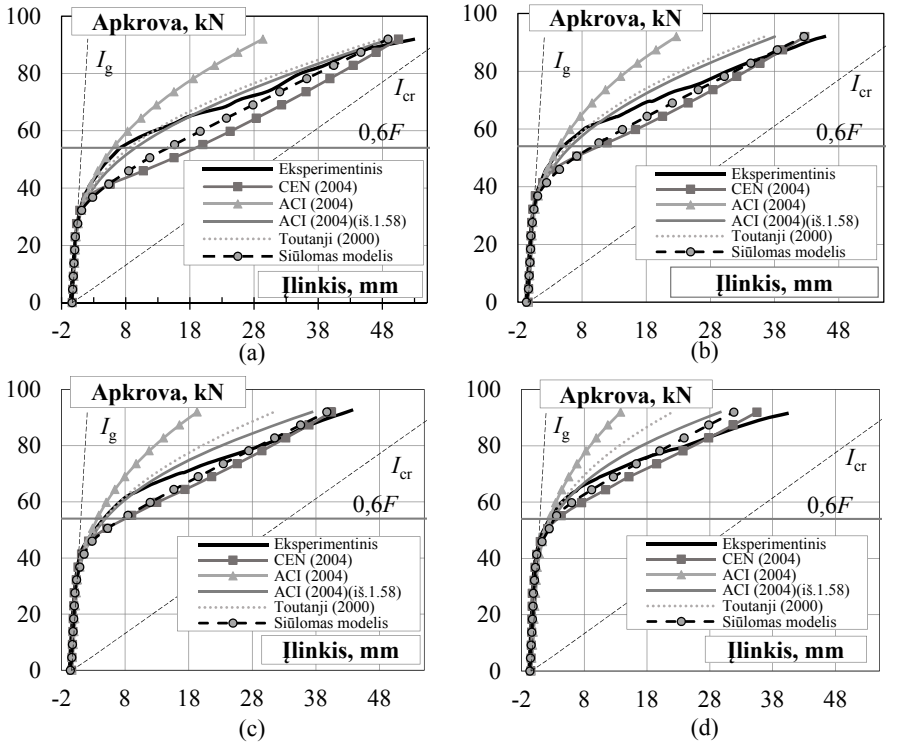

S3.2 pav. Iš anksto įtemptų gelžbetoninių sijų su bazalto pluošto armatūra apskaičiuotų ir eksperimentinių jėgos ir įlinkio diagramų palyginimas: 1 serijos (a); 2a serijos (b); 2b serijos (c); 3 serijos (d)

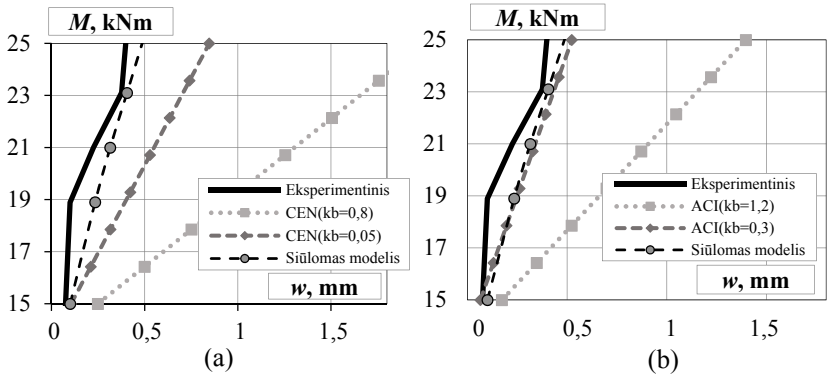

S3.3 pav. 1 serijos eksperimentais nustatyto ir apskaičiuoto plyšio pločio reikšmės, kai koeficientas k_b: pagal Euronormas (a); pagal JAV projektavimo normas (b)

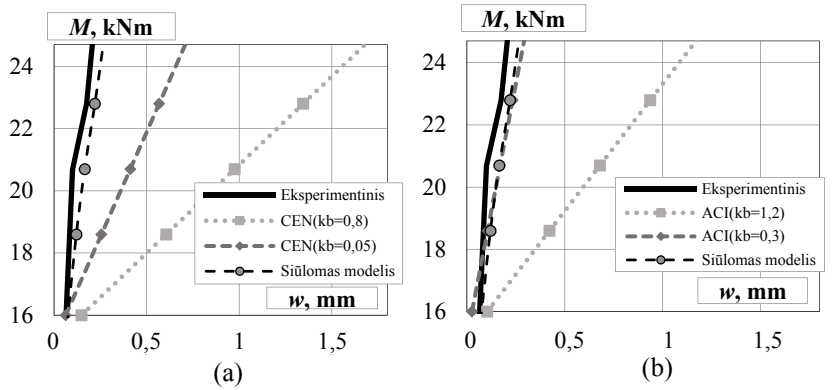

S3.4 pav. 2 (SSI-5,6) serijos eksperimentais nustatyto ir apskaičiuoto plyšio pločio reikšmės, kai koeficientas k_b: pagal Euronormas (a); pagal JAV projektavimo normas (b)

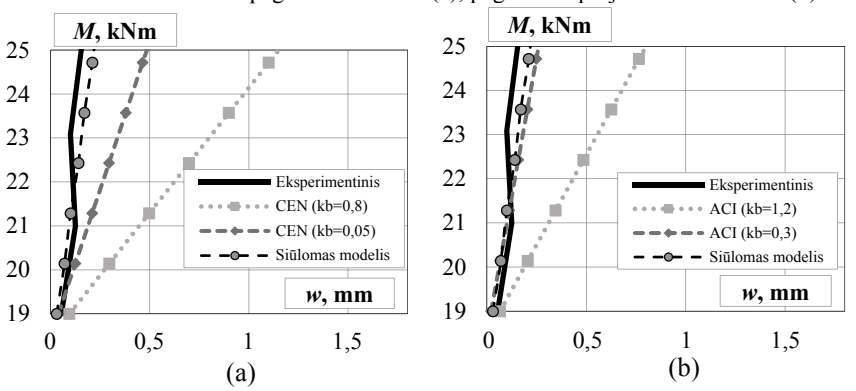

S3.5 pav. 3 serijos eksperimentais nustatyto ir apskaičiuoto plyšio pločio reikšmės, kai koeficientas k_b: pagal Euronormas (a); pagal JAV projektavimo normas (b)

S3.2 lentelė. Eksperimentiškai nustatytų relaksacijos nuostolio reikšmės

Išankstinis įtempimas	Serija	Bandinio Nr.	Likutinis išankstinio įtempimo dydis, %	Nustatytas relaksacijos nuostolis, %	Vidutinis relaksacijos nuostolis, %
		BP-1		5,42	
$0,4f_u$	1 Serija	BP-2	94,28	5,76	5,72
		BP-3		5,98	
		BP-4		6,01	
$0,45f_u$	2 Serija	BP-5	93,96	6,09	6,04
		BP-6		6,02	
		BP-7		6,5	
$0,55f_u$	3 Serija	BP-8	93,33	7,1	6,67
		BP-9		6,4	

Lyginant projektavimo normas, tiksliausi plyšio pločio skaičiavimo rezultatai gaunami remiantis JAV projektavimo normomis, kai $k_b = 0{,}3$.

Siekiant tiksliau nustatyti išankstinės įtempimo jėgos liekamąjį dydį priklausomai nuo įtempių relaksacijos nuostolių buvo atlikti bazalto pluošto armatūros strypų įtempių relaksacijos bandymai. Bandiniai buvo suskirstyti į 3 serijas priklausomai nuo išankstinio įtempimo dydžio 40 %, 45 % ir 55 %. Pasirinktas bandinių relaksacijos laikas – 1000 h. Apkrovimo žingsnis 200±50 N/mm^2. Pasiekus reikalingą įtempimo lygį bandiniai toliau neapkraunami ir laikomi 120±2 sekundžių. Laiko intervalai, kada nuskaitomi indikatorių rodmenys: 1, 3, 6, 15, 30, 45 minutės, 1, 2, 4, 10, 24, 48, 72, 96, 120 valandų, vėliau, kas 24 valandas. Eksperimentinės bazalto pluošto armatūros relaksacijos nuostolio reikmės (%) pateiktos S3.2 lentelėje. Remiantis eksperimentinių tyrimų rezultatais buvo nustatytos bazalto pluošto armatūros strypų įtempių relaksacijos kreivės, kurias tiksliausiai galima aprašyti logaritminėmis įtempių relaksacijos koeficiento φ_r diagramomis. Priklausomai nuo išankstinio įtempimo dydžio jos pateiktos S3.6a–S3.6b paveiksluose.

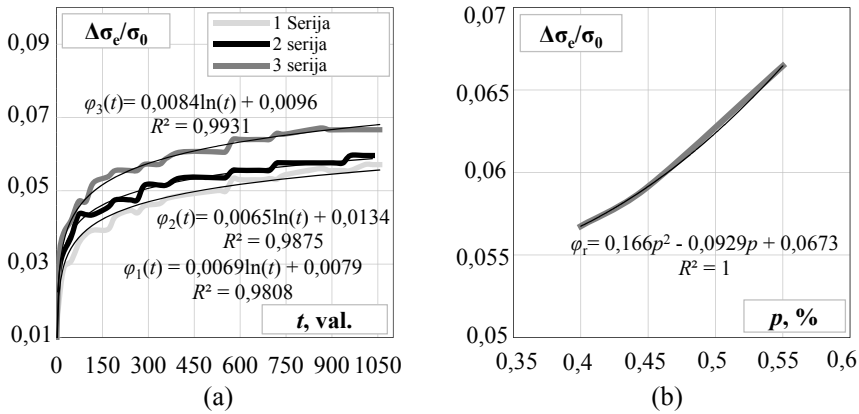

S3.6 pav. Eksperimentinės relaksacijos koeficiento priklausomybės: priklausomai nuo įtempimo dydžio (a); priklausomai nuo įtempimo dydžio, kai t = 1000 h (b)

Remiantis eksperimentų rezultatais pasiūlyta įtempių relaksacijos koeficiento apskaičiavimo formulė:

$$\varphi_r = (0{,}166p^2 - 0{,}0929p + 0{,}0673)\ln(t) + 1\,. \qquad \text{(S1.5)}$$

Atlikus išankstinių įtempių nuostolių analizę gauta, kad remiantis eksperimentinėmis relaksacijos koeficiento φ_r reikšmėmis (S1.5 formulė) bazalto pluošto armatūros išankstinių įtempių nuostoliai nuo 0,85 %; 1,16 % ir 3,01 % didesni nei priimant šio koeficiento reikšmes pagal Banibayat (2015) pasiūlyta priklausomybę. Atsižvelgiant į tai, nustatyta, kad bazalto pluošto armatūros relaksacijos elgsena priklauso nuo išankstinio įtempimo dydžio reikšmės t.y. didėjant išankstinio įtempimo jėgos dydžiui, armatūros relaksacijos nuostolio reikšmė taip pat didėja.

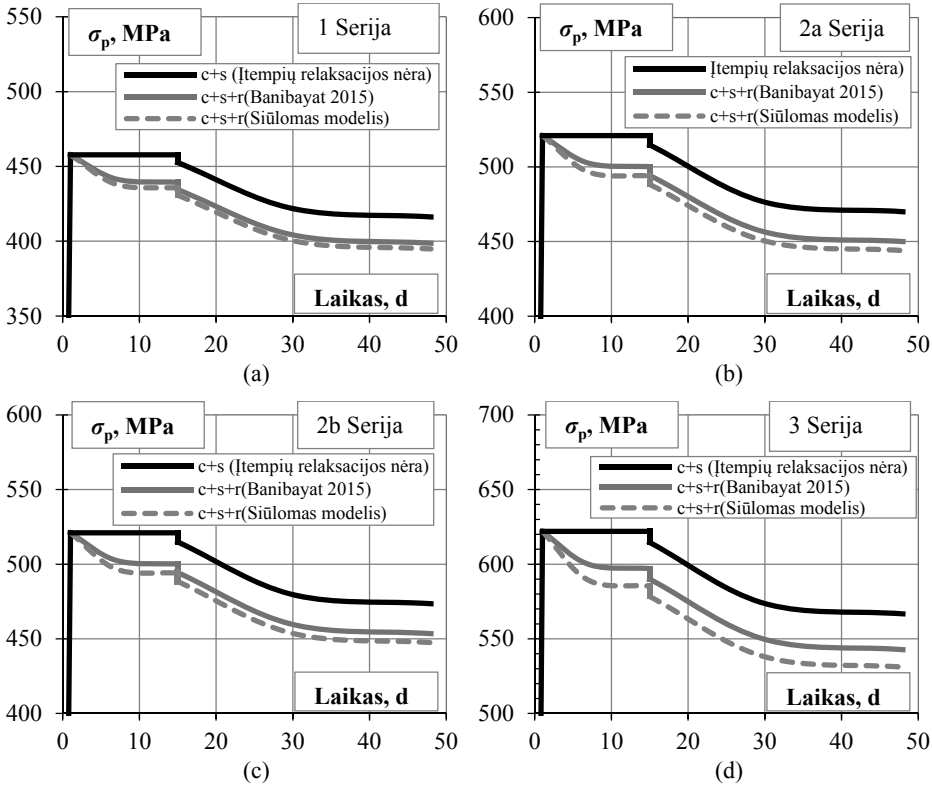

S3.7 pav. Iš anksto įtempto gelžbetonio lenkiamų sijų su bazalto pluošto armatūra įtempių armatūroje pasiskirstymas: 1 Serijos (a); 2a Serijos (b); 2b Serijos (c); 3 Serijos (d)

S3.7a–S3.7d paveiksluose pateikti pradinių bazalto pluošto armatūros įtempių ir laiko priklausomybės grafikai. Esant 40 % išankstinio įtempimo dydžiui (S3.7a pav.) pradiniai armatūros įtempiai netolygiai mažėja, kai skaičiavimuose vertinama iš karto patiriama bazalto pluošto armatūros įtempių relaksacija. Kai išankstiniai armatūros įtempiai padidėja iki 45 % (S3.7b–S3.7c pav.) ir 55 % (S3.7d pav.), armatūros įtempių nuostoliai padidėja netolygiai. Iš minėtų grafikų matyti, išankstiniai armatūros įtempių nuostoliai apskaičiuoti pagal pasiūlytą metodiką yra didesni nei apskaičiuoti remiantis Banibayat (2015) metodika. Pasiūlytoje metodikoje yra vertinamas armatūros išankstinio įtempimo dydis, kuris turi įtakos armatūros įtempių relaksacijos elgsenai. Tuo tarpu minėtoje Banibayat (2015) metodikoje yra priimta, kad įtempių relaksacijos reikšmė yra pastovus dydis, o tai prieštarauja eksperimentinių tyrimų rezultatams. Eksperimentiškai pagrįstos bazalto pluošto armatūros įtempių relaksacijos elgsenos vertinimas leidžia tiksliau apskaičiuoti iš anksto įtemptosios bazalto pluošto armatūros įtempių relaksacijos nuostolius.

Bendrosios išvados

Apibendrinus atliktų tyrimų rezultatus galima teigti, kad:

1. Literatūros analizė parodė, kad projektavimo normose nėra pateiktų įtemptosios bazalto pluošto aramatūros įtempių relaksacijos nuostolio reikšmių konstrukciniams skaičiavimams atlikti.
2. Bazalto pluošto armatūros relaksacijos elgsena skiriasi nuo įprastosios plieno armatūros t. y. priešingai nei plieninės armatūros atveju, kai armatūros įtempių relaksacija vertinama įtempiams pasiekus apie 50 % jos tempiamojo stiprio, iškart patiriama bazalto pluošto armatūros relaksacija didėja proporcingai nuo pat įtempimo pradžios.
3. Remiantis pasiūlytu skaičiavimo metodu efektyviąjai išankstinei įtempimo jėgai nustatyti, galima tiksliai įvertinti bazalto pluošto armatūros įtempių nuostolius dėl relaksacijos priklausomai nuo elemento apkrovimo stadijos.
4. Pasiūlytas skaičiavimo metodas leidžiai tiksliai nustatyti įtempių ir deformacijų pasiskirstymą skerpjūvyje. Gautos apskaičiuotų deformacijų reikšmės 3,5 % didesnės už eksperimentų rezultatus. Atlikta analizė parodė, kad naudojant siūlomą skaičiavimo metodiką gaunama mažesnė paklaida, lyginant su kitų autorių metodikomis.
5. Eksperimentinai tyrimai patvirtino pasiūlytos metodikos tinkamumą, kai yra atsižvelgiamą į išankstinį apgniuždymą skaičiuojant efektyvųjį inercijos momentą pagal JAV projektavimo normas. Neatsižvelgiant į tai, gauti apskaičuoti įlinkiai 56 % mažesni už eksperimentiškai nustatytus įlinkius.
6. Remiantis pasiūlytu įlinkių skaičiavimo metodu gautos teorinės apkrovos ir įlinkio priklausomybės atitinka eksperimentiškai ištirtų kreivių pobūdį.
7. Pasiūlytas plyšio pločio skaičiavimo metodas, pagrįstas išankstinio elemento apspaudimo ir betono traukumo deformacijos vertinimu, užtikrina adekvačią iš anksto įtemptais bazalto pluošto armatūros strypais armuotų betoninių elementų pleišėtumo analizę. Gautos plyšių pločių teorinės reikšmės 25–30 % viršija eksperimentines.
8. Šiame darbe aprašyti unikalūs bazalto pluošto armatūros strypų įtempių relaksacijos eksperimentiniai tyrimai. Tyrimai parodė, kad esant išankstinių įtempių reikšmėms 40 %, 45 % ir 55 % gautos atitinkamos įtempių relaksacijos nuostolio reikšmės 5,75 %, 6,04 % ir 6,67 %.
9. Eksperimentiniai tyrimai parodė, kad išankstinis bazalto pluošto armatūros įtempimas padidino sijų standumą. Sijos, kurių armatūra buvo įtemta 40 %, 45 % ir 55 % nuo tempiamojo stiprio, atitinkamai gauti 33 %, 40 % ir 47 % mažesni įlinkiai nei neįtemtosios sijos.
10. Pasiūlyta bazalto pluošto armatūros įtempių relaksacijos koeficiento, kuris priklauso nuo išankstinio įtempių lygio bei mechaninių armatūros savybių, apskaičiavimo formulė.

Annexes[1]

Annex A. Declaration of Academic Integrity

Annex B. The Co-authors' Agreement to Present Publications Material in Dissertation

Annex C. Copies of Scientific Publications by the Author on the Topic of Dissertation

[1]The annexes are supplied in the enclosed compact disc

Mantas ATUTIS

ANALYSIS OF FLEXURAL BEHAVIOUR OF CONCRETE BEAMS PRESTRESSED WITH BASALT FIBER REINFORCED POLYMER BARS

Doctoral Dissertation

Technological Sciences,
Civil Engineering (02T)

IŠ ANKSTO ĮTEMPTAIS BAZALTO PLUOŠTO STRYPAIS ARMUOTŲ LENKIAMŲJŲ BETONINIŲ ELEMENTŲ ELGSENOS ANALIZĖ

Daktaro disertacija

Technologijos mokslai,
statybos inžinerija (02T)

2018 10 08. 13 sp. l. Tiražas 20 egz.
Vilniaus Gedimino technikos universiteto
leidykla „Technika“,
Saulėtekio al. 11, 10223 Vilnius
http://leidykla.vgtu.lt
Spausdino BĮ UAB „Baltijos kopija“
Kareivių g. 13B, 09109 Vilnius